

**onesteel**



---

The Regolith Expression of Cu-Au mineralisation  
within the Northern region of  
the Project Mawson area, NE Eyre Peninsula,  
South Australia

**Chad Brian Hicks**

**Geology and Geophysics, School of Earth and Environmental Sciences,  
University of Adelaide, Adelaide, SA 5005, Australia**

**A Manuscript submitted for the Honours Degree of Bachelor of Science  
University of Adelaide October 2010**

**Supervised by Dr. Steven M. Hill**

**Co-Supervisor: Prof. David Giles**

## ABSTRACT

The Gawler Craton is a well documented region, and is important because of the many IOCGU style deposits, it hosts. The Eyre Peninsula lies within this district and also within the Olympic Cu-Au province, and OneSteel's current IOCGU exploration also lies within this Cu-Au-rich domain. There has been strong evidence from data gained since the late 1990's by various companies, which suggests that approximately 50km south-west of Whyalla, proximal to Iron Duke, Iron Duchess and Iron Baron, is potential IOCGU mineralisation. Currently; gravity, magnetics, and existing calcrete data are being used to try and assess the validity of the suggested mineralisation, but further exploration is inhibited by extensive regolith cover. To overcome this problem; a vegetation and calcrete sampling program were conducted, targeting the major north-south trending structures throughout the area. From the study, the outcomes were; to uncover the landscape evolution of the area, characterise a biogeochemical signature of the deposit and a plant species which best suits the biogeochemical signature and landscape, and most importantly to suggest potential drilling targets from anomalous Cu-Au results.

The regolith expression was obtained from a regolith-landform map compiled throughout this project period; and western myall (*Acacia papyrocarpa*) pearl bluebush (*Maireana sedifolia*) and calcrete were used to characterise the biogeochemical and geochemical signature of the study area, also known as Project Mawson. The area of interest for this particular manuscript targets the northern half of the Project Mawson area, with a companion study being undertaken in the south of the region (Mitchell, 2010). The commodity elements chosen for detailed analysis included (Au, Cu and U), with secondary mineral trace elements (Al, Fe, Ca, and Zr), and pathfinder and mineralisation accessory elements (Ce, Co, Y, La, Pb, Ag and Zn). The results from this study have highlighted anomalous zones of mainly Cu and Au, particularly in the vegetation results, and there is also a strong structural relationship with these anomalies. This association and the highly anomalous results, indicate that a further biogeochemical survey would be a sound approach for further exploration, but a strong emphasis needs to be put on the understanding of the landscape; as it has the potential to alter soil profiles and to shift anomalous concentrations of target elements. Taking these factors along with others discussed throughout the following manuscript into consideration, would increase the quality of data returned from a future survey, and overall highlight zones of interest and therefore delineate potential drilling targets.

**Contents**

ABSTRACT.....	2
1. INTRODUCTION.....	6
1.1 Previous Exploration.....	8
1.2 IOCGU Background.....	9
2.0 STUDY AREA.....	11
2.1 Location and Landuse.....	11
2.2 Geology.....	11
2.3 Geomorphology.....	14
2.4 Mineralisation.....	15
2.5 Regolith.....	16
2.6 Climate.....	16
2.7 Vegetation.....	17
3.0 METHODS.....	19
3.1 Biogeochemistry.....	19
3.1.1 TRANSECT SAMPLING.....	19
3.1.2 CONTAMINATION.....	20
3.2 Geochemistry.....	20
3.2.1 REGOLITH CARBONATE (CALCRETE) SAMPLING.....	20
3.2.2 GEOCHEMICAL SAMPLING OF HELIX DATA.....	21
3.3 Regolith-Landform Mapping.....	21

3.4 Analysis of Results.....	21
4.0 RESULTS.....	23
4.1 Regolith-Landform Mapping.....	23
4.1.1 AEOLIAN SEDIMENTS.....	23
4.1.2 ALLUVIAL SEDIMENTS.....	23
4.1.3 SHEET-WASH SEDIMENTS.....	24
4.1.4 COLLUVIAL SEDIMENTS.....	24
4.1.5 PALAEO-DRAINAGE SYSTEMS.....	25
4.1.6 EXPOSED BEDROCK.....	25
4.2 Geochemical and Biogeochemical Element Suites.....	25
4.2.1 WESTEWRN MYALL ( <i>Acacia papyrocarpa</i> ) ELEMENT ASSOCIATIONS.....	26
4.2.2 PEARL BLUEBUSH ( <i>Acacia papyrocarpa</i> ) ELEMENT ASSOCIATIONS.....	27
4.2.3 CALCRETE ELEMENT ASSOCIATIONS.....	29
4.2.4 SPATIAL ASSOCIATION OF ELEMENT ANOMALIES.....	30
5. DISCUSSION.....	32
5.1 Landscape Evolution Model.....	33
5.2 Relationships between Species.....	33
5.3 Relationship between Biogeochemistry and Geochemistry.....	36
5.4 Significance of Data.....	38
5.4.1 CURRENT DATA.....	38
5.4.2 HELIX DATA.....	39
5.5 Models for Target Element Dispersion and Residence.....	40



5.6 Implications for Mineral Exploration.....	45
6. CONCLUSION.....	47
7. ACKNOWLEDGEMENTS.....	49
8. REFERENCES.....	50
9. FIGURES AND TABLES.....	
10. APPENDICES.....	
11. REGOLITH-LANDFORM MAP AND LEGEND.....	

## **1. INTRODUCTION**

Iron-Oxide Copper Gold Uranium (IOCGU) deposits have been highly prospective in Australia since the discovery of the world class Olympic Dam deposit. Deposits such as Olympic Dam are important because of their enormous size and therefore economic significance, and for providing precious metals to the growing, Australian and world populations. The greatest implication to this style of deposit is the difficulty in locating them when covered by a significant thickness of overburden (Hedger and Dugmore, 2001). Along with this issue there is also the problem of the wide variation of IOCGU systems since it is a collective term that includes a broader spectrum of mineralisation styles. Deposits such as Olympic Dam and Prominent Hill illustrate this as they have different alteration styles but are both believed to be IOCGU deposits (Skirrow, 2004). There is also more than one way that they can form, including fluid mixing, and multiple fluid sources, which adds to the challenge of identifying mineralisation (Skirrow, 2004). Another factor that increases the difficulty of exploration is that there are no depth constraints available on mineralisation, so this factor cannot be used to help define an approximate region for the zone of mineralisation.

The main exploration issue with IOCGU deposits, such as Olympic Dam, is that the mineralisation needs to be either exposed or a geophysical anomaly needs to be drilled to uncover significant mineralisation. This kind of exploration, which is generally based around drilling, is very expensive and the level of uncertainty involved with this technique is high. Even though there is uncertainty when using geophysical data to try and discover IOCGU deposits, it is becoming increasingly easier, as geophysical techniques utilising gravity and magnetic measurements are becoming more detailed and the manipulation of the data is advancing. However, even with the progression of geophysical techniques it is very difficult to understand exactly where a commodity lies and what its shape is without extensive drilling. An alternative technique that can accompany the geophysical data and potentially help define the shape or location of a deposit is geochemistry. However, assessing the chemical fertility of the material which covers potential mineralisation can be difficult when there is a significant depth of overburden. As well as this, geochemical sampling media, such as calcrete or soils, can also give false anomalies in areas with a complex landscape history because most overburden has been transported to some degree. Therefore it is necessary to have a sound understanding of the landscape evolution and current landforms within the area of interest, which could have an effect on the expression of mineralisation.

A cheap solution that can be used to penetrate through the cover to sample the buried *in-situ* geology is biogeochemistry. Plant biogeochemistry has been defined as ‘a method of exploration involving the chemical analysis of plant tissues to assess the presence and nature of underlying mineralization, bedrock composition, bedrock structure (faults, joints and folds), and the chemistry of the soil, surficial sediments, and associated groundwater’ (Dunn, 2007). The basis of the technique is to analyse plant tissue of a specific species, checking for anomalous concentrations of particular target elements. By analysing the concentration within a particular plant organ it is possible to suggest where mineralisation is or if any pathfinder elements or commodity elements are present. In most cases either the twigs or leaves are the target organ; even though the plant roots are the organ that accesses the chemical signature of the underlying *in-situ* bedrock, the chemical fertility can still be measured in other organs.

The technique has been around for many years with records dating to 1898, suggesting that the ash of plants around mines had elevated levels of particular elements (Dunn, 2007). Since the late 1800s the technique has undergone continual modification and many studies have been undertaken looking at aspects such as biogeochemical, geobotanical and phytomining studies (Dunn, 2007). There is also the use of the technique for mineral exploration, with companies such as Argo Exploration utilising the technique to find IOCG mineralisation (Herbert, 2008). The limited use of this technique within Australia is due to the belief, that there are many other more popular surficial sampling techniques such as calcrete, ferruginous material and soil sampling, and the fact that there is a limited understanding and recognition of the value of biogeochemistry and its potential applications to mineral exploration, particularly for Australian vegetation (Lowrey & Hill, 2006).

Since 2006, there has been a slight increase in the use of biogeochemistry as an exploration tool throughout Australia, and there has been some excellent results yielded for companies including Minatour Exploration Ltd and Dominion Mining Limited. Dominion’s Challenger Gold Mine was sampled using *Maireana sedifolia* with results showing elevated levels of Au at 0.7 ppb (Lintern & Sheard, 1999). The results for Minatour at Tunkillia which is becoming one of the best expressed mineralisation case studies through biogeochemistry are also very impressive, with multiple species being sampled, and *Maireana sedifolia* yielding concentrations of up to 0.9 ppb for Au and 0.44 ppm for Pb (Lintern and Sheard, 1999).

The region of interest is the project Mawson area, approximately 50 km south-west of Whyalla (Figure 1), and from both recent and older work undertaken in the area it is prospective for IOCGU mineralisation. The mineralising zone which was drilled late 2009, is interpreted to be an IOCGU anomaly, and also corresponds with a significant north-south trending structure that runs throughout the study area. The issue at present is the continuation of exploration, where the region is covered extensively by approximately 30 m of transported regolith, such as sheetwash and aeolian sands which inhibit some geochemical exploration techniques (G. Johnson, personal communication, February, 2010). Plant biogeochemistry may be able to overcome the exploration challenge of transported regolith, by using deep rooted species such as western myall (*Acacia papyrocarpa*) and pearl bluebush (*Maireana sedifolia*). It may be possible to identify element anomalies that can be used to narrow down possible regions of mineralisation, therefore improving the chance of finding mineralisation when drilling prospective targets.

### **1.1 Previous Exploration**

The geology of the Middleback Ranges has been extensively studied, but mostly because of the iron-rich Middleback Formation within the metamorphosed sediments of the Hutchinson Group. There has also been some previous iron-oxide copper gold exploration, which is summarised in Table 1, with the more influential work being undertaken by Equinox Resources in 1997 and 1998 and Helix Resources from 1999 to 2001.

The later work by Helix was part of a joint venture with BHP and although there were some interesting results producing geochemical anomalies, the program ended in 2003 because of a dispute over the ownership of mineral rights (Wilson, M 2004). Helix had spent \$1.54 million in identifying two significant mineral occurrences at the Moola Prospect and Princess Prospect (Figure 2). Exploration techniques used by Helix included RC drilling, calcrete sampling, Diamond Drilling, RAB/Aircore Drilling and Ground Electromagnetics (Table 2). Figure 2 shows the location of each program, and Table 3 highlights significant results reported by Helix which will later be correlated with data from this study. Helix's annual report of 2002 (Cairns, 2003) also identifies possible prospective areas within the Princess, Moola and Highway prospects, and has suggested some possible exploration approaches which may be used to constrain these findings, all of which are summarised in Table 4.

Prior to this, Equinox Resources undertook a geochemical survey of the area, identifying multiple anomalies of Cu, Cu-Au, Au, and Cu-Pb-Zn. The majority of these have been associated with areas of Broadview Schist and or major N-S trending structures, of which some are truncated by the Charleston Granite (Parker, 1998). Figure 3 shows the approximate locations of these anomalies, with a majority being defined throughout the very north and south of OneSteel's current tenement. These anomalies along with the Helix data help define targets, and mineralisation occurrences, with perhaps the most valid understanding being that a majority of these anomalies correlate with the major structures running north-south throughout the region.

Current exploration for IOCGU mineralisation which has been led by OneSteel's Exploration Manager Geoff Johnson was announced late November of 2009 (OneSteel, 2010). This is based on interpretation that the tenement holds high potential for IOCGU mineralisation, and that the area has all of the attributes required for mineralisation, discussed in section 1.2. A diamond drill hole on one of the calcrete anomalies identified by Helix has identified the likely source of the calcrete anomaly, showing native copper and also other host minerals and alteration styles (Cave, 2010; Jones, 2010), and throughout 2010 there has been detailed geophysics, aerial photography, and digital elevation modelling also undertaken for the entire region.

## **1.2 IOCGU Background**

There are four main constants that are required and recognized in the major Australian IOCGU deposits:

- There has to be evidence that shows there has been a major thermal event
- There needs to be the presence of trans-crustal sutures which link up to brittle-ductile shears or brittle-ductile faults that were also active during the hydrothermal event; and,
- There also needs to be two fundamentally different fluids which interact to form mineralogical and geochemical variations which relate to IOCG deposits (Skirrow, 2004).

Geophysical tools such as magnetic and gravity data can be very useful for finding this style of deposit but overall can produce a fairly broad signature and in some cases can give incorrect signatures. As mentioned throughout the introduction, exploration for IOCGs has been particularly challenging because of the wide variation of IOCG deposits, alteration styles, styles of formation, poor depth constraints, and the need for a sound understanding of the structures in the area since they are conduits and traps for migrating fluids (Skirrow, 2004), but still, the IOCGU style of deposition has been of interest for a long time and a lot of study has gone into their formation. Skirrow *et al.* (2006) have produced an IOCGU potential map of South Australia (Figure 4), taking into account factors such as; rock units of the Gawler Ranges, faults/shear zones, copper geochemistry, hydrothermal alteration assemblages and zones, and host sequence units considered important in localising IOCG alteration and mineralisation (Skirrow *et al.* 2006). The Project Mawson study area is within the green dashed line of the potential map (Figure 4), which denotes the second highest IOCG potential based on the components listed above. This potential map is supported by the Olympic Cu-Au province (Figure 5), which highlights the major IOCG prospects throughout South Australia and the Gawler Craton, and also highlights two main corridors of IOCG deposits. This study area is shown by the yellow and red star within the more western, Moonta corridor and also within the Olympic Cu-Au province; therefore it is in a highly prospective setting.

## **2.0 STUDY AREA**

### **2.1 Location and Land-use**

The project Mawson area is part of OneSteel's tenement within the Middleback Ranges, which is approximately 50 km south-west of Whyalla, South Australia (Figure 1). The main landuse for the region is mining through the extraction of iron-ore from Iron Baron, Iron Prince, Iron Duke and Iron Duchess which are all located throughout the Middleback Ranges, with the current operational pit being the Iron Duke (Wilson, 1999). Currently the study area is also used for sheep grazing, and some cropping to the east of the ranges.

### **2.2 Geology**

The Palaeo- to Mesoproterozoic rocks of the Middleback Ranges are a part of the eastern Gawler Craton, more specifically they represent the Moonta and Cleve Subdomains which are made up of Palaeoproterozoic metasediments, metavolcanics, and plutonic rocks. These Palaeoproterozoic rocks form what is known as the Hutchinson Group, which has been broken down to form a subgroup of semi-pelitic and chemical sediments known as the Middleback Group which also hosts the massive iron-ore deposits of the Middleback Ranges (Neumann & Fraser, 2007).

The basement to the area and the formations which underlie the Hutchinson Group are not well understood, and there is great controversy as to what the basement of the area is. One belief is that unconformably below the Hutchinson Group is the Miltalie Gneiss dated to  $2003 \pm 18$  Ma (Vassallo & Wilson, 2002) which consists of pink pegmatic segregations within a grey biotite-rich thinly banded granodioritic to tonalitic host (Parker & Fanning, 1998). A second belief is that the Miltalie gneiss is actually unconformably above the Sleaford Complex which is the basement to the area and also a lot of the Eyre Peninsula as seen in Figure 6 (Parker & Fanning, 1998). Aposing this and also the first theory is recent research undertaken by Fraser et al. (2010), who obtained ages of 3150Ma from a granite outcrop located within the project Mawson area. The proposed theory is that the granite represents Meso-archean granite known as the Cooyerdoo Granite, which in the past has been thought to exist in only the Yilgarn and Pilbara Cratons of Western Australia. This information, is the most recent for the area, and seems to put to rest the argument of what the basement of the Middlebacks actually is. Figure 7 shows the proposed interpretation of where the Cooyerdoo granite sits, and given this it is plausible to suggest that the Miltalie Gneiss and Sleaford Complex aren't the basement, and that they lie unconformably above one another and the Cooyerdoo Granite.

The Hutchinson Group itself consists of 8 fining upward sequences (Neumann & Fraser, 2007), and of these, five make up the Middleback group. Sitting stratigraphically and unconformably above the basement is the Warrow Quartzite, which is a massive to flaggy quartzite sequence (Curtis, 2007) which varies in thickness, most-likely due to being deposited in a series of extensional rift basins (Parker & Fanning, 1998). Sitting above this is the Middleback Group; the first two units are believed to represent marine, shallow water to intertidal chemical sediments and are known as the Katunga Dolomite and Lower Middleback Jaspilite. Above this are the Cook Gap Schist, the Upper Middleback Jaspilite, and the Yadnarie Schist which mark the top of the Hutchinson sequence and possibly a transgressive event given the interpretation of the rocks as being deep water clastic sediments (Parker & Fanning, 1998). There are also numerous conformable amphibolites within the Cook Gap Schist, which have a quartz tholeiite composition and are believed to represent mafic volcanic extrusions or mafic sills intruded very early before deformation (Parker et al. 1985)

The top of the Hutchinson Group marks an unconformity at approximately 1820Ma, the same time as the intrusion of the Wertigo Granite ~1760 (Parker & Fanning, 1998). The intrusion of the Myola Volcanics followed approximately 1791 ±4Ma which was accompanied by the Broadview Schist as seen in Figure 8 (Parker & Fanning, 1998). The sequence is now represented by a series of deformed felsic volcanics and fine grained gneisses, in the Middleback it is represented by inter-banded porphyritic rhyolite and rhyodacite, fine-grained felsic and hornblende-bearing gneisses and fine grained amphibolites, due to the volcanics undergoing upper greenschist to lower amphibolite facies metamorphism (Curtis, 2007; Parker & Fanning, 1998). The mineralogy of these rocks has been studied intensely because of their importance with respect to hosting mineralisation (Cave, 2010; Jones, 2010). Within the core obtained from the Moola drill hole there has been sericite and chlorite alteration observed within the rhyodacite, and mineralisation has been observed within large to small veinlets (Cave, 2010; Jones, 2010). The sulphide mineralisation consists of multiple generations of pyrite and chalcopyrite with minor sphalerite, and within the shear zone occurs as secondary copper mineralisation such as malachite and native copper (Cave, 2010; Jones, 2010)

The next major event was the intrusion of the 1740Ma McGregor Volcanics which are massive, dark grey, porphyritic to non porphyritic rhyodacite and rhyolite with minor basalt, dacite with some inter-bedded volcanoclastic grit, which may be associated with the above Moonabie Formation which is made up of grey/purple volcanoclastic grit (Wilson, 2000).



The youngest formation in the sequence is the Mesoproterozoic, Corunna Conglomerate dated at 1585Ma (Curtis, 2007) which caps the sedimentary sequence and consists of pebble to boulder conglomerate with inter-bedded sand and siltstones (Wilson, 2000). Associated with this conglomerate is the Hiltaba suite which intruded at  $1585 \pm 2$ Ma as the Charleston granite, which has recently been identified as a possible source of the potential IOCGU mineralisation (Cave, 2010). The granite itself is a massive, homogeneous, pink, phenocrystic granite with coarse, pink K-feldspar phenocrysts in a medium to coarse-grained quartz–biotite–green plagioclase groundmass (Parker & Fanning, 1998), and it intrudes not only the Corunna Conglomerate but also the McGregor Volcanics and Moonabie formation (Parker & Fanning, 1998).

The youngest intruding volcanics of the area are believed to be the porphyritic rhyolite dykes of the Gawler Range Volcanics (Parker & Fanning, 1998) but there have been no exposures observed within the Whyalla map sheet. However it is believed that the northwest trending rhyolite dykes located just west of Iron Baron are an equivalent to similar dykes of the Gawler Range Volcanics observed near Corunna on the Port Augusta map sheet (Parker & Fanning, 1998). The dykes that have been observed have been defined as massive, pink, porphyritic rhyolite containing abundant K-feldspar and quartz phenocrysts and they occur as dykes which intrude granites to the west of the Middleback Range (Parker & Fanning, 1998).

Above the Corunna Conglomerate which has been intruded by the volcanics discussed above are a variety of Tertiary sediments which are related to deep weathering profiles (Parker & Fanning, 1998). Included in these sediments are massive ferricreted conglomerate talus deposits which contain large concentrations of mineable iron ore and overlie kaolinised basement which may be derived locally from honeycomb veining within nearby ironstone. There is also Silcrete which lines the eastern and western sides of the Middleback Ranges however there is no interpretation of why the silcrete is observed at the same geological and topographical position (Parker & Fanning, 1998).

The Quaternary sediments of interest are the calcareous deposits observed in Figure 9. The two hard calcrete deposits which formed during the middle to late Pleistocene are the Ripon Calcrete and the Bakara Calcrete (Parker & Fanning, 1998) and their importance relates to the current geochemical exploration in the area. The Ripon calcrete is the most consolidated of the calcareous deposits, it is generally observed as hard calcrete sheets, of buff to pink colour, and is often overlying nodular calcrete soil profiles (Parker & Fanning, 1998). The overlying profile in most cases refers to what is known as the Bakara calcrete or the Bakara Soil. The Bakara calcrete is often less consolidated and is

composed of more nodular to biscuity calcrete, and often contains a significant amount of re-worked Ripon calcrete (Parker & Fanning, 1998). The final layer of interest which is also the youngest of the quaternary sediments is the Loveday Soil; it is a soft, powdery, off white to brown calcareous soil and holds some importance with respect to the current IOCGU exploration (Parker & Fanning, 1998).

### 2.3 Geomorphology

The landscape of the Middleback Ranges has been shaped by relatively complex periods of deformation, with the major deformation and manipulation of the landscape occurring between 1850Ma and 1590Ma within the Kimban Orogeny and also 2300Ma when the basement to the area was effected by the Sleaford Orogeny (Parker & Fanning, 1998). Since this period the area has not been majorly disrupted, as the Gawler Craton has not been affected by tectonic forces since approximately 1450Ma (Schwartz et al. 2006). However there was a fourth deformational event believed to be associated with Wartakan deformation, which was responsible for fluid movement along structures. Since this period, neo-tectonics have continued throughout the quaternary, shaping the current landscape.

The formation of the Hutchinson group is believed to relate to a period of marine transgression (Vassallo & Wilson, 2001<sub>2</sub>) where the sea level rose and sediments were deposited in a series of extensional basins prograding from west to east (Figure 10)( Parker & Fanning, 1998). Since deposition the sediments have been heavily deformed, undergoing 3 stages of deformation throughout the Kimban Orogeny, which have been identified throughout the Cleve-Cowell area, and a detailed tectonic history has been summarised (Parker & Fanning, 1998). The most important event with respect to landscape formation is  $KD_3$  or the third recorded deformation of the Kimban Orogeny, because it is believed to be responsible for between 4 and 6 km of uplift, which occurred approximately 1740-1710Ma (Parker & Fanning, 1998). Figure 11 is a schematic describing very simply a possible scenario for how the Middleback Ranges came to be at the surface. Since  $KD_2$ , the second deformation of the Kimban Orogeny deformed the Hutchinson Group, and Myola Volcanics which were at a depth of approximately 20km (Jones, 2010), it is plausible to suggest that deformation occurred at a depth of approximately 20km. Accompanying this was the latter  $KD_3$  event, which reflects the uplift mentioned above, is also associated with the formation of major north-south trending shear zones and mylonite belts in the region, including the Kalinjala shear zone (KSZ) (Parker & Fanning, 1998). These north-south trending structures may represent splay faults from the Kalinjala Zone or may be independent structures; however it is more than likely that the events were initiated throughout the same time period. Following this, there was a period of minor

tectonic influences, accompanied by erosion and exhumation that most-likely led to the uncovering of the Middleback Ranges.

Throughout the region, there are many north-south trending fault scarps which appear to be youthful features (Miles, 1951) associated with the formation of the Pirie Basin, which hosts the Quaternary sediments of the coastal plains (Parker & Fanning, 1998). These structures have shaped the current landscape; causing uplift, exposing tertiary limestones and other underlying bedrock, and also influencing the drainage system throughout the area. The uplift has produced regionally topographic high features with heights of 35m, 20m and 3.5m for the Murninnie scarp, Randell scarp, and Roopena fault respectively (Robert, 2006). These scarps have not only disrupted the Quaternary sediments, and created new drainage systems but also interrupted other drainage systems, with Figure 12 showing how the uplift of the Ash Reef scarp has disrupted the flow path of the paleo channels that it dissected. The age of these scarps has been placed throughout the quaternary with ages of 975,000 years for the Murninnie scarp and 525,000 years for the Randell scarp (Robert, 2006). These are only relative ages calculated from a palaeo-seismicity study along the Roopena fault (Crone et al., 2003), but even so, they do constrain the approximate age of the uplift to the quaternary; and given that the formation of the Pirie Basin and uplift of the Flinders Ranges and Cleve Uplands was around this time (Parker & Fanning, 1998) the suggested ages most-likely represent the correct time period (Robert, 2006) for the events which helped shape the landscape observed today.

The contemporary landscape of the Middleback Ranges consists of low and undulating plains with scattered north south trending elevated regions related to either the quaternary tectonic development (Figure 13) or the older fault splays or faults that have been re-activated by younger neo-tectonics. There is also the effect of the Middleback Range, which is the major control of drainage in the area, with a majority of the drainage running off the eastern side of the range and then draining to the south in the large depression observed in Figure 22. This drainage and the drainage which reflects the younger neo-tectonics both control the flow of sediments and the landscape that is developing today, with drainage systems modifying sediment transport directions and erosion manipulating the topographic features of the area.

## **2.4 Mineralisation**

The host rock for mineralisation is interpreted as the Myola Volcanics which were emplaced within the Hutchinson Group approximately 1791 Ma. The mineralisation is believed to be hosted within veinlets, and the sulphide mineralisation consists of multiple generations of pyrite and chalcopyrite with minor sphalerite (Cave, 2010; Jones, 2010). There is also secondary copper mineralisation, in the form of malachite and native copper which has been observed at the surface; the malachite in the Helix RC workings (Table 3), and the native copper within the drill core located at 703668mE, 6331356mN (GPS co-ordinates AGD 66) and old mine workings along SZ1 identified in figure 76. The mineralisation dominantly has an isotopic signature representing a crustally-derived metal source with minor mantle input, and fits within the generic IOCGU parameters of the Gawler Craton (Cave, 2010; Jones, 2010). The mineralisation has also been identified within the major north-south trending structures.

## **2.5 Regolith**

The surrounding regions of the Middleback Ranges are arid and with the exception of the ranges, have low topographic relief. This dry climate and minimal topography influence the landscape processes, with the dominant regolith units being composed of sheetwash plains, palaeo-drainage systems, and aeolian dunes. Regolith carbonates in the form of calcrete, are mainly exposed on topographically high settings, but are buried by up to 2 m elsewhere. In the lower areas, such as valleys and depressions, alluvial sediments dominate the regolith and carbonates are less obvious but still most-likely exist at greater depth. Therefore when targeting carbonates for exploration it would be advisable to concentrate on the rises and highest points of sheet-wash plains. Overall the dominant transport of alluvial material is eastwards off of the ranges, then south through a prominent drainage system mapped as Aed on the attached regolith-landform map (Figure 19). The ranges are dominantly composed of the Middleback Sub-group, and is a north-south trending structure, which influences the remaining landscape of the study area. Off of the ranges alluvial drainage depressions flow to the east which have formed very distinct fan systems that drain into multiple depressions or sheet-wash plains at the base of the range-front. In contrast, the western side of the ranges is dominated by dune systems which in some areas over-ride the Middleback Group on the range-front.

## 2.6 Climate

The Middleback Range's climate is semi arid to arid and is mostly of Mediterranean type. Temperatures vary depending on the season with average winter maximums of 17.5° C and minimums of 5.7° C, and summers averaging a maximum of 29.2° C and a minimum of 16.9° C often accompanied with weekly periods exceeding 40° C (WeatherZone, 2010). Wind direction and speed varies throughout the region because of the effects of topography, but is generally SSW (WeatherZone, 2010). The sea breeze has an effect on the region all year round, starting off slight in the morning and slowly building a more dominant southerly component throughout the day. The rainfall is only 250 mm per annum which is strongly outweighed by the mean annual evaporation of 2150 mm (WeatherZone, 2010).

## 2.7 Vegetation

Most of the vegetation in the study area has been cleared for agriculture, with scattered regions of a formerly dense mallee scrub remaining throughout sandy regions and along roads (Figure 23) and fence lines (Parker & Fanning, 1998). The vegetation types in the area form dominantly, a chenopod shrub-land; which carries shrubs such as pearl bluebush (*Maireana sedifolia*), bladder saltbush (*Atriplex vesicaria*), and bluebush daisy (*Cratystylis conocephala*), an upper storey characterised by black oak (*Casuarina pauper*), bullock bush (*Alectryon oleifolium*) and western myall (*Acacia papyrocarpa*) (Lange and Sparrow, 1992), and also a sparse forbland with copper burr possibly *Sclerolaena napiformis* and *Sclerolaena diacantha* along with many other exotic species within each storey of vegetation.

The western myall (*Acacia papyrocarpa*) and pearl bluebush (*Maireana sedifolia*) were the two target species for the biogeochemistry program. The western myall (Figure 14) grows greater than 6m tall (Lange and Sparrow, 1992), has a broad canopy and is also believed to have an extensive root system. Figures 15 and 16 show the lateral extent of the roots of this species, and given the ability of the plant to grow to 1000 years old (Facelli and Brock, 2000; AALBG, 2010) in an arid climate, its root system must penetrate to a great depth; similar to that of the river red gum (over tens of metres) (Hulme & Hill, 2005). The plant itself has a shady umbrella like crown, and produces yellow flowers after heavy rainfall. The wood is dark brown, hard and durable and its foliage is needle like and silvery grey in colour (Facelli and Brock, 2000; AALBG, 2010).

Pearl bluebush (*Maireana sedifolia*) has been used for biogeochemical sampling in many other projects including a biogeochemical survey undertaken at Challenger Gold Mine (Lintern and Sheard, 1999). The species observed in Figure 17 is *Maireana sedifolia*, it is a multi-branched shrub which grows to approximately 1.5 m and has a root system which can penetrate over 10 m (Hill et al. 2005) In some cases it has been suggested by core loggers that the root system has been observed at over 20 m depth within the core and it is for this reason along with the fact that it has been documented to penetrate over 10m (Hill et al. 2005) that the plant has been chosen. Another factor which makes this particular species more viable to exploration is its higher tolerance to grazing (H. Facelli, personal communication, June 2, 2010), which makes it more abundant and is therefore easier to sample than species such as *Atriplex vesicaria* which also inhabits the region but is diminished because of overgrazing (H. Facelli, personal communication, June 2, 2010).

### 3.0 METHODS

#### 3.1 Biogeochemistry

##### 3.1.1 TRANSECT SAMPLING

Western myall (*Acacia papyrocarpa*) and pearl bluebush (*Maireana sedifolia*) were the target species for the biogeochemistry sampling program, and there were differences between their sampling approaches. Western myall (*Acacia papyrocarpa*) were used for the first round of transect sampling, at a sample spacing of approximately 500 m, with 5 km north-south spacing's between the east-west orientated transects shown in Figure 18. Transect 1 was slightly different to the others, instead of being an opportunistic sample line, the samples were more orientated around the Moola Drill Hole, hence the scattering of samples within this particular transect. Overall, 81 samples of western myall (*Acacia papyrocarpa*) were taken from the target organ which was the phyllodes, and their location is shown in Figure 18. The second sampling program which targeted the leaves of pearl bluebush (*Maireana sedifolia*), followed the same transects as the western myall (*Acacia papyrocarpa*) but at a lesser spacing, of a still opportunistic 250 m. This approach was used to help narrow down potential anomalies within the western myall (*Acacia papyrocarpa*) data, by sampling in similar locations to the western myall (*Acacia papyrocarpa*) and also between each sample, a representation of the space between each western myall (*Acacia papyrocarpa*) was obtained. Overall 106 bluebush were sampled, and special care was taken to make sure there was a strong overlap between the results of the two species.

The sample technique was identical for each species, firstly the sample location was recorded (GPS coordinates using AGD 66), accompanied with plant and regolith expression descriptions. The leaves/phyllodes were taken from around the canopy of both species of plant, and then stored in unbleached paper bags labelled either WM 001-081 or BB001-106. Storing the samples in these bags not only reduces contamination from the outside environment but also reduces sample sweating, which can be a major problem with more succulent species like *Maireana sedifolia*. The bags are not sealed but instead the tops rolled over several times to allow the samples to still breathe whilst still reducing the possibility of contamination.

The samples are then dried at approximately 60 degrees to remove moisture and reduce the possibility of sample decay. From here the samples are crushed to a fine powder, which can be done prior to being sent using a grinder. For this project, the western myall samples were sent straight to

ACME in Vancouver, Canada, where they were milled and assayed for a specific array of elements (ICP-MS), and the bluebush were milled at Adelaide University and then sent to ACME for analysis (ICP-MS). The results were returned in an Excel spreadsheet and were analysed using programs such as loGas and ArcGIS.

### **3.1.2 CONTAMINATION**

While sampling plant media it is important to consistently minimise contamination, therefore jewellery is removed when sampling and trimming tools are disregarded. The main issues which effect sampling within the Middleback Ranges are dust due to roads, and the age of plant growth which can vary seasonally and may also be affected by the degree of grazing. Dust problems can be overcome by sampling away from main roads and tracks, but even though there are plenty of regions not affected by dust, issues with landowners and the restriction of only travelling on some properties and also along premade tracks meant that the samples were mainly taken along access roads. Even though this had the possibility of introducing errors to the data, the issue was more or less overcome, by taking samples a few hundred metres from tracks and also from trees that were sheltered in thickets.

The other major issue with sampling was plant growth especially when sampling pearl bluebush. This was only an issue along particular transects, and the main reason seemed to be overgrazing. Figure 19 shows the mapped region, and highlights areas where most vegetation has been removed, most-likely due to clearing and overgrazing.

## **3.2 Geochemistry**

### **3.2.1 REGOLITH CARBONATE (CALCRETE) SAMPLING**

The sampling of calcrete was taken along the same transects as the bluebush (Figure 21). The samples were obtained using a variety of techniques dependant on the depth of burial, and strength of the transported material. In most cases a soil auger was used, as the calcrete in the northern region is generally nodular and has a small clast size. There were some regions where the calcrete was shallow and in more tabular sheets, and could therefore be dug up using either a crow bar or grub hoe. The main concern with using these tools is not introducing a source of contamination. Once collected, the calcrete samples were put into labelled soil sample bags (Calcrete NM001-057), and a sample location recorded (GPS coordinates using AGD 66). Prior to the samples being sent to a laboratory, they were split, to allow access to remaining material once results have been returned,



and they were then re-bagged, labelled and sent to Genalysis Laboratories, Perth, WA, where the analysis was undertaken.

### **3.2.2 GEOCHEMICAL SAMPLING OF HELIX DATA**

There were also samples taken along specific co-ordinates which overlap with the data obtained by Helix in 1999. This was done to try and check the accuracy of the previous data, as it is highly possible that in some cases the sampled material may not have been calcrete. The sample locations (Table 5) are in the northern and southern parts of the area, and have been taken at the same location as the Helix data. The sampling technique was identical to the above, and the samples were treated identically to the transect samples, and were also analysed by Genalysis, which were also used by Helix in 1999 (Wilson, 1999).

### **3.3 Regolith-Landform Mapping**

To aid the interpretation of the analytical results, the area has been regolith-landform mapped. The map has been created at a 1:20,000 scale and is highly detailed showing sub-division of alluvial plains, alluvial drainage depressions, sheet wash plains, and variably weathered erosional regions (Figure 22). A lot of the mapping area has been orthophoto interpreted with minor ground survey to identify specific units and to make sure assumptions made during photo interpretation were correct. The geological map has been used to identify exposed bedrock and prominent structures. A detailed topographic map was used to help identify drainage channels. The map was created manually on a clear sheet of film at approximately A1 size and then scanned to create a digital copy. The map was then constructed using an image manipulation program called GIMP, and then it was input into ArcGIS where it was geo-rectified using known locations. The final map contains 26 units which are discussed both in the legend attached as Figure 20 and also in section 4.1 of the results. The map has been used to interpret landscape processes which control the accumulation and dispersion of elements.

### **3.4 Analysis of Results**

The analytical results returned from ACME, have been processed in many programs including: loGas, Excel, ArcGIS, and Statistica. The main issue with the analysis of results is identifying the final suite of elements to be presented and discussed within the constraints of this manuscript. The main elements focussed on are Cu, Au, U, Pb, Zn, Ag, Sn, Y, Ce, La, Al, Fe and Zr. The main outputs from this data are: the dendrogram, scatter plots and line graphs, with the use of normal probability

restricted to determining only the concentration ranges for each element to be used in IoGas or ArcGIS. Throughout 5.2 the relationships between species are discussed, and it is mentioned that it is possible to normalize the data. This has been done for the Cu concentrations of results from proximal myall and bluebush samples; the gradient of the line from Figure 61 was used to establish a constant that could be used to normalize the data. Tables 6 and 7 show the normalized data, for both myall to bluebush and bluebush to myall respectively, with the calculations for the constant being observed in Tables 6 and 7.

## **4.0 RESULTS**

### **4.1 Regolith-Landform Mapping**

The mapping area is dominated by transported material, such as aeolian, sheet-wash and alluvial sediments. Most of the landforms include erosional and depositional plains, channels and drainage depressions. The drainage in the area, which has been controlled by the uplift of the ranges and later neo-tectonics, flows east and west off the hills and then on the eastern side runs into a major depression which drains to the south. The regolith-landform map (Figure 22) includes:

Aeolian Sediments;

Sheet-wash sediments;

Alluvial sediments;

Colluvial Sediments; and,

Weathered Bedrock;

#### **4.1.1 AEOLIAN SEDIMENTS (ISps and ISul)**

The western extent of the mapping area is dominated by aeolian material which forms two main subgroups based on landform; longitudinal dunes (ISul) and sand plains (ISps). Both units consist of well-rounded and well-sorted, red-brown quartz, fine sand. The units are generally bound to the western side of the ranges and in most cases are densely vegetated with bluebush (*Maireana spp.*) and either mallee or myall.

#### **4.1.2 ALLUVIAL SEDIMENTS (Aed, Apd and Afa)**

Alluvial sediments have been transported by water within drainage depressions and depositional plains, corresponding to the lowest parts of the area. There are three alluvial units sub-divided based on landform. Sediments mapped as Aed, are alluvial sediments within drainage depressions, sediments labelled Apd are in depositional plains, and sediments labelled Afa are at the base of moderate to high topographic relief. Aed's generally contain multiple clast lithologies, including; quartz, ironstone, calcrete, granite, maghemite, and conglomerate, and they are generally sub-rounded to sub-angular in shape. Clast sizes are sand and clay, which vary between channels and proximal and distal settings. Apd RLUs have a lower flow rate, and therefore the sediment sizes are decreased, with the most recognisable feature being the existence of dominantly fine, sandy-clay.

Afa units have a distinct fan shape and are generally the coarser of the alluvial sediments. Two different fan systems are identified, correlating to primary and secondary fan development. The primary fans form at the base of topographic relief and are the dominant style of fan and then there are secondary fans which develop as the accommodation space for the primary fans is filled and fans accrete outwards and laterally (Figure 24).

All of these units are well preserved, especially along the eastern side of the Ranges (Figure 84); with the alluvial fan sediments flowing down the hill into the Aed and Apd units depositing finer more reworked sediments. The Apd and Aed units host a diversity of flora as they are the focal point for water, so species such as *Casuarina pauper* and many local grasses and shrubs occupy these units.

#### **4.1.3 SHEETWASH SEDIMENTS (CHep, Cher, CHpd)**

Sheetwash sediments have been transported along a relatively flat land surface by a large volume of water within shallow overland flow. It can be difficult to interpret flow direction, although flow vectors such as the ones in Figure 25 can be identified. There are 3 sheetwash units, which are subdivided by landform expression. The CHpd units have a fine grained sand or clay which contain multiple lithic fragments, such as; quartz, maghemite, calcrete, granite and ironstone, varying in size up to ~15 cm. They occur within low depositional settings, possibly adjacent to Apd or Aed units. The CHep units are in areas with more topographic relief and therefore are eroding sediments. The Cher units are sheetwash erosional rises, which correspond to areas of higher topographic relief.

Morphologically these three units are similar but they do have their distinctions, which are mostly based on grain size. Units of low topographic relief tend to receive fine grained sediments and small lithic fragments; therefore they are dominated by clay and sand. With greater elevation, larger fragments and sediments are mobilised, providing the second distinction between sediments on erosional rises (coarse fragments) and erosional plains (fine fragments). The low topographic relief and the sporadic flora distribution which generally includes species such as western myall (*Acacia papyrocarpa*) and emu bush (*Eremophila spp.*) are the most obvious features which distinguish sheet-wash units. They may also have diagnostic features such as contour banding (Figure 26) and flow paths (Figure 25).

#### **4.1.4 COLLUVIAL SEDIMENTS (Cer)**

Colluvium includes sediments transported predominantly by gravity. This material mostly occurs along significant topographic highs, such as rises and hills. Colluvial sediments are differentiated here by their landform and topographic relief, being found on an erosional rise (Cer), and commonly occurring on the sides of hills around exposed bedrock. They generally include large fragments > 1 m in diameter, with units composed of mostly angular to sub-angular lithic fragments, with minor bedrock outcrop and a regolith composed of mainly medium to coarse grained sands. Vegetation is generally sparse.

#### **4.1.5 PALAEO-DRAINAGE SYSTEMS (Lpd)**

There are many drainage depressions which host ephemeral flow. Most of the Lpd units trend along the western side of the Middleback Ranges, but occur as only pockets surrounded by aeolian sediments. It is possible that these areas, which in some cases still pool water throughout times of intense rainfall, may have been joined and been a part of a much larger drainage depression, much like the one observed today on the eastern side of the ranges. These units occupy areas of low relief and contain fine grained sediments, with lithic fragments ranging from rounded to sub-angular in shape. The unit is generally sparsely vegetated, and dominated by saltbush and bluebush.

#### **4.1.6 EXPOSED BEDROCK (SSel, SSer, SMer, SMep)**

Bedrock throughout the area has been split based on its lithology and landform. The difference between landform refers to the difference in elevation, with units found upon higher elevation being denoted a low hill, and the lower units; rises or plains, depending on the variance of relief. The major interest in these units is their geology, so the major granitic and Hutchinson Group sediments of interest have been split to show their spatial distribution. The sediments have also been classed on their rate of erosion.

### **4.2 Geochemical and Biogeochemical Element Suites**

The following elements have been chosen for detailed assessment, based on their local abundance, expression of mineralisation and previous exploration undertaken within the area. Along with this there has also been an influence from studies undertaken on IOCGU mineralisation within Australia, with elements such as Ce, La, Ag, Mo, W, Bi, Zn, Co, Pb and U typically associated with this mineralisation style (Hitzman & Valenta, 2005). Only a few of these elements have been chosen for focus, as they cover a broad range of IOCGU deposits. The elements which have been chosen have

been split into two different groups, a biogeochemical and geochemical suite. The target elements of each suite can be grouped into 3 sub-sets, which are summarised below.

#### Biogeochemistry

1. Mineralisation commodity elements (Cu, Au, U)
2. Pathfinder elements and mineralisation Accessory elements (Pb, Zn, Ag, Sn, Y, Ce, La)
3. Secondary mineral trace element host elements potentially associated with detrital contamination (Al, Fe, Zr)

#### Geochemistry

1. Mineralisation commodity elements (Cu, Au, U)
2. Pathfinder elements and mineralisation Accessory elements (Pb, Zn, Ag, Sn, Y, Ce, La, Co)
3. Secondary mineral trace element host elements (Al, Fe, Ca, Zr)

The figures discussed throughout the results and discussion section have been created in ArcGIS, Statistica, and Iogas, and the ranges for each element listed in the corresponding legends were determined from normal probability plots (appendix 1). The data presented throughout the Spearman's Matrix has been split into 5 equal groups to help assess the strength of the relationships, and Table 8 describes these divisions. Throughout the text Yttrium is discussed as being a REE, as it behaves the same as a REE and is commonly discussed in this way (Dunn, 2007).

#### **4.2.1 WESTERN MYALL (*Acacia papyrocarpa*) ELEMENT ASSOCIATIONS**

Copper, Au, and U are the main mineralisation commodity elements, with figures 34, 37, and 77 showing their concentration within western myall overlain on the geological and regolith-landform maps of the area.

Throughout the region Cu is generally relatively abundant with the major anomalies being listed in Table 9. These anomalies of up to of 20 ppm, 36 ppm, 33 ppm and 43 ppm also relate to regions previously identified as prospective. One of these elements associated with Cu is Zn and the X-Y scatter plot of Cu and Zn (Figure 27) shows a reasonable correlation. There is also a moderate correlation in the spearman matrix (Table 10), with the line graph of the samples (Figure 28) also demonstrating the high abundance of both elements, especially within samples 3, 13, 17, and 19. Copper also shows a moderate correlation with some of the other target elements, mainly Fe and Ag, with weak relationships between the other main commodity elements.

Gold has only minor anomalies, and produces data striping throughout most of the X-Y scatter plots of the data (Appendix 3), suggesting values approaching analytical detection limits. Relationships between other target elements include a strong relationship between Au and Ag (Figure 29) and a similar relationship between U and Cu, which is also backed up by weak correlations within Table 10. Although these relationships are weak, they are important.

Uranium is recognised as a commodity within an IOCGU system, but varies considerably between different IOCGU systems. Throughout the study area, U levels are considerably low, and therefore drawing a correlation between it and any other target elements is difficult. The X-Y scatter plots for this region observed in Figure 30, exhibit mainly data striping due to low concentrations, however there is a moderate correlation with the host elements: Al, Fe and Zr, (Table 10). This suggests that the low levels of U are a representation of the U which is within the soil minerals.

These host elements; Al, Fe and Zr, represent either contamination of sample by dust if results are high, or if results are low they may be representing the clays and oxides within the soil. Given that the results are low, they are most-likely representing the make-up of the soils. There is a strong correlation between Al and Fe which represents the clays and Fe-oxides within the soil, and there are also associations with Zr and La which suggests these elements are also abundant within clays.

#### **4.2.2 PEARL BLUEBUSH (*Maireana sedifolia*) ELEMENT ASSOCIATIONS**

Pearl bluebush (*Maireana sedifolia*) has similar biogeochemical trends to western myall, but there are some significant differences with respect to both concentration and elemental association. Similar to western myall; Cu, Au, and U concentrations are overlain on the geological and regolith-landform maps of the Middleback Ranges (Figures; 35, 38 and 78). Trends throughout the region correlate with the western myall data, given that sample sites were proximal, and therefore trends discussed are strongly correlated with those in section 4.2.1, however the concentrations do vary and element associations also have their differences

The commodity elements Cu, Au and U show only weak to moderate correlations with one another; however, this is expected given the correlations drawn with the other species sampled. Copper's strongest correlation is with U, and it is evident within both spearman's correlation (Table 11); which identifies a moderate correlation, and also the X-Y scatter plot of the two elements (Figure 31); which shows a broad but very much positive relationship. Copper also has a strong relationship with

Zn which has been identified and discussed throughout section 4.2.1, and this relationship is most-likely portraying the same correlation as that discussed above.

An association which is unique to *Mariana sedifolia* is the relationship between Cu and the target host elements. This association, observed in Figure 32 and within spearman's correlation matrix (Table 11) may represent contamination of samples, however if this is the case, it would be expected that results would be high for Al and Zr. Levels are slightly elevated, mainly along the Kimba Road, but even when these elevated results from transect 3 (Figure 21) are removed, the correlations stay approximately the same, suggesting that the trend is not related to contamination but instead to the species. Another correlation which may be related to the Al and Zr anomalies is the moderate correlation between Cu and the REE, but this association is discussed more thoroughly later in this section.

Gold within pearl bluebush has similar element association to that observed within the western myall data, only there are less observable relationships. The best relationship for Au is its weak association with Ag observed within Figure 32, which is followed by a very weak correlation within the spearman's matrix (Table 11), and the X-Y scatter plot of the 2 elements (Figure 34). There is also a weak relationship in spearman's data for Zn, but this is not represented in any of the other figures or tables used to demonstrate the element associations.

Uranium is another element which follows similar trends to the western myall data, only the associations observed are a lot stronger than those previously identified. Throughout the study area U levels are considerably low, with many below detection limit, and therefore drawing a correlation between it and any other target elements is difficult. The X-Y scatter plots in Figure 33 follow the same trend as *Maireana sedifolia*, exhibiting mainly data striping due to the low concentrations. A strong correlation is shown in the dendrogram (Figure 32), with a strong correlation between U and Fe, as discussed in section 4.2.1, and also U with the host elements and REE.

This REE association occurs with not only Fe but also U, Pb, Zn and Sn, and may be related to the elevated Zr and Al levels within the bluebush and calcrete data. All sampling media show the strong relationship between the REE and, Al & Zr, and this has been discussed further in section 5.5. The possibilities include: that the elements may be concentrated by lichens and mosses growing in calcrete and they are enriching the calcrete results, the regolith may be enriched in the elements because of the associated landforms, or the samples may be contaminated with dust.



Also important to this study is the association between relationships observed in previous exploration and relationships observed throughout this study. The main anomalies of interest are discussed later, however, the relationships that Zn has with many other elements for both species is noteworthy. Zinc has moderate to strong relationships with Pb, Cu, Au and Sn, and its correlation with the commodity elements is interesting. Where and why these anomalies occur is addressed in sections 5.5, but there is a strong association between the commodities and Zn and it may be used as a pathfinder to identify mineralisation.

#### **4.2.3 CALCRETE ELEMENT ASSOCIATIONS**

Geochemistry is one of the most used exploration tools, and often identifies approximate mineralisation when aspects such as residence and dispersion are taken into account. Throughout the study area calcrete has a patchy distribution, which is discussed further in section 5.4.1; however, it still hosts significant geochemical anomalies. Given the possible problems with the quality of previous data as discussed in section 5.4.2, one of the most important elements to consider for a calcrete study is Ca. Figure 35, demonstrates the close relationship that Ca has with commodity elements Au and Cu, which demonstrates that the results should be significant. Another interesting correlation is the negative correlation between Ca and Fe. This is observed in Table 12, and Figure 36, with the line graph of the two elements showing high Fe corresponding to low Ca.

Gold is the commodity which is normally associated with geochemical exploration, and mostly has a strong relationship with Ca. This has already been demonstrated above, however, Au also has a close relationship with Cu (Figure 35 and Table 12), and also within the X-Y scatter plot of the two elements. Cobalt is weakly correlated with Au (Table 12), however it is not the direct correlation which is important. Often Co can occur as a spatial halo for Au, giving high values around the Au anomalies (Dunn, 2007), and this is the case for these samples.

Copper is the most important commodity in this system and correlates with not only Au but also Zn and Co. The correlation with Zn is shown within Table 12 where it is identified as a very weak association. Copper also has a weak relationship similar to the relationship between Au and Co, but given that there are no other spatial associations for these elements it can be dismissed. Copper has also been known to have associations with U, but for calcrete this has been dismissed as have other U relationships, because of its very low abundance.

Zinc is abundant in the area and its biogeochemical relationships in the area also occur in the calcrete data. A major correlation is with Pb, where it has a strong correlation within spearman's data (Table 12) and Figure 35, and also shows a linear resemblance on the X-Y scatter plot (Figure 37). There is also a strong relationship with Cu which has been discussed, and also strong relationships with Co and Fe identified using multiple techniques (Figure 37 and Table 12).

Aluminium has multiple correlations, and most-likely represents elements that are found within the soil, resulting in elements such as La, Y, Zr, and Fe having strong relationships. There are also relationships drawn with Co, Sn and Zn, and all can be identified in spearman's matrix (Table 12) and the X-Y scatter plots for Al (Figure 38). A negative correlation occurs with Ca, indicating that high levels of calcium equate to a good quality calcrete sample, as opposed to the low Ca and high Al. Zr also shares this correlation with calcium, with high levels of Ca relating to low levels of Zr and vice-versa.

There are a further 19 samples which have been taken from the within the tenement boundaries. These samples have been taken as an overlap from data collected by Helix, with a simple correlation of results being used to check how consistent the data is. Some samples correlate well with others, but there are some differences, discussed further in section 5.4.2. Unfortunately Ca cannot be compared because it is not included in the Helix analytical suite, however relationships can be drawn for elements such as Au, As, Cu, Ni, Pb, and Zn. Copper is one of the most important elements, and overall samples seem to correspond well with the Helix data (appendix 4). Trends are the same with peaks in the data corresponding well for both media, but the concentrations vary for each, some being higher in the Helix data and some higher within the current data. Zinc and Ni also show this correlation, with concentrations ranging, but trends being similar (Appendix 4). An association which is interesting and may be used to fit some sort of significance to the helix data is the concentration of Ca within the new data with Cu levels in both sets of data. If high Cu concentrations are observed for the new data and also high Ca values, but low Cu concentrations in the old data, it may be that the old data does not represent a calcrete sample; however this type of association is discussed in more depth within section 5.4.2, as mentioned above.

#### 4.2.4 SPATIAL ASSOCIATION OF ELEMENT ANOMALIES

Copper has been recognised throughout the region, and is the most anomalous of all the commodity elements. A majority of the high concentrations of Cu are observed scattered throughout the region, but the two species show very similar spatial distributions (Figures 39 and 40), with the scattering reflecting the distribution of the main structural features running through the region. There is also a slight correlation with the Myola Volcanics near the Myola (Figures 39 and 40) and Moola prospects, which is accompanied by undifferentiated granite. A majority of the anomalies are within either alluvial or depositional units (Figures 39 and 40), but still relate to underlying structures, as transect 3 has an anomaly near the top of a drainage depression but the signature does not extend downstream, and is therefore more-likely a representation of the material under the regolith cover.

Gold shows only a few anomalous readings, but there are still some observable associations. The calcrete data best shows lithological relationships (Figure 41), with two of the larger sample peaks occurring within the Broadview Schist, which is surrounded by Myola Volcanics. Along with the lithological associations there are also strong structural controls similar to Cu, only the anomalous values are limited to certain structures (Figures 42 and 43). Transect 3 has an arbitrary anomaly at the foot of the ranges, within alluvial sediments (Figures 42 and 43), and may link with an unmapped structure, or could be a representation of the material eroded from the ranges.

Uranium has some associations with Cu and Au, with anomalies corresponding to the same regions, however, the concentrations of U are low; however given its association with the commodity elements it is important.

Aluminium and Zr follow similar relationships and spatial patterns, as they are mostly an indicator of dust contamination (Figures 44 and 45). Given the association with contamination and their low bioavailability (Dunn, 2007), it is unlikely that the results for these elements reflects the underlying geology (Figures 44 and 45). The strongest spatial association for Al and Zr is within bluebush and calcrete samples taken along the Kimba Road which may be a representation of dust contamination (Figures 45 and 46). Western myall is fairly low in both Al and Zr, with the few values above detection limit correlating with mostly alluvial sediments (Figure 44).

Lead, Ag and Zn, are common elements throughout the area, and their main anomalies correlate with one another and also have relationships with commodity elements. The spatial distribution of these elements is most-likely related to the north-south trending structures throughout the area. Lead follows this trend, with anomalous values along known structures that are abundant in Cu

and/or Au, but also has anomalous values along the Kimba Road which may be related to contamination (Figures 47 and 48). Silver is the same as Pb, with high values in all three species at the western end of transect 3 (Figures 49, 50 and 51). Zinc is more abundant in the area, as most values seem to be anomalous; however, there is still a strong structural association.

The rare earth elements (REE) are mostly uniform over the area, with the only major values along the Kimba Road. Myall show few anomalous values, but bluebush and calcrete both have a strong association with the Kimba Road sites (Figures 52 and 53). The anomalous values throughout the area are low, but the association with the samples taken along the road needs to be further considered, as it corresponds with a major N-S structure but could also be from detrital contamination.

## 5. DISCUSSION

### 5.1 Landscape Evolution Model

The landscape of the study area has undergone complex changes. Prior to the Tertiary, after deposition of the Hutchinson Group, there was a large period of deformation and weathering of bedrock, which created much of the transported regolith.

To the east of the mapping area are Tertiary limestones, which may represent the Melton Limestone or an equivalent. It is possible that there are Tertiary to Quaternary limestones within the project area that are related to a marine transgression. A companion study to the south of the area (Mitchell, 2010) has found evidence for weathered limestone (Melton Limestone) associated with a marine transgression within a large embayment (Mawson Embayment) between the Middleback and Moonabie ranges. The main observation which indicates a palaeo-embayment is the calcareous rock observed throughout the centre of the Mawson area, which has a morphology (Figure 54) and chemical composition suggesting it is a marine limestone. Figure 55 shows the concentration of copper and gold observed throughout the Equinox calcrete data, and there seems to be a strong spatial relationship for the commodity element concentrations. Samples in the north and south exhibit strong geochemical anomalies but the middle area which is topographically lower seems to host low trace metal concentrations. Along with this odd trend in the results, is also a difference in morphology, to the north and south the calcrete seems to be nodular and has a distinct horizon within the soil (Figure 56), and in the centre of the Mawson area within Mitchell's study area, the calcrete or marine limestone occurs as massive tabular sheets (Figure 57). This is a very similar scenario to that occurring on the Yorke Peninsula near the newly found Hillside deposit where the calcrete also seems to have two sub-populations (Dietman, 2009). The belief being that one population is a marine sourced, weathered limestone and the other is terrestrial based pedogenic carbonate, which seems to be an equivalent to that seen in this study area.

Throughout the marine transgression within the Mawson embayment, it is possible that the Moonabie Ranges and surrounding topographically high points were small islands, and this correlates well, because the topographically high points throughout these regions have no large tabular sheets, only nodular calcrete which most-likely formed at a later period. Following the marine transgression was a marine regression, which would have resulted in a large drainage depression running from the northern end of the ranges through to the south observed in Figure 22. Remnants of this relates strongly to ferruginous mottled weathered bedrock flanking silicified palaeo-sediment (probably

alluvial), and also the distribution of maghemite, along with the swampy depressions throughout the area that may also represent palaeo-drainage remnants. In the central-north of the mapping area are scattered silcrete occurrences (Figure 58) along a N-S trend (Figure 59), which all seem to be at a similar elevation and contain rounded quartzose clasts. Along with this, there is also ferruginous mottled weathered bedrock observed at 706338mE 6339923mN (GPS co-ordinates, AGD 66), which flank one of the large silcrete outcrops. Figure 60 demonstrates the formation of both the silcretes and the mottled zone during the regression period, highlighting how they formed together. Another piece of evidence which suggests there was a large north-south trending drainage depression is the association with rounded maghemite. To the north, near the mottled zone, sub-angular to angular maghemite was distributed throughout current drainage depressions, but to the south, east of Ash Hall; polished rounded maghemite is associated with the silcrete occurrences. This suggests that there has been transport in a north to south direction, and it is most-likely correlated with the regression event and/or transgression event within an embayment to the south.

The change from transgression/ embayment to regression period most-likely left behind alluvial sands, which also formed large strand plains. However, none of these are observed today, so after this period it is likely that the aeolian and sheet-flow processes have reworked the sands into the dunes observed throughout the area today (Figure 59). Throughout this re-working period, the limestone would've also undergone weathering to form some of the calcrete observed today. Following this, continual re-working and formation of calcrete are continued, and on-going neo-tectonics have shaped the current landscape and influenced the colluvial sediments and alluvial fans observed along the range-front.

## **5.2 Relationships between species**

Many studies have targeted the differences of element uptake between particular species and also the differences between different genera and the results differ on both accounts. Some species relate very closely to other similar species, yet some can vary, and when looking at genera the differences can be even bigger. Ideally a biogeochemistry program should target only one plant species (Dunn, 2007) but since this study uses 2 very different species from different genera, comparisons of the two need to be made.

Both species express buried mineralisation along major north-south trending structures, which is a good indication that the technique is effective in both cases. The difference is in the concentrations

for these expressions, and also the type of elements being up-taken. The main elements of interest are the commodity elements, and since there has been minimal U detected, the elements which are best associated with mineralisation are Cu and Au and they have therefore been correlated with one another. Two methods have been used to describe the relationships between Cu and Au for the two species; X-Y scatter plots, and simple 'location vs. concentration' graphs. The more influential of these two elements is Cu because it has been identified more times throughout the survey and therefore there is a large data set to analyse. Figure 61, the X-Y scatter plot of the Cu concentrations shows an approximate straight line relationship, indicating a strong correlation between the species, and Figure 62 also shows this relationship.

Western myall has a higher concentration of Cu than pearl bluebush when compared from the same or adjacent locations. This difference may be an effect of many phenomena, including; depth of root penetration, sample location (results may represent one small quartz vein being accessed by only one of the two species), plant morphology, and time of year of sampling. All of these are plausible suggestions, but to better understand why this association occurs, a detailed study of the two species needs to be undertaken.

Gold results are different to Cu, with Figure 63 indicating that there is a negative correlation between the two species, which is supported by Figure 64, however these figures do indicate that both species express mineralisation, only at different locations. An explanation for this may be the difference in morphology of each species, specifically depth of root penetration; plants maybe accessing different depths within the soil profile and picking up varying signatures. A study undertaken by Jose Facelli, University of Adelaide which is yet to be published (H. Facelli, personal communication, June 2, 2010) concluded that some pearl bluebush in the Middleback Ranges have root systems which penetrate to only a very shallow depth. This may be the reason why there are differences between species; the bluebush maybe sampling shallower, perhaps sampling the calcrete which has been known to concentrate gold, whereas the myall may be sampling medium which is deeper, less weathered and therefore more enriched in commodity elements. On the other hand, the study undertaken by Facelli (H. Facelli, personal communication, June 2, 2010) may have been limited in locating the tap root of the species. Figure 65 highlights the implications of Facelli's study, where it shows how a tap root could be easily identified as a lateral root, and disregarded.

Another suggestion for the difference of results is the time of year each sampling media was collected. Many studies have been undertaken to try and narrow down the understanding of variation of concentration for a particular species throughout the year (Dunn, 2007). Many species

have been studied, and each show varying results between each species and also between each element within each species when sampling living tissue (Dunn, 2007). Therefore it is advised to keep sampling to a specific period throughout the year, but given that this is a one year study, infill using a different species could not be undertaken at the same time a year later, so therefore the difference in results may be a representation of the differences between sampling times. There are many reasons why the time of year can affect the species, but the most significant may be growth rate of foliage. This is well understood for western myall, the species is believed to have cyclic growth, with maximum and most growth between November and February (Ireland, 1997). This is an important factor, as growth rates affect the concentration of target elements (Dunn, 2007), and therefore sampling periods should be kept to a minimum and if re-sampling is needed the effects of growth, have to be taken into consideration.

Another attribute which needs to be assessed is the difference in elemental uptake for each plant, and there has already been many studies undertaken regarding this. Unfortunately western myall are poorly understood with respect to their biogeochemical expression of mineralisation and elemental uptake. However the difference between species and the expression of certain elements has been demonstrated throughout the results, particularly through Sn concentrations. Tables 13 and 14 show the concentrations of Sn in each species, and there is a major difference, with myall expressing levels mostly below detection limit and bluebush showing results up to 6 times the detection limit. This is most-likely a morphological difference between the species, but to better understand the relationships between other species and actual % of variation for each element, a more detailed study is needed.

Along with this there is also the inconsistency observed for Au within biogeochemistry which makes it hard to correlate the two species. Dunn (2007) advises great caution with respect to the interpretation of low levels of Au in vegetation due to the 'nugget' effect; which relates to sampling media which demonstrates extremely higher values than the actual concentration of the overall sample. Dunn (2007) also advises that it is important to be very suspicious of single point Au anomalies given the 'nugget' effect, and generally poor reproducibility, especially in circumstances when no path-finder elements are observed. This is the case for the Mawson data, but there are factors such as structural controls which have been discussed in section 5.5 that indicate the results observed are correct representations.

Given the multiple anomalies observed for Cu and that it is the commodity of interest, the correlation between the 2 species for it is the most important. Given the positive correlation



discussed above for the 2 species, it is possible to assign a value to the data which will normalize the data so the entire dataset can be viewed at once, offering a better representation of the data. The method used to produce the constant which normalizes the data is discussed in section 3.4, and the normalized data can be observed in Tables 6 and 7. However, this is only an estimate, and it is more of an aid to gain perspective over the entire data-set.

### **5.3 Relationships between Biogeochemistry and Geochemistry**

Another important relationship is the difference between the biochemistry and geochemistry results. Once again the commodity elements will be used to discuss these correlations, focusing mainly on Cu and Au.

Western myall and calcrete have been sampled proximal to one another at 9 sample locations, and these samples are shown in Table 15. To test the similarity between the two exploration techniques, these samples have been graphed in Figures 66 and 67, and X-Y scatter plots of the two have also been used to demonstrate the relationships between the key elements (Figures 68 and 69).

Unfortunately Au concentrations at these sample points are generally low, limiting the ability to identify a significant relationship, but there is some spatial relationships observed for both which are discussed later in section 5.5. Copper shows some correlation within the last 5 samples, but a poor correlation for the first 4 samples. This correlation is also shown in Figure 70 which shows the spatial relationships between western myall and calcrete, there is no spatial relationship but there does seem to be a strong structural control.

Pearl bluebush and calcrete were sampled adjacent to one another and therefore the samples are mostly proximal. Due to the increased sample size, a more accurate correlation can be calculated for the bluebush- calcrete association, but it seems this had little effect on the outcome. Gold, once again shows a patchy correlation, most-likely a representation of the patchy Au anomalism. The scatter plot of the data (Figure 69) shows a negative correlation, but this is influenced by the higher samples recorded in calcrete, if this data were removed the correlation would be higher. The scatter plot shows a very poor relationship and this may be a result of the 'nugget' effect (Dunn, 2007).

Copper, shows a similar relationship to Au, with a negative correlation in the scatter plot (Figure 68), but there is some correlation when observing the line graph of the two sets of data (Figure 71). At locations; 9, 10, 17, 18, 19, 29, 35, 36 and 37 there are moderate relationships, with both sampling media showing a similar trend. This indicates a relationship between the calcrete and bluebush, which is also backed up by Zn concentrations through the area. Since Zn is so abundant, a correlation

between the bluebush and calcrete Zn concentrations has been used to check the Cu relationship, and both the scatter plot (Figure 72) and line graph (Figure 73) of the Zn data show that there is a relationship between bluebush and calcrete data.

The two biogeochemistry sampling media have their differences and also have their own differences with the geochemical data. One possibility which could explain the variation of the relationships between each species and calcrete, is the time of sampling, given that there is a stronger relationship with bluebush and these two sampling medium were taken at the same time of year. It is known that calcrete can function differently, depending on aspects such as rainfall (Tyler, 2004) because of microbial activity and its effects on calcrete composition (Tyler, 2004). Time of sampling may be the variable which causes this change but instead of the differences in calcrete, it may also be the factor causing the differences between species. Many studies have been undertaken trying to understand the differences in sampling plant tissue throughout different times of the year, and this has been discussed throughout section 5.4.1, and given that the two species were sampled at different times, this may represent why the relationships between each species and calcrete may occur. A final explanation for the differences observed may be different degrees of proximity, where the samples of bluebush were taken at the same location (GPS; AGD 66, Zone 53), whereas western myall were only proximal with an average variation of approximately 50 m for the closely selected species (Table 15) or with the two outliers removed, an average of approximately 10 m.

There seems to be some relationships between the biogeochemistry and geochemistry, but there are also some differences between each plant species which add another dimension of variation to the plant to calcrete correlation. Even though each technique exhibits different concentrations, it is important to note that each technique is still expressing buried mineralisation. This conclusion can be made because most sample anomalies from current data and data obtained from Equinox Resources and Helix Resources (Cairns, 2003; Parker, 1998; Wilson, 1999; Wilson, 2000; Wilson, 2004) are correlated with the major structures in the area identified on the Whyalla 250k map sheet (Figure 59). It is also possible that the anomalies which are scattered throughout the area also align with structures that have not been identified, and may soon be proven from interpretation of further gravity and magnetic surveys. The differences which are observed may relate to many variables which have been discussed throughout, and it may be that all techniques need to be utilised to correctly represent mineralisation due to the many factors which affect each exploration tool.

#### **5.4 Significance of Data**

Quality analysis and Quality checks have been performed throughout three main stages of this program, to ensure that errors from factors such as sample contamination and laboratory analysis are kept to a minimum. Sampling can introduce some major contamination, so; hands were kept clean, jewellery was removed, sampling was contained to thickets where samples weren't as prone to dust contamination, and samples from individuals were taken from around the crown of the tree to reduce chances of the 'nugget effect'. The true values of the laboratory were also tested by adding in duplicates of random samples, and Tables 16, 17, and 18 show the average standard error for each element within each sampling medium. Along with this there were also standards and blanks analysed by the laboratory, which forms the third stage of QA/QC. Pulp duplicates were analysed, to test the repeatability of individual samples, standard solutions were used to test the precision and accuracy of the laboratories analysis, and also blanks were used to test if the equipment or analytical technique is producing and cross contamination.

The results from the errors analysis (Tables 16, 17, 18) indicate that the V14 samples and duplicates produced by ACME are slightly more precise than the blind duplicates added, unknown to the laboratory. Therefore there may be errors within the data produced by the laboratory, but these errors are only a minor issue, because the anomalous values within the data are very high, and are therefore only slightly affected by the calculated errors.

##### **5.4.1 CURRENT DATA**

In most biogeochemical sampling programs a significant check to test the confidence of the data is to assess the rare earth elements within the data. A data set which correctly identifies elemental abundance and one which has minimal errors should have REE concentrations which aren't necessarily the same but which follow the same trends. Figure 74 shows the concentrations of Y, Ce and La on the y axis and the sample numbers on the X axis for pearl bluebush. The graph depicts the very strong relationship between the rare earth elements, and the same trend is observed for western myall (Figure 75.).

For the geochemical data, a filter has been added, and Table 19 shows the level of certainty of results for each calcrete sample. This has also been proved by (McQueen et al., 1999) with the belief that higher Ca concentrations are better able to host higher Au concentrations in mineralised settings. The breaks calculated for the spatial association maps of Ca represent 5 concentration groups; with the two lowest groups representing samples which contain less than 10% Ca. The

scatter plot of Ca and Au show that at lower concentrations of Ca, Au is less abundant. The cause of this relationship is most likely due to a poorly constrained (and therefore inconsistent) sampling method. Given the rather complex landscape evolution of the area it is possible that some of the more barren results with lower commodity element concentrations may represent sampling media which isn't nodular calcrete. In some cases, in the field there were sites where ironstone was being cemented in a calcareous layer making it look like calcrete, and it is possible that some of this may have been sent to the labs for analysis. As observed in Figure 36, this is most-likely the case, as some of the samples which contain very minimal Ca percentages, also contain very high Fe levels compared to the rest of the samples.

Another possibility is that the sampling media collected may only represent a calcareous horizon instead of nodular calcrete. It was noted at some sample locations that the sample was not nodular calcrete, and therefore it would be expected that the Al (clay) and Zr (sand) concentrations at these sites would be significantly higher. Figure 46 demonstrated this, at sites where Zr and Al are elevated the sample has a low Ca percentage, and it is likely that instead of the nodular calcrete a calcareous layer was sampled, possibly the Loveday soil discussed in section 2.2. The effect of this seems to be negligible, as commodity and other target elements vary in concentration throughout these results, but if used, these results should be treated with great caution, as they may not be representing underlying mineralisation.

#### **5.4.2 HELIX DATA**

As previously discussed OneSteel have a significant amount of data available to help aid current exploration, but there is a major issue with using some of this data because it is not well documented as to how the data were obtained especially with respect to the calcrete data. The data which was obtained around 10 years ago appears to have been poorly constrained because only part of the region has available calcrete for sampling, but the Helix calcrete surveyors were able to obtain a sample at every gridded site (even where calcrete could not be found upon return visits during this study).

From the data shown in Table 20, some of the new data correlates well with respect to the older data (appendix 4). Even though some samples follow a similar linear trend to others, there are still significant differences with respect the concentrations observed. This may have been due to an analytical error; however it is more likely a result of poor sampling technique. If incorrect media has

been sampled or if the calcrete taken was only a calcareous layer as opposed to more nodular calcrete, there may be variation in the results obtained between surveys.

To add to this, there are also samples which show very little linear correlation (appendix 4), which can be explained by similar means to that previously discussed, however from field observations it is plausible to suggest that the incorrect media has been sampled. This was especially important at 703177mE, 6334505mN (GPS co-ordinates AGD 66) where workings from the Helix program were located, and instead of a small sample of calcrete at the surface, there was a pile of crushed up quartz and granite chips (Figure 85). This particular site was then re-sampled correctly auguring to a deeper depth, however the material obtained had a different morphology to the rest of the calcrete taken from the northern area. The two sets of results are displayed in Table 20 and depict a strong relationship; leading to the belief once again that sampling techniques used to obtain the old data were poor.

A simple test to check the validity of the calcrete samples would be to check Ca %, which should indicate whether calcrete has been sampled. Unfortunately the data obtained in 2000 (Wilson, 2000) has a poor array of results and in some cases Ca % have not been recorded. This is the case for the locations sampled, so it is not possible to check the Ca %, but the current Ca % along with the target elements show some indications of whether calcrete has been correctly sampled at each site. This is particularly evident for sample 17 (703177mE, 6334505mN), Table 20 shows that Ca levels are extremely low in the new data, but the trends between both data sets (current data and Helix data) are similar (Appendix 4.17). This indicates that the material tested in both cases gives the same signature, and the sampling media is not likely to be Calcrete given the low Ca %, and therefore this particular data point should be disregarded. Data points with low Ca % also returned low values of Cu and in some cases elevated levels of Fe, this is a common association, and may relate to similar findings within the rest of the data discussed above (section 5.4.1). It is possible that the material sampled was only carbonate coated Iron-stone, and therefore has very little concentrations of the commodity elements, and instead has elevated Fe %. Therefore samples with a low Ca % and/or high Fe % should be treated with caution.

### **5.5 Models for Target Element Dispersion and Residence**

Throughout the area 3 main controls need to be considered in association with the identified anomalies, including: lithology, landscape and structure. All of these factors are extremely important and play roles in dispersing and concentrating elements and therefore understanding these

associations will help better understand the biogeochemical and geochemical signature of this deposit.

The area as discussed has been highly deformed, leaving many fault/shear structures throughout the mapping area (Parker & Fanning, 1998) which have so far been the focus for exploration, with the only Diamond drill hole ( Moola Drill hole) being focused along a north-south trending structure (Figure 76). The main structure, drilled late 2009 will be referred to as SZ1, it is the largest of the multiple fault system, and throughout sections has outcropping quartz. Figure 76 shows the geology of interest for this project, and SZ1 is marked on this figure, along with the other major structures discussed.

Copper has more spatial associations than all other target elements, and this is perhaps the most important association given that it is the element of interest. Figures 39 and 40 show the distribution of Cu over the study area and its strong structural association is made obvious by the structures of interest being highlighted. SZ1 has the most anomalies along its length, with peaks being observed in transect 1 and 2 for both plant species, and along transect 2 within the calcrete data (Figure 77). SZ2 is only anomalous in the plant samples and has been picked up along both transect 1 and 2, and SZ3 is a structure which stands out very well on the surface, and in air photo, and also has anomalous values being detected in both western myall and pearl bluebush. Two interesting associations are the anomalies along SZ4 and SZ5 observed in the bluebush (Figure 39) and calcrete data (Figure 77) respectively. The calcrete hosts an extremely high value, over 100 ppm, which isn't represented in the other media, and the anomaly along SZ4 is also not represented in other data.

Along with this strong structural control, there are associations with other factors such as, regolith and lithology which can account for the accumulation of target elements. Transect 5 for the western myall data shows elevated results for Cu along two separate structures, but there are also high results not correlated with any structures or lithology (Figure 39). The most-likely explanation for this is the association shown in Figure 39, with all samples being in either an alluvial or depositional setting. There is also another drainage depression which is un-mappable due to size, and it along with the depositional landform, may be accumulating Cu from the eastern and western end structures, causing enrichment along this particular transect. Another regolith-landform association is that shown in Figure 77, along transect 3. The highest anomaly along this transect which has a reading in excess of 100 ppm Cu, isn't directly related to a structure, but can be related to the structure only a few 100 metres to the west. Along with this there is also a slightly decreased anomaly downstream of the 100 ppm sample and it is likely that the signature expressed

downstream is a representation of the higher sample upstream. This association is also made a third time, with the plant samples expressing anomalous values further downstream. It may be that the geological mapping is in need of further refinement and the highest reading may represent a structure, but the effect of drainage can still be observed with the reduced signature being expressed in the creek.

The main association for Gold throughout the area is with the major structural features, with very similar associations to Cu being observed. SZ2 hosts one of the most significant Au anomalies, with anomalous values being detected along transect 1 (Figure 42) and transect 2 (Figure 43). These anomalies which link in with the structure are also surrounded by the Myola Volcanics and undifferentiated volcanics, which is encouraging given that these are believed to host mineralisation. There is also an association with the Broadview Schist, which is surrounded by Myola Volcanics (Figure 41). The eastern and western ends of transect 3 have strong results but neither lay on a fault and instead lie within alluvial settings (Figure 43). The sediments to the west are the more interesting of the two, and more than likely represent the material in the side of the hills, but more testing is needed to check the significance of this assumption. The anomaly to the east, observed in Figure 41, is another anomaly related to alluvial sediments, and it is associated with the same alluvial system as the sample that retained 100 ppm Cu and it is likely that Au is showing the same association as the Cu anomaly.

Uranium has been recognised in some IOCGU systems, but the concentration of it can vary considerably; with Prominent Hill, a large IOCG, having minimal U (Skirrow et al. 2007), and Olympic Dam, also an IOCG, being a world class U deposit (Skirrow et al. 2007). Throughout the results, concentrations of U are very low but there does seem to be some trends with Cu and Au's spatial distributions, with anomalies corresponding to the same regions. This is a well documented relationship, if there is Cu and Au with traces of U it is very likely that the biogeochemical signature being observed represents an enriched underlying rock, possibly mineralisation (Dunn, 2007). This is the main association that should be taken from Uranium, as its levels are too low to be significant for further U exploration, but it can be used as a pathfinder to check if the Cu and/or Au levels being portrayed are representative of something prospective, an error, or another issue such as the 'nugget' effect.

Aluminium and Zr have been identified as the elements which can indicate possible sources of contamination, or even incorrect sampling methods, therefore the main observation of interest is whether high values correspond to contamination, or to regions where Al and Zr are concentrated

such as alluvial channels or palaeo-surfaces. Overall the results are minimal for the entire region; with the exception of transect 2 which adjacent to the Kimba Road. This strong relationship is possibly related to airborne contamination, given that most plants do not typically take up large amounts of Al and Zr (Dunn, 2007) and that dust is being stirred up by passing traffic. The anomalous values however are only observed within the bluebush, but this is expected given the hairy surface morphology of the leaves which can capture dust.

Another possibility for these readings is that the plants are taking up these elements, which is very possible given that the results obtained are within alluvial and depositional plains (Figure 78), which field observations were also noted as being more clay and sand rich than surrounding regolith units. It is also possible that the rock types in the area account for the accumulation of Al in the soil, because it is known that the breakdown of feldspars in areas such as zones of alteration, can account for a higher than normal concentration of Al in foliage (Dunn, 2007), and given the close proximity of feldspar bearing granites, this is a possibility.

Since the deeper rooted species only show low readings for Al and Zr it is possible that the shallow rooted species are sampling the clay and sand rich profile instead of penetrating through this material. The calcrete results for this region were also higher in Al and Zr than surrounding regions (Figure 46), and since a majority of the samples were augured it cannot be that the samples were contaminated by airborne dust. The explanation for this is that the calcrete samples that were collected, were taken from soil profiles that are changing so quickly that the calcareous material is not able to form nodular calcrete; and instead form only calcareous horizons that are richer in clay and sand, and therefore the assay results have a higher abundance of elements associated with clay and sand. This association was noted when sampling the material, with most samples taken along the Kimba road being a mix of calcareous material and red, brown, fine sands and clays, possibly a representation of the Loveday soil.

Given the above, it is plausible to suggest that the best explanation for the elevated Al and Zr levels along transect 2 reflect both contamination and the effects of clay and sand rich soils, however the most important factor is the effect these levels have had on results. In this case the elevated levels seem to have had no major effect, as the anomalies along transect 2 contain some of the most spectacular results in the region, and are still expressing structural zones which have a very high possibility of hosting mineralisation. Therefore these higher Al and Zr results do not affect the results directly as targets for further exploration are still produced from the data, but if further sampling is



to continue, it may be a good idea to avoid sampling in high traffic areas that could potentially contaminate samples.

Silver, Pb and Zn are three elements which all follow similar spatial trends, with nearly all anomalous values being detected along the north-south trending structures. Being pathfinder elements, it is expected that results elevated in the commodity elements will also be elevated in these trace elements and this is the case for the enriched samples. Zinc is perhaps the most important of these elements as it is highly abundant and also correlates very well with Cu, Au and the major structures throughout the area (Figures 79 and 80). These zones are in some cases also enriched in Ag and Pb, but Pb also has some other strange patterns. Transect 2 which has been heavily discussed above is also enriched in Pb (Figures 81 and 82), which may represent contamination. Given that surrounding Pb levels are low, it is very likely that the anomalous values are a signature of leaded gasoline, given the proximity to the road, and that the gases from leaded petrol can leave a lingering signature for between 150 and 5000 years (Dunn, 2007). However it is believed that plants need Pb as an essential component and can therefore accumulate up to 6ppb for their own use, however this has not been fully proven (Dunn, 2007), and is virtually useless for these anomalies given they are commonly in the 100s to 1000s of ppb.

The REE have a similar spatial distribution to Al and Zr, with relatively low background levels and a strong association with the Kimba Road (Figure 53). The enrichment is observed only within the calcrete and bluebush data, and may be caused by one of many mechanisms. It is known that certain lichens can accumulate REE elements from factors such as rainfall and dust, which indicates that there is possibly a source of dust contamination given the low rainfall of the area, and the already considered possible dust contamination (Tyler, 2004). It is also believed that dust contamination can result in elevated levels within plants, which is represented by the Bluebush data, as REE are abundant within clays and sands (Dunn, 2007). Therefore the same issue that has been continually discussed is the conclusion for these results, may be an effect of dust contamination, but may also be related to the elemental composition of the soil, which may be concentrated in calcrete; through lichen building processes (Tyler, 2004) or in plants through element up-take.

Other mechanisms that are able to transport and concentrate elements which have been discussed in great depth by (Aspandiar et al., 2006) include both Phreatic and Vadose mechanisms such as; Advective transport, Chemical and electrochemical transport, Capillary action, Gaseous processes, Plant Uptake, and Bioturbation.

These methods account for the dispersion and residence of target elements throughout the regolith or transported cover and plant material, and as mentioned are covered in detail by (Aspandiar et al., 2006). The more detailed study produced multiple mechanisms which are listed in Table 21, and mostly sub-categorize the mechanisms listed above. Figure 83 shows how a plant is able to express mineralisation that is undercover, and the mechanisms discussed above also help to understand how this occurs. Plants have also been able to adapt their root systems (Aspandiar et al., 2006) to better grasp essential metals such as Cu and Fe in varying landform settings given that different physiology is needed for different regions, depending on factors such as; rainfall, soil pH, mineral abundance, depth of soil profile and groundwater depth. These adaptations however are poorly understood for individual species, and therefore it is difficult to know which species are the most effective at concentrating elements specific to mineral exploration.

It also needs to be understood how a plant can change the environment it is in, not only can the plants themselves become enriched but there is also the possibility of the soils they reside in also becoming enriched. This occurrence is brought about by the accumulation of plant matter around the base of a plant, given that the foliage is anomalous in specific elements, the soil it breaks down and forms after falling from the plant will also be enriched in these elements. This association is therefore also important for recognising the significance that plants have with respect to calcrete formation, and therefore geochemical sampling. Since plants are able to concentrate the elements within themselves and soils, it is likely the carbonates that form within these soils will also be enriched. Along with this there is also the ability of the plant to sample the calcrete, which may possibly hyper-accumulate the same elements which the tree has already accumulated and then released back into the soils when dropping its leaves. Given that the hyper accumulation may occur within all sampling medium, these aspects should be heavily regarded when analysing results from either a biogeochemical or geochemical survey, as anomalous values may not represent an abundance of an element, but instead biological processes which concentrate essential elements for that particular species.

### **5.6 Implications for Mineral Exploration**

The biogeochemical and geochemical sampling programs that have been undertaken throughout the study area show strong correlations between commodity elements and the major north-south trending structures throughout the area. Along with this there has also been many other spatial associations recognised and associations between sampling media, and the importance of these results and associations relates solely to further exploration and suggestions for further exploration.

A majority of the anomalous commodity element concentrations lie directly on top of the major north-south trending structures, which are also accompanied by elements such as Ag and Pb. Along with the direct relationship there are also some distal associations with the structures observed, and this relates to the effects of the associated landforms which have been discussed throughout section 5.5., highlighting the importance of a regolith-landform map for identifying transported elemental signatures.

A lot of the Australian continent is covered by thick regolith, with the Project Mawson area being no exception, and this complicates exploration, when using techniques such as; geophysics, and geological & geochemical mapping. Testing the biogeochemical signature and the near surface chemical fertility which is a much cheaper alternative has proven to be not only a cost-effective approach, but also a much more suitable exploration approach. The results obtained and discussed thoroughly above, highlight extensive regions of interest, which can now be targeted with more precise exploration techniques, in particular drilling.

The regolith-landform map has been used to discuss anomalous values which potentially portray a different signature to the underlying geology, with the landform setting complicating the results of the surveys. Calcrete as discussed has undergone an interesting formation, and is not found throughout the entire area, with areas identified on the regolith-landform map as paelo-swamps having no calcrete formation. The map also explains the higher Al and Zr levels, so given the thickness and complexity of the cover, and the ability of the regolith-landform map to explain these relationships; it is a necessary tool for further exploration.

Western myall and pearl blush are the only sampling media plentiful enough to efficiently conduct a biogeochemical survey throughout the northern region of project Mawson and both media have proved their significance in biogeochemistry, exhibiting anomalism. Pearl bluebush has already been identified as a good mineral exploration target species, but very little work has been done on the myall as target species for an exploration program (Thomas, 2004). This work shows the ability of the species to penetrate to a considerable depth, and possibility sample the underlying bedrock directly. Given the lateral extent of the root system along with its obvious ability to penetrate to depth, the species would be well suited for other sampling programs, as would the pearl bluebush, with the only consideration being to reduce contamination risks.

## **6. CONCLUSION**

The project Mawson area offers a range of anomalous values for multiple target elements, in a range of different areas. The biogeochemistry seems to best represent the underlying chemical signature, with calcrete being not only patchy but also poorly formed throughout extensive areas. Both biogeochemical sampling media produce expressions of potential mineralisation, with some overlap. The only factors which could depict the better sampling medium are; depth of penetration, contamination, and plant distribution. Given that there have been some issues with pearl bluebush, with respect to possible contamination, it could be suggested that western myall are a more advantageous sampling medium, particularly for regional surveys, since it seems that the myall are able to penetrate much deeper than pearl bluebush. Putting these factors aside there is the issue of availability of species, given the scattered distribution of the vegetation, especially the western myall.

Future exploration throughout project Mawson should be pursued, given the anomalous values throughout the region, and the best type of program to continue with narrowing down drilling targets would be a biogeochemical survey. The approach however needs to be different given that the sampling should be more orientated around the major structures in the area, but overall still in an east-west orientation. An ideal survey would consist of multiple transects with 5-10 samples at a spacing of approximately 50 m, located along known structures. Special detail would need to be taken when interpreting the results from this survey as it has been proven throughout, that the landscape plays a major role in concentrating target elements. However the attached regolith-landform map and landscape evolution (section 5.1) depicts most of the misleading relationships that may be identified. Figure 84 denotes a possible sampling program, idealised from the Cu, Cu-Au, Cu-Zn, and Ag-Zn anomalies that have been identified from this study.

The strong relationship identified between structures and the commodity elements is accompanied by relationships with the Myola Volcanics and Broadview schist which are believed to host mineralisation (Cave and Jones, 2010). There are two possibilities for the signature perceived; the mineralisation may be bound by the north-south trending structures throughout the area, or the elevated commodity element concentrations within the structures may represent underlying mineralisation. The latter suggests that the structures in the area are bringing the signature of the underlying mineralisation up stratigraphy, to a depth that can be portrayed by techniques such as biogeochemistry, whereas the prior explanation suggests that the signature actually represents the

in-situ mineralisation, not a signature of deeply buried mineralisation. Both scenarios are plausible, given the current data available, but to define these theories and validate the proposed mineralisation suggestions, the exploration suggested above along with drilling of potential targets needs to be initiated.

## **7.0 ACKNOWLEDGEMENTS**

I would like to thank Steven Hill for his guidance and assistance throughout the duration of this Project, his knowledge and commitment have made this an exciting and interesting project. I would also like to thank Geoff Johnson and the boys from OneSteel for their contribution and support on the project, and give a special mention to Charlotte Mitchell, Hose Facelli, and Dave Giles for their contributions, and finally the lads from the “gold room” for their contributions and many distractions throughout the year.

## **8. REFERENCES**

- Aspandiar, M.F., Anand, R. and Gray, D., 2006. Mechanisms of element dispersion through transported cover: A review. CRC LEME Report 230.
- Cairns, B., 2003. Middleback Ranges Project –South Australia EL 2763, Annual report for the year ending 30th October 2002, Helix Resources.
- Cave, B., 2010. Copper-Gold Exploration in the Middleback Ranges: Source(s) of Fluids and Metals. The University of Adelaide BSc (Hons) thesis (unpublished).
- Crone, A. J., Martini, P. M. D., Machette, M. N., Okumura, K. & Prescott, J. R. (2003). Paleoseismicity of two historically quiescent faults in Australia : Implications for fault behaviour in stable continental regions, *Bulletin of Seismological Society of America* 93(5): 1913-1934.
- Curtis, S., 2007. The geology and mineral potential of the Port Augusta area, eastern Gawler Craton. PIRSA, Geological Survey Branch, Report Book 2007/6.
- Dietman, B., 2009. Regolith Expression of buried Cu-Au Mineralisation. The University of Adelaide BSc (Hons) thesis (unpublished).
- Dunn, C. E., 2007. Biogeochemistry in Mineral Exploration - Handbook of Exploration and Environmental Geochemistry, Volume 9, 2007, Pages xiii-xviii, 1-460.
- Facelli, J. M. and Brock. D. J. 2000. Patch dynamics in arid lands: localized effects of *Acacia papyrocarpa* on soils and vegetation of open woodlands of South Australia. - *Ecography*'23: 479 49L.
- Fraser, G. L., McAvaney, S., Neumann, N. L., Szpunar, M. & Reid, A. Discovery of Early Mesoarchean crust in the eastern Gawler Craton, South Australia. *Precambrian Research*, Volume 179, Issues 1-4, May 2010, pp. 1-21
- Hedger, D. And Dugmore, M., 2001. Geochemical detection of deeply buried mineralisation below the Mundi Mundi Plain, Curnamona Province – Implications for discovery success. *MESA Journal*, 21:50-51.

Herbert, H.K., 2008. Diamond Drilling at Intercept Hill project Yields exciting results - Drilling to recommence in February; Calcrete Geochemical sampling program nearing completion at Toondulya. Project ASX/Media Release, 31<sup>st</sup> January 2008.

Hill, S.M., 2009. Vegetation sampling in the Gawler Craton. CRC LEME, Publication-guides.

Hill, S.M., Brown, A., Hulme, K.A., Petts, A., Reis, N., and Mayo, A., 2005. Using biogeochemistry and Geobotany to explore through Transported Cover for Mineralisation. Abstracts CRC LEME Minerals Exploration Seminar, Perth WA - 25 May 2005, pp. 27-30.

Hitzman, M.W., & Valenta, R.K., 2005. Uranium in Iron Oxide-Copper-Gold (IOCG) Systems. Society of Economic Geologists, Inc., *Economic Geology*, v. 100, pp. 1657–1661.

Hulme, K.A. & Hill, S.M., 2005. River Red Gum Biogeochemistry Associations with substrate: Bedrock penetrators or Stream Sediment Amalgamators? In: Roach, I.C. (ed.), *Regolith 2005, Ten Years of CRC LEME*, pp. 146-151.

Ireland, C., 1997. Sustaining the western myall Sustaining the western myall woodlands : ecology and management. Thesis (PhD), University of Adelaide, Dept. of Environmental Science and Rangeland Management, 1997.

Lintern MJ and Sheard MJ, 1999. Regolith studies related to the Challenger Gold Deposit, Gawler Craton, South Australia. *CRC LEME, Open File Report 78*.

Lange, R.T., Sparrow, A.D., 1992. Growth rates of western myall (*Acacia papyrocarpa* Benth.) during the main phase of their canopy spreading. *Australian Journal of Ecology*, 17: 315-320.

Lowrey J.R. and Hill S.M., 2006. Plant biogeochemistry of Au-mineralisation buried by an Aeolian Dunefield: Tunkillia SA: in Fitzpatrick, R.W. and Shand, P. (editors) *Regolith 2006 – Consolidation and dispersion of ideas*. CRC LEME, Perth, 217–220.

Johnson, G., 2009. Introduction to IOCG Mineralisation, OneSteel presentation, OneSteel.

Jones, R., 2010. Copper-Gold Exploration in the Middelback Ranges: Conditions of Mineralisation. The University of Adelaide BSc (Hons) thesis (unpublished).



McQueen, K.G., Hill, S.M. and Foster, K.A., 1999. The nature and distribution of regolith carbonate accumulations in Southeastern Australia and their potential as a sampling medium in geochemical exploration. *Journal of Geochemical Exploration* 67, (1999) 67-82.

Miles, K.R., 1951. Tertiary Faulting in North-eastern Eyre Peninsula, South Australia. Published by permission of the Director, Department of Mines, South Australia. *Trans. Roy. Soc. S. Aust.*, 75, September 1952.

Mitchell, C., 2010. The Regolith Expression of IOCG mineralisation within the Southern region of the Project Mawson area, NE Eyre Peninsula, South Australia, The University of Adelaide BSc (Hons) thesis (unpublished).

Neumann, N.L. & Fraser, G.L. (Eds.), 2007. Geochronological synthesis and Time-Space plots for Proterozoic Australia. *Geoscience Australia Record* 2007/06.

OneSteel, 2010. Half Year Statutory Net Profit After Tax \$117m, Half Year Underlying Net Profit After Tax \$119m-ASX RELEASE, 16 February 2010

Parker, A.J., 1998. "Myola" Exploration License EL2228, Eastern Gawler Craton, South Australia- Annual Technical Report 8<sup>th</sup> November 1996 -7<sup>th</sup> November 1997, Equinox Resources.

Parker, A.J., & Fanning, C.M., 1998. Explanatory Notes for the Whyalla 1:250 000, Geological Map-SHEET SI53-8 International Index. Geological Survey of South Australia.

Parker, A.J. , Fanning, C.M. , Flint, R.B. 1985 Geology. In: Twidale C.R., Tyler M.J., Davies M. ed. Natural history of Eyre Peninsula. Royal Society of South Australia 1v p21-55.

Parker, A.J., PhD, Flint, R.B., B.Sc. (Hons), and Broken Hill Proprietary Co. Ltd., 1983. Whyalla Sheet. Geological Survey of South Australia, Department of Mines and Energy, Adelaide.

Robert, A., 2006. Tectonic Geomorphology studies in South Australia : Whyalla's Scarps and Billa Kalina Basin. The University of Melbourne, Report of Second Year of Prédكتورat Ecole Normale Supérieure de Paris March 2006- August 2006.

Schwarz, M.P., Morris, B.J., Sheard, M.J., Ferris, G.M., Daly, S.J. and Davies, M.B., 2006. Gawler Craton Summary. South Australian mineral explorers guide, chapter 4, 1-5.

Skirrow, R.G., 2004. Iron oxide Cu-Au deposits: An Australian perspective on their unifying characteristics. *Dynamic Earth: Past, Present and Future*. Abstracts of the 17th Australian Geological Convention, Hobart, Tasmania. February 8 - 13, Geological Society of Australia, Abstracts No. 73, p.121.

Skirrow, R.G., Bastrakov, E.N., Barovich, K., Fraser, G.L., Creaser, R.A., Fanning, M.C., Raymond, O.L. and Davidson, G.J., 2007. Timing of Iron Oxide Cu-Au(-U) Hydrothermal Activity and Nd Isotope Constraints on Metal Sources in the Gawler Craton, South Australia. *Economic Geology*, v. 102, pp. 1441–1470.

Skirrow, R.G., Fairclough, M., Budd, A., Lyons, P., Raymond, O., Milligan, P., Bastrakov, E., Fraser, G., Hight, L., Holm, O., and Williams, N., 2006. *Iron oxide Cu-Au (-U) potential map of the Gawler Craton, South Australia*. (First Edition), 1:500 000 scale, Geoscience Australia, Canberra. ISBN: 1 920871 76 4 (print); ISBN: 1 920871 78 0 (web)

The Australian Arid Lands Botanic Garden (AALBG). (2010). Plants at the AALBG – Western myall (*Acacia papyrocarpa*). Retrieved May 5, 2010, from [http://www.australian-aridlands-botanic-garden.org/general/plants/p\\_spec/wemy.htm](http://www.australian-aridlands-botanic-garden.org/general/plants/p_spec/wemy.htm)

Thomas, M. In: Roach I.C. ed. 2004. Biogeochemical Data Ranges from Tunkillia Prospect, Central Gawler Craton, South Australia. *Regolith 2004*. CRC LEME, pp. 362-364.

Tyler, G., 2004. Rare earth elements in soil and plant systems – A review. *Plant and Soil* 267: 191–206, 2004.

Vassallo, J.J., & Wilson, C.J.L., 2001. Palaeoproterozoic regional-scale non-coaxial deformation: an example from eastern Eyre Peninsula, South Australia *Journal of Structural Geology*, 24, Issue 1, January 2002, 1-24.

Vassallo, J.J., & Wilson, C.J.L., 2001<sub>2</sub>. Structural repetition of the Hutchison Group metasediments, Eyre Peninsula, South Australia *Australian Journal of Earth Sciences* (2001) 48, 331–345.

WeatherZone. (2010), data from Bureau of Meteorology. Whyalla Ap Climate. Retrieved April 3, 2010, from <http://www.weatherzone.com.au/climate/station.jsp?lt=site&lc=18120>

Wilson, M., 1999. Technical report no. 2235, Middleback Ranges Project –South Australia EL 2109,  
Annual report for the year ending 5 October 1999, Helix Resources

Wilson, M., 2000. Technical report no. 2238, Middleback Ranges Project –South Australia EL 2109,  
Annual report for the year ending 5 October 2000, Helix Resources

Wilson, M., 2004. Annual Report Exploration License EL2763 (Eyre BHP Alliance – Middlebacks), Helix  
Resources.

### **Figure Captions**

**Figure 1.** Regional Locality Map, Project Mawson, SA (source: minerals.pir.sa.gov.au)

**Figure 2.** Locations of each exploration programme undertaken by Helix Resources throughout the Project area (source: Wilson, 2000)

**Figure 3.** Location of significant results observed by equinox resources (source: Parker, 1998)

**Figure 4.** IOCG potential Map for South Australia (source: Skirrow, et al. 2006)

**Figure 5.** Map of South Australia highlighting the Olympic Cu-Au province and Moonta and OD corridors (modified from Skirrow et al, 2007)

**Figure 6.** Map showing the distribution of the Sleaford Complex over the Eyre Peninsula (source: Fraser et al, 2010)

**Figure 7.** Believed interpretation of where the 3150Ma Cooyerdoo Granite is emplaced (source; Fraser et al., 2010)

**Figure 8.** Geological events and rock types of the Middleback Ranges (Parker & Fanning, 1998)

**Figure 9.** Quaternary Sediments of the Middleback Ranges (Parker & Fanning, 1998)

**Figure 10.** Interpreted deposition Environment of the Hutchinson Group (source: Vassallo and Wilson, 2001)

**Figure 11.** Basic schematic explaining how the exhumation of the Middleback Ranges and the emplacement

**Figure 12.** The Ash Reef Scarp disrupting paleo-drainage to the east of the Middleback Range (source: Miles, 1951)

**Figure 13.** Map of Quaternary fault scarps (source: Robert, 2006)

**Figure 14.** A large mature Western Myall which has been used to test the biogeochemical signature of underlying mineralisation

**Figure 15.** A large western myall's roots spreading laterally more than 20m

**Figure 16.** A large western Myall's roots which have travelled approximately 30 m laterally before penetrating the overburden.

**Figure 17.** Pearl Bluebush which has been used as a target species for the biogeochemical survey

**Figure 18.** Aerial photo of the study area, with marked western myall transects.

**Figure 19.** Aerial photo of the region identifying vegetation changes due to overgrazing

**Figure 20.** Legend for Regolith-Landform Map

**Figure 21.** Aerial photo of the mapping area, showing the sample locations for Pearl bluebush and Calcrete

**Figure 22.** Regolith-Landform Map of the project area

**Figure 23.** Preserved thicket of Mallee around and along fence line

**Figure 24.** Evolution of alluvial fan development, identifying primary and secondary fan development

**Figure 25.** Flow vectors, indicating the southern direction of sheet flow, observed along transect 1

**Figure 26.** Contour banding giving stripy distribution of gravels, which can be used to identify sheet-wash plains.

**Figure 27.** X-Y Scatter plot for Cu and Zn from western myall data

**Figure 28.** Line graph showing concentrations of Cu and Zn for multiple western myall samples

**Figure 29.** Dendrogram, showing relationships between the target elements for western myall

**Figure 30.** X-Y Scatter plots of Uranium with other target elements for western myall

**Figure 31.** X-Y Scatter plots of Copper with other target elements for pearl bluebush

**Figure 32.** Dendrogram, showing relationships between the target elements for pearl bluebush

**Figure 33.** X-Y Scatter plots of Uranium with other target elements for pearl bluebush

**Figure 34.** X-Y Scatter plots of Au with other target elements for pearl bluebush

**Figure 35.** Dendrogram, showing relationships between the target elements for calcrete

**Figure 36.** Line graph showing concentrations of Ca and Fe for multiple calcrete samples

**Figure 37.** X-Y Scatter plots of Zinc with other target elements for calcrete

**Figure 38.** X-Y Scatter plots of Aluminium with other target elements for calcrete

**Figure 39.** Spatial Association Map for Cu western myall element distribution

**Figure 40.** Spatial Association Map for Cu pearl bluebush element distribution

**Figure 41.** Spatial Association Map for Au calcrete element distribution

**Figure 42.** Spatial Association Map for Au western myall element distribution

**Figure 43.** Spatial Association Map for Au pearl bluebush element distribution

**Figure 44.** Spatial Association Map for Al and Zr western Myall element distribution

**Figure 45.** Spatial Association Map for Al and Zr pearl bluebush element distribution

**Figure 46.** Spatial Association Map for Al and Zr calcrete element distribution

**Figure 47.** Spatial Association Map for Pb pearl bluebush element distribution

**Figure 48.** Spatial Association Map for Pb calcrete element distribution

**Figure 49.** Spatial Association Map for Ag western myall element distribution

**Figure 50.** Spatial Association Map for Ag pearl bluebush element distribution

**Figure 51.** Spatial Association Map for Ag calcrete element distribution

**Figure 52.** Spatial Association Map for La western myall element distribution

**Figure 53.** Spatial Association Map for La pearl bluebush element distribution

**Figure 54.** Morphology of the calcrete in centre of the Mawson area, which may be a weathered marine limestone (tertiary age)

**Figure 55.** Geological map, which highlights significant calcrete anomalies throughout the Mawson project area (source; Parker, 1998)

**Figure 56.** Nodular calcrete observed in the northern region of the project Mawson area, within the soil as distinct horizon

**Figure 57.** Massive tabular sheets of calcrete that may be a marine limestone

**Figure 58.** Silcrete observed at 706920mE 6339959mN and 706567mE 6339674mN (GPS coordinates AGD 66) which is scattered throughout the project area (figure 59)

**Figure 59.** 250K Whyalla Map sheet (source; Parker et al., 1983)

**Figure 60.** Illustration showing the formation of the silcretes and surrounding mottled zone

**Figure 61.** X-Y scatter plot of Cu concentrations from pearl bluebush and western myall samples

**Figure 62.** Line graph showing the concentration of Cu at each sample point for pearl bluebush and western myall

**Figure 63.** X-Y scatter plot of Au concentrations from pearl bluebush and western myall samples

**Figure 64.** Line graph showing the concentration of Au at each sample point for pearl bluebush and western myall, depicting a negative correlation between the two species

**Figure 65.** Morphology of a common tap root, showing the lateral deviation of the root before it penetrates to a greater depth

**Figure 66.** Line graph of Cu concentrations for proximal calcrete and western myall samples

**Figure 67.** Line graph of Au concentrations for proximal calcrete and western myall samples

**Figure 68.** X-Y Scatter plot of Cu concentrations from proximal calcrete and western myall samples

**Figure 69.** X-Y Scatter plot of Au concentrations from proximal calcrete and western myall samples, only shows minimal points because of overlap of results

**Figure 70.** Spatial Association Map for Cu western myall and calcrete element distribution

**Figure 71.** Line graph of Cu concentrations from proximal calcrete and pearl bluebush samples

**Figure 72.** X-Y Scatter plot of Zn concentrations from proximal calcrete and western myall samples

**Figure 73.** Line graph of Zn concentrations from proximal calcrete and pearl bluebush samples

**Figure 74.** Line Graph showing relationships between the REE for pearl bluebush

**Figure 75.** Line Graph showing relationships between the REE for western myall

**Figure 76.** The geology of interest for this project, with the main structures of interest highlighted and defined, with SZ1 hosting the Moola Drill Hole (modified from Parker et al. 1983)

**Figure 77.** Spatial Association Map for Cu calcrete element distribution

**Figure 78.** Spatial Association Regolith Map for Al and Zr for pearl bluebush element distribution

**Figure 79.** Spatial Association Map for Zn western myall element distribution

**Figure 80.** Spatial Association Map for Zn pearl bluebush element distribution

**Figure 81.** Spatial Association Map for Pb pearl bluebush element distribution

**Figure 82.** Spatial Association Map for Pb calcrete element distribution

**Figure 83.** Typical tree cycle showing the ability of a plant to pick an underlying mineralisation from using capillary suction; which forces the rise of mineralized water to the evaporation front (source: Aspandiar, 2006)

**Figure 84.** Alluvial fan on eastern side of the northern region of the Middleback Ranges

**Figure 85.** Quartz/ Granite chips found at 703177mE, 6334505mN (GPS co-ordinates AGD 66), the location of a sample point within the Helix Geochemistry Survey, chips may represent sample material, values of Ca very low when re-sampled.

**Figure 86.** Possible future biogeochemical sampling program, (transects represent location not size, parameters are defined throughout section 6

Figure 1





Figure 2.

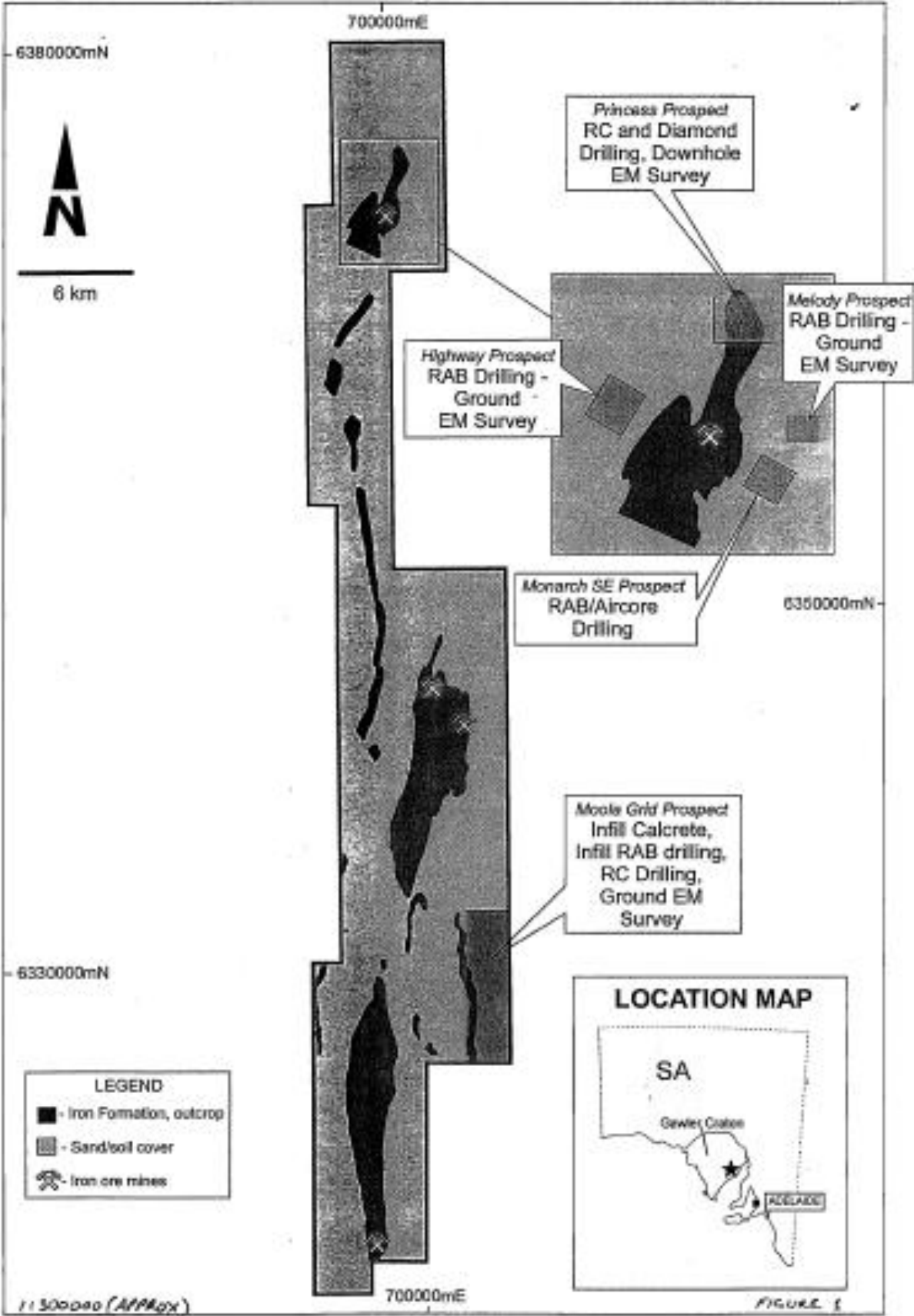


Figure 3.

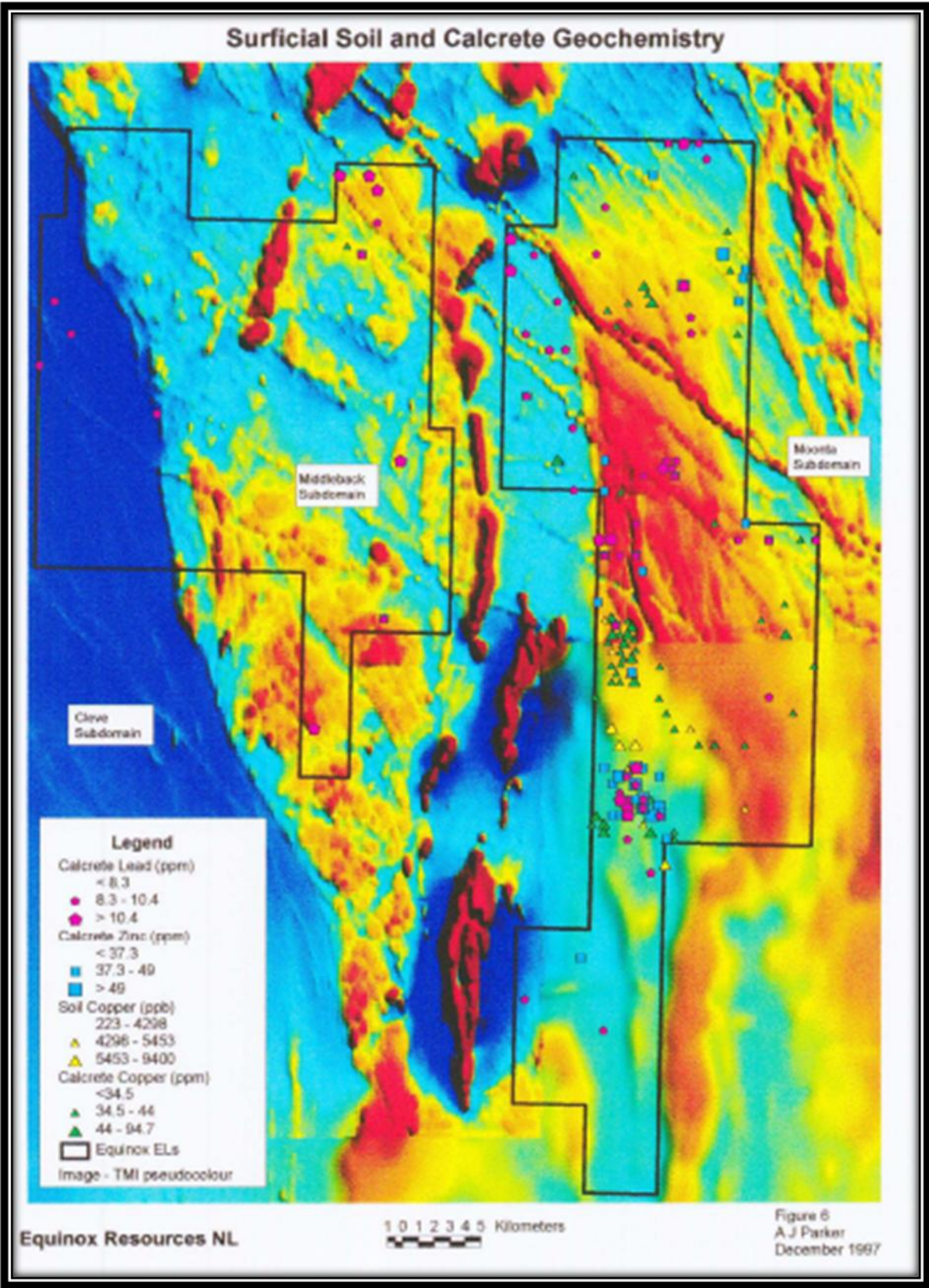




Figure 4.

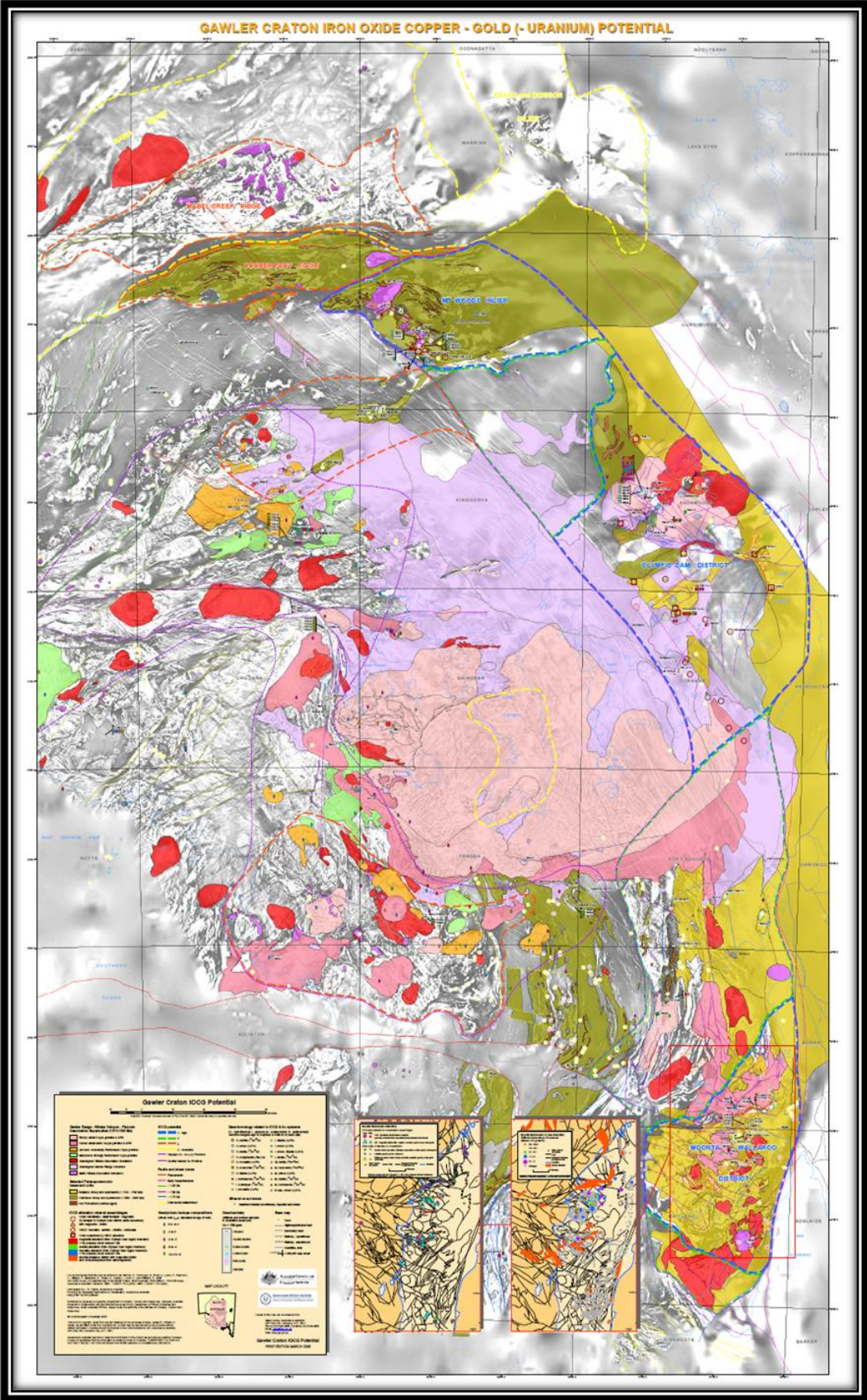


Figure 5.

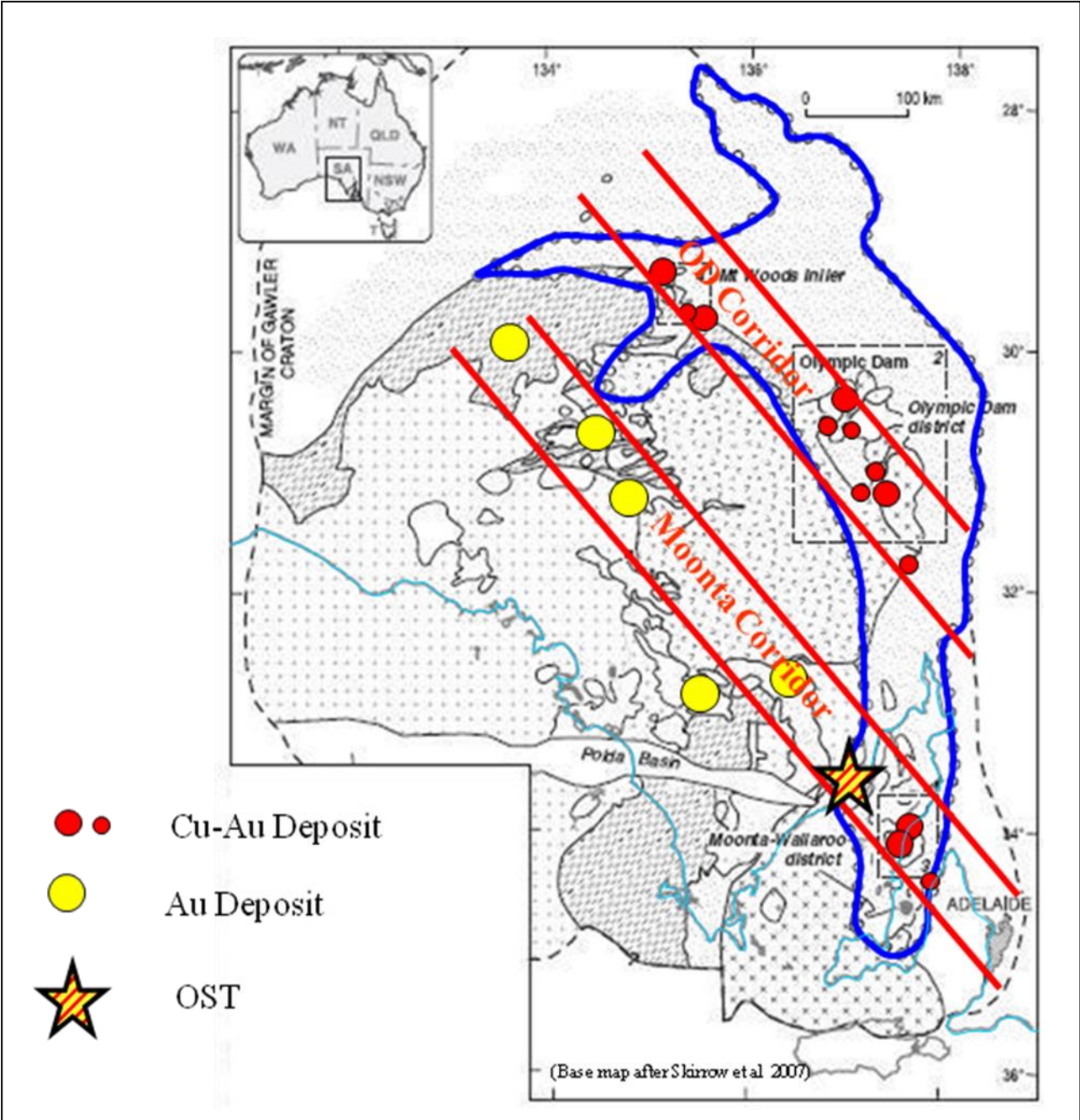




Figure 6.

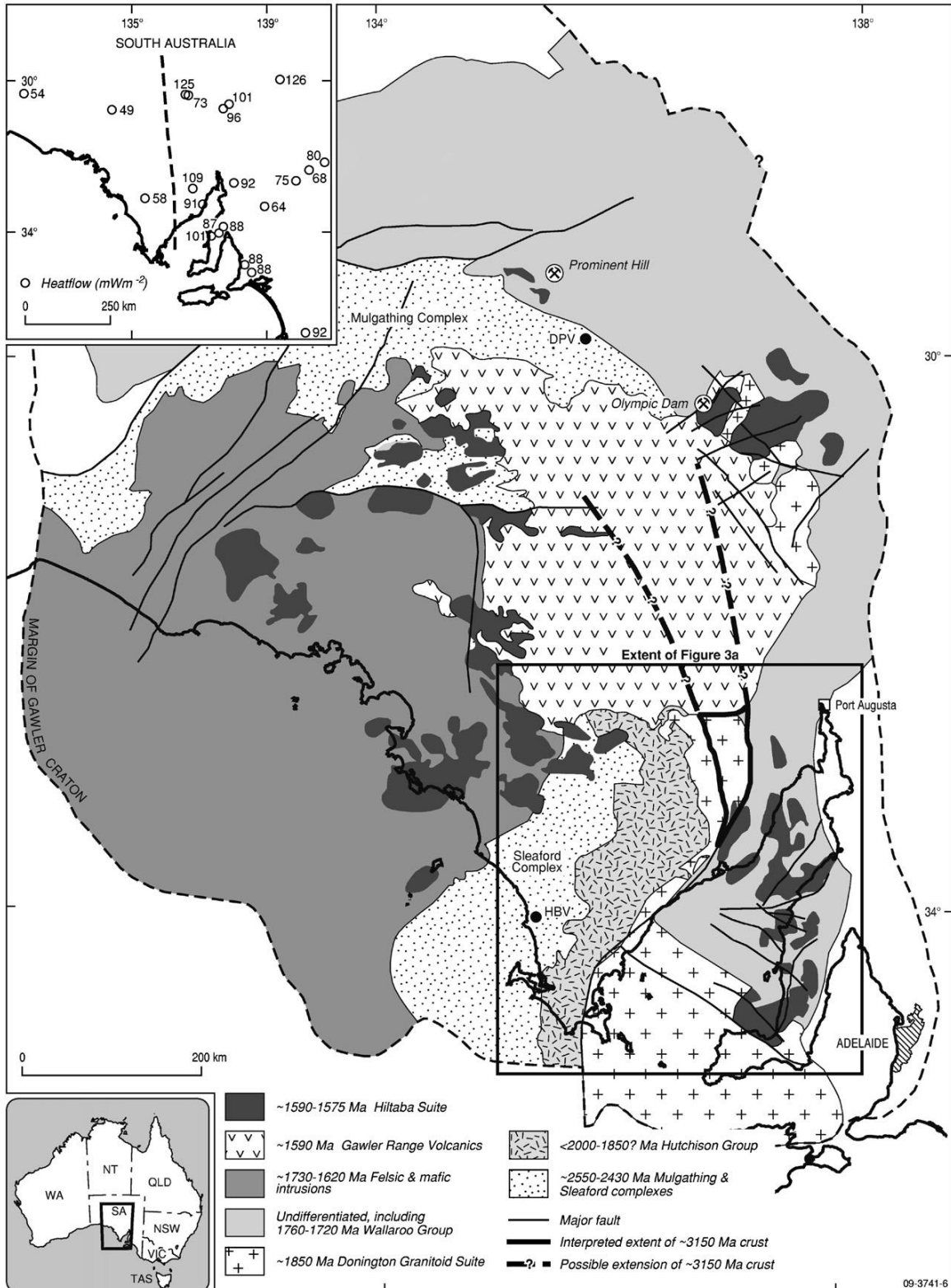
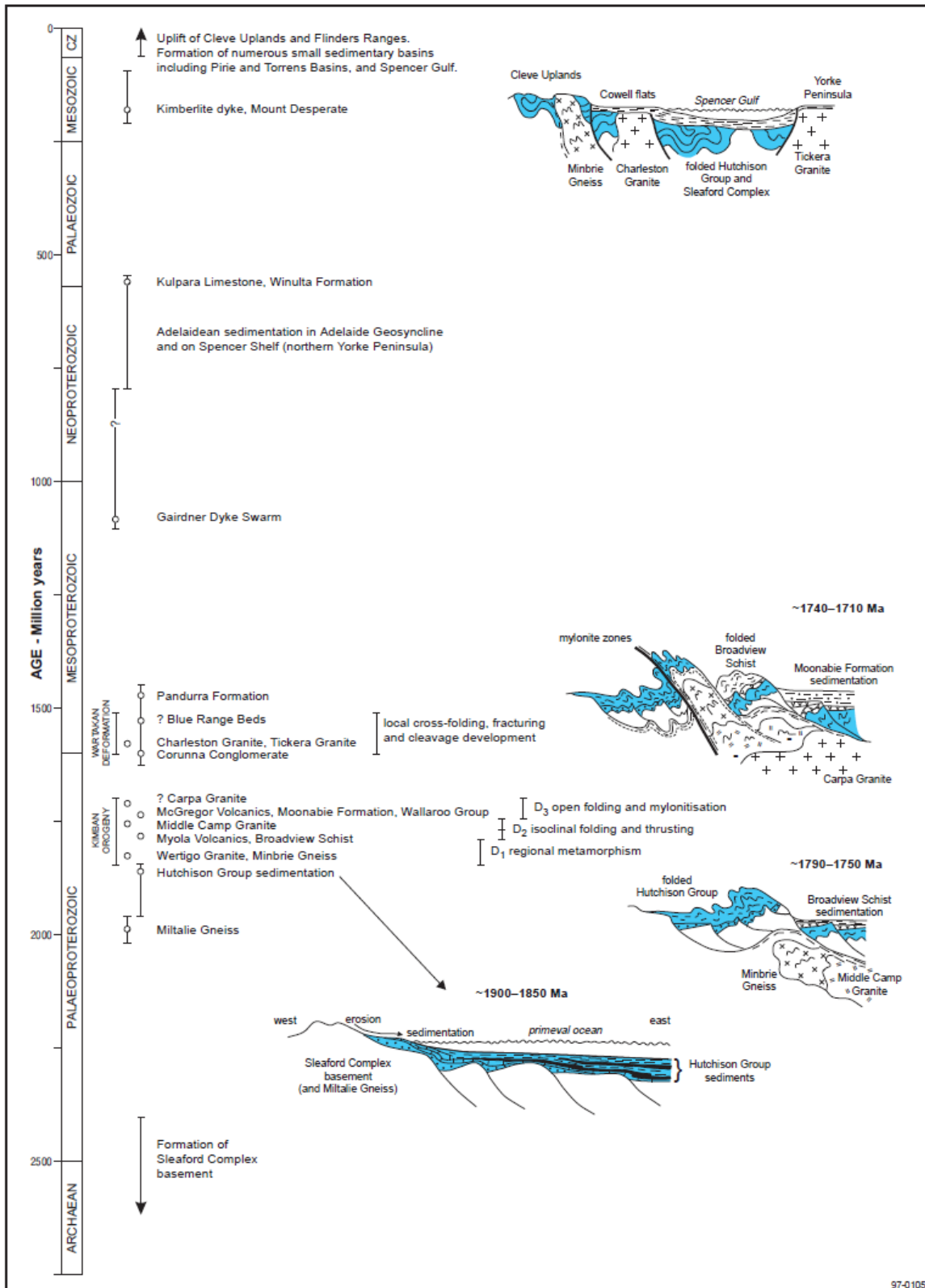


Figure 7.



Figure 8.





Regolith Expression of Cu-Au mineralisation within the Northern region of the Project Mawson area,  
NE Eyre Peninsula, South Australia

Figure 9.

Age	Stratigraphic unit and symbol	Lithology	Thickness (m)	Comments	
QUATERNARY	HOLOCENE	Semaphore Sand (Qhb)	White quartz and shelly quartz sand.		Modern beach and beach dune deposits of the present coastline.
		(Qh)	Undifferentiated alluvial sand, gravel and sandy clay of modern drainage channels, or thin, red-brown, sandy clay soil developed on thick Pooraka Formation. Loveday Soil at top of Pooraka Formation.		Calcrete surface either not present, eroded away or deeply buried by fluvial/solifluction sediment.
		(Qm)	Unconsolidated talus deposits.		Found flanking most of the steep, inland hills and ranges.
	LATE PLEISTOCENE	St Kilda Formation (Qhk)	Unconsolidated, laminated saline clay and silt with intervening quartz and shelly sand ridges. Yellow to grey in colour and often carbonaceous.		Interbedded marine, beach ridge and estuarine deposits of the coastal regions.
		(Qhl)	Lacustrine clay, silt, salt and gypsum deposits of the inland lakes. Unconsolidated in part but often have hard gypsaceous crusts.		Basal deposits equivalent in age to the St Kilda and Yamba Formations.
		(Qg)	Unnamed, fine gypsaceous silt and gypsaceous quartz sand.		Forms anolian dune deposits on the margins of the inland lakes.
	EARLY PLEISTOCENE	Moomba Sand (Qhb)	Off-white at the surface to pale yellow-orange at depth, quartz sand. The yellow sand contains soft, vertical carbonate pipes (Foshinga Soil).	5-15	Forms the prominent west-northwest-trending linear self dunes of the inland regions.
		Loveday Soil	Soft, powdery, off-white to creamy brown calcareous earth.	<0.5	Is developed on and within units below.
		Wabuna Formation (Qwb)	Pale red-brown to orange quartz sand with soft, powdery carbonate (of Loveday Soil).		Forms a basal member in the cores of inland self dunes (Moomba Sand).
		Pooraka Formation (Qpp)	Unconsolidated red-brown gravelly to clayey sand and gravel.	<5	Contains soft, powdery carbonate of Loveday Soil near top.
		Bakara Soil (Qca)	Nodular to biscuity calcrete of buff to pink colour.	0-1	May contain reworked Ripon Calcrete (not differentiated).
		Glanville Formation (Qgg)	Calcreted shelly grit and sand.	<1	Occurs only very rarely along the coastline and beneath Spencer Gulf.
	UNDIFFERENTIATED MAPPING UNITS	Ripon Calcrete (Qca)	Hard calcrete sheets of buff to pink colour often overlying nodular calcrete soil profiles.	0-1	Hard pan on well-developed calcareous soil profiles.
		(Qpl)	Red-brown clayey sand and sandy clay with local gravel beds. May be locally mottled and often contains vertical carbonate and gypsum pipes at the top.	<4	Semiconsolidated and may be equivalent to Telford Gravel.
(Qp2)		Undifferentiated Quaternary profiles comprising thin, red-brown, sandy and clay soil veneers over relatively thick gravel and gravelly sand of the Pooraka Formation.	<6	Clay may represent Callabonna Clay.	
	(Qp1)	Undifferentiated, thin, red-brown, sandy clay soil and gravel developed on and containing reworked calcrete (Bakara Calcrete mainly).	<3	Red-brown clay may represent Callabonna Clay, and gravel may represent Pooraka Formation equivalents. Calcrete crops out locally.	

97-0015



Figure 10.

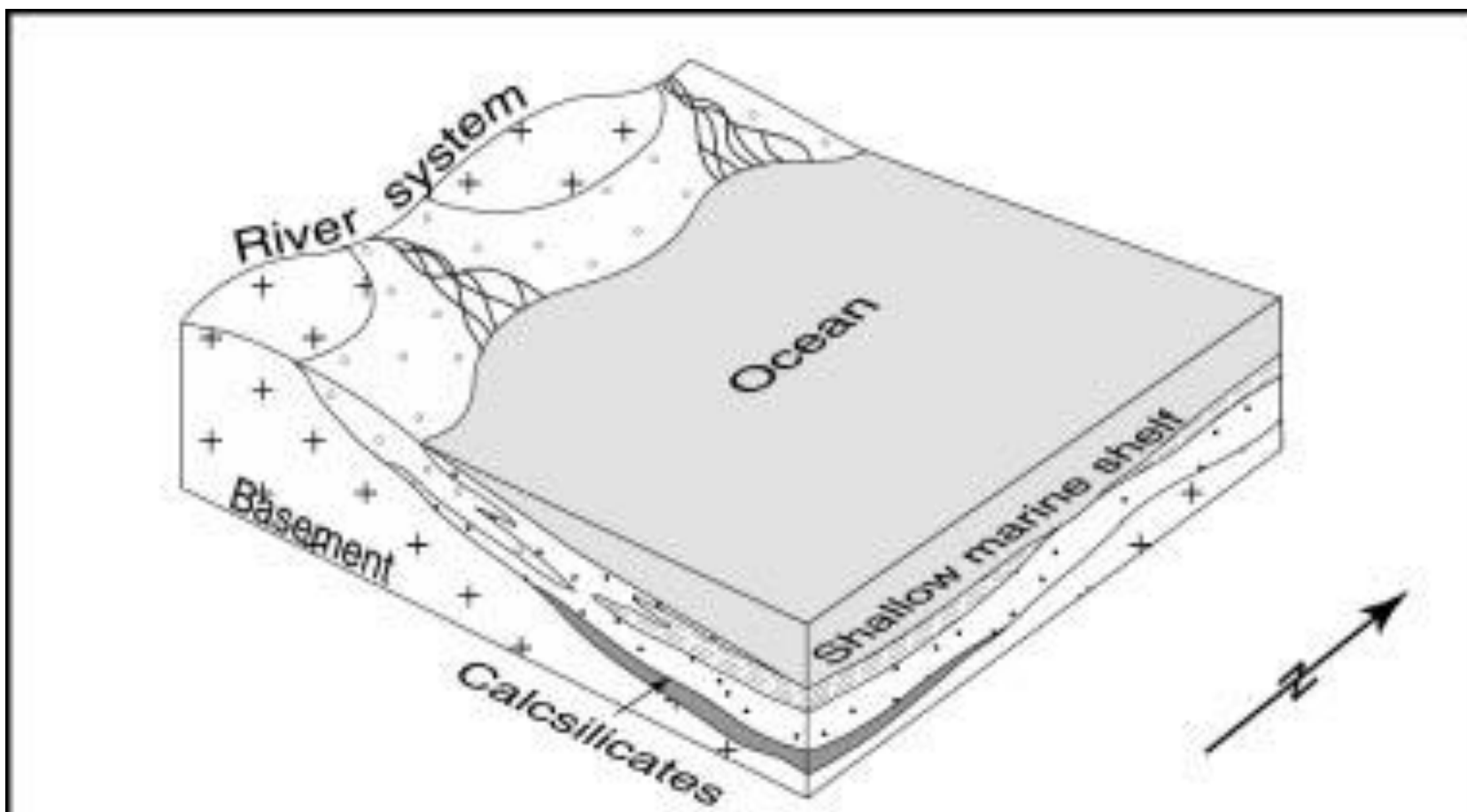


Figure 11.

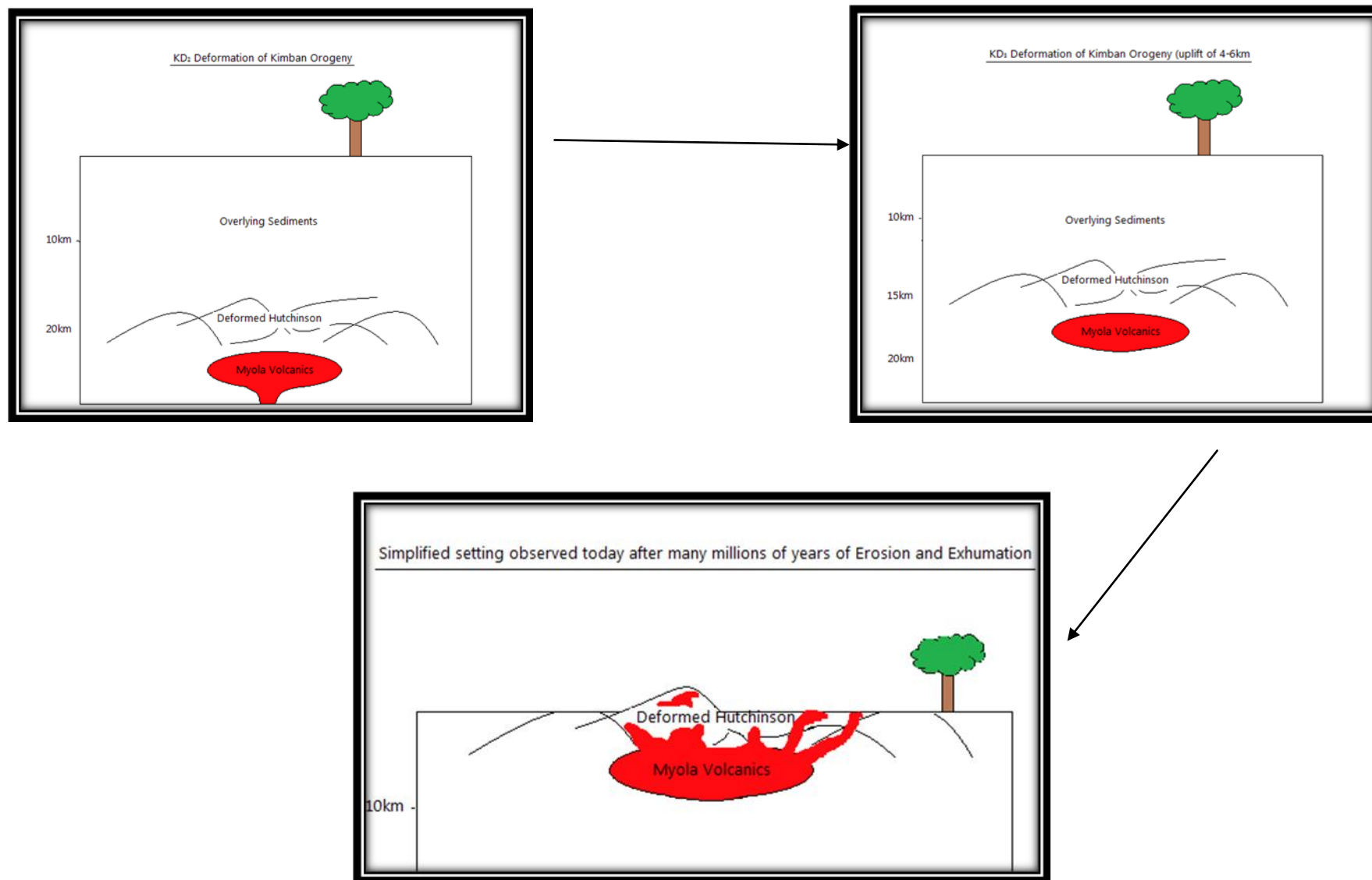


Figure 12.

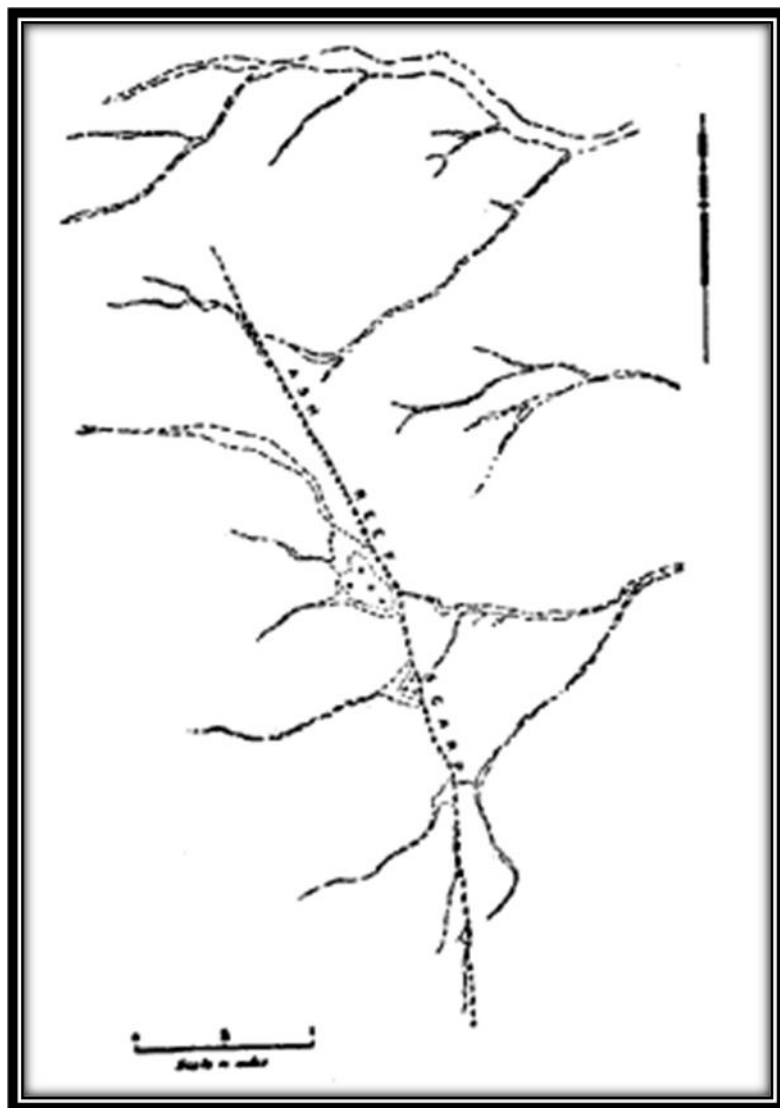


Figure 13.

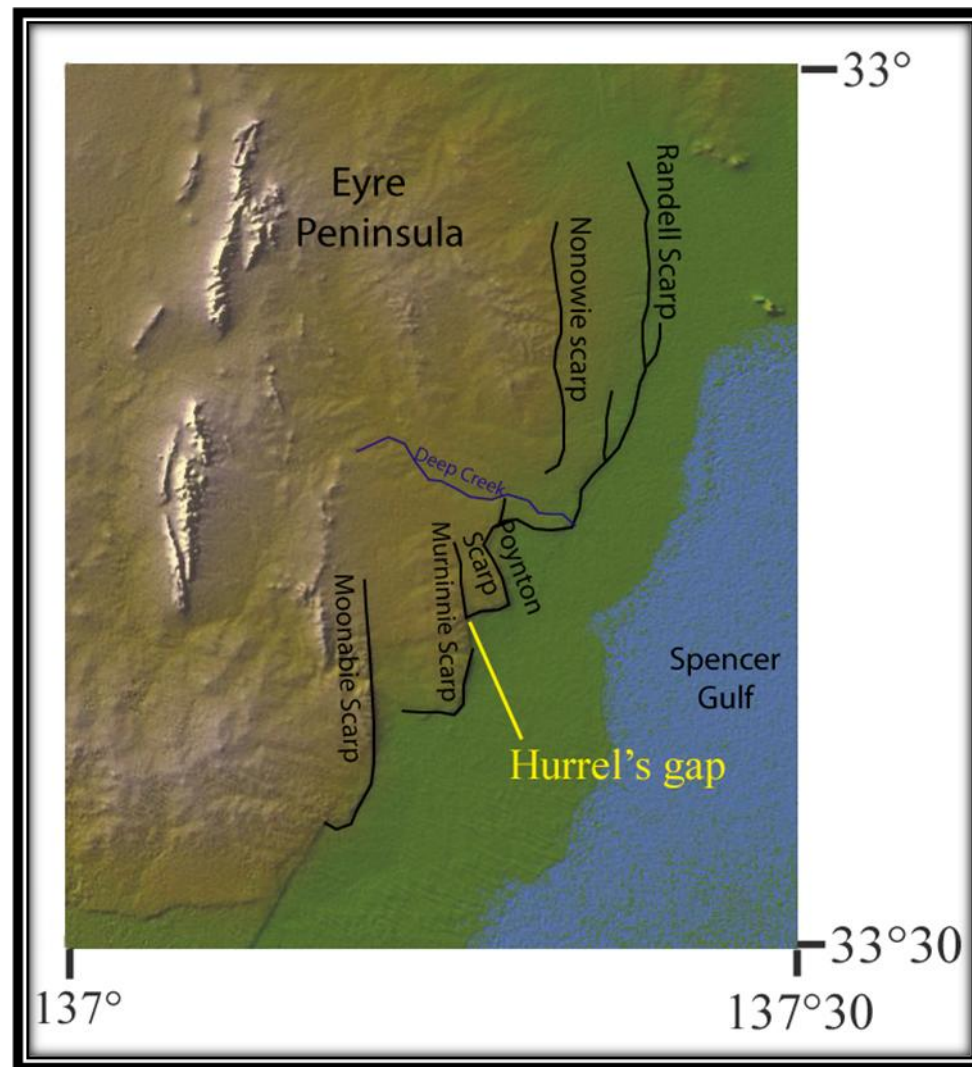


Figure 14.



Figure 15.





Figure 16.



Figure 17.





Figure18.

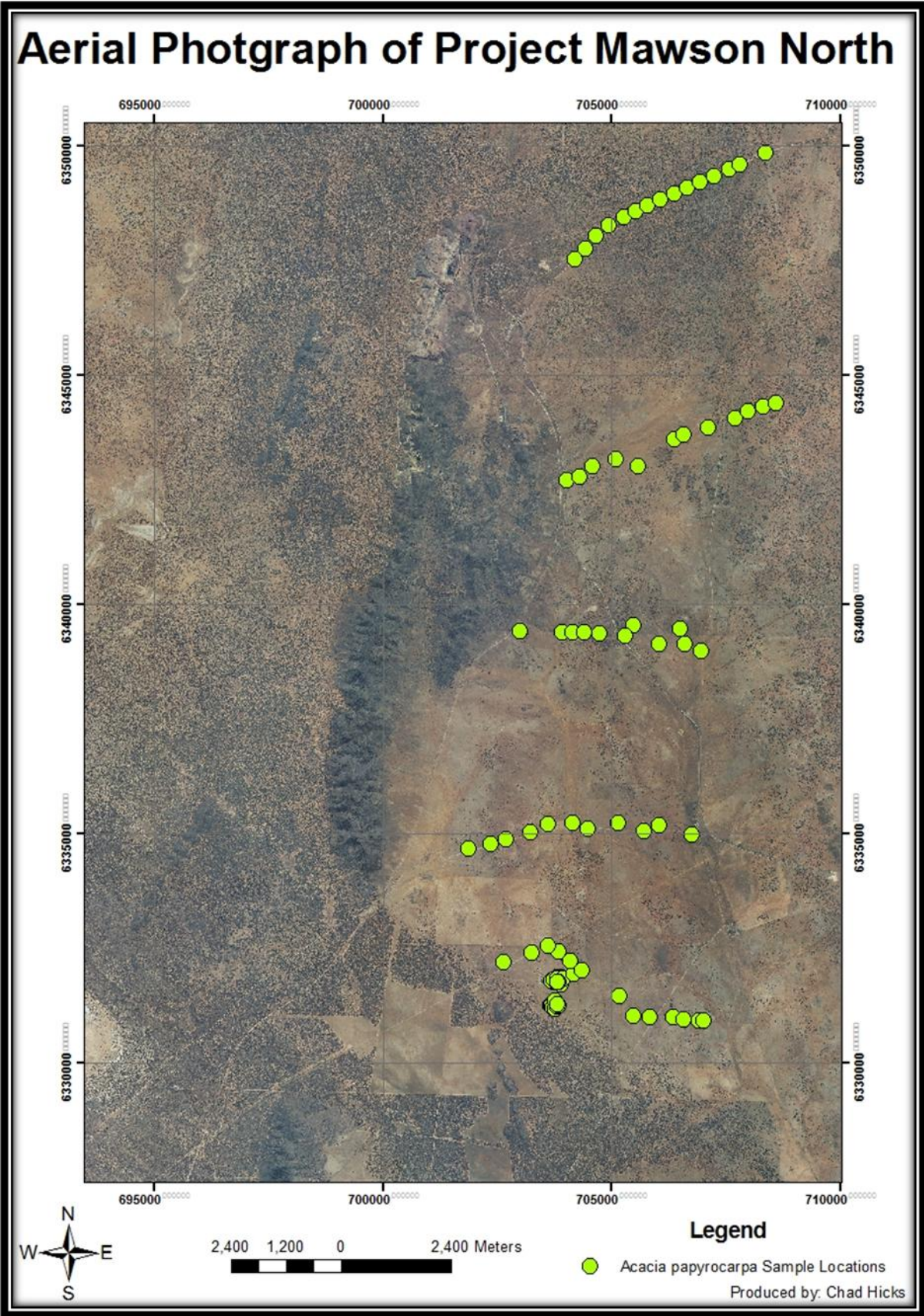
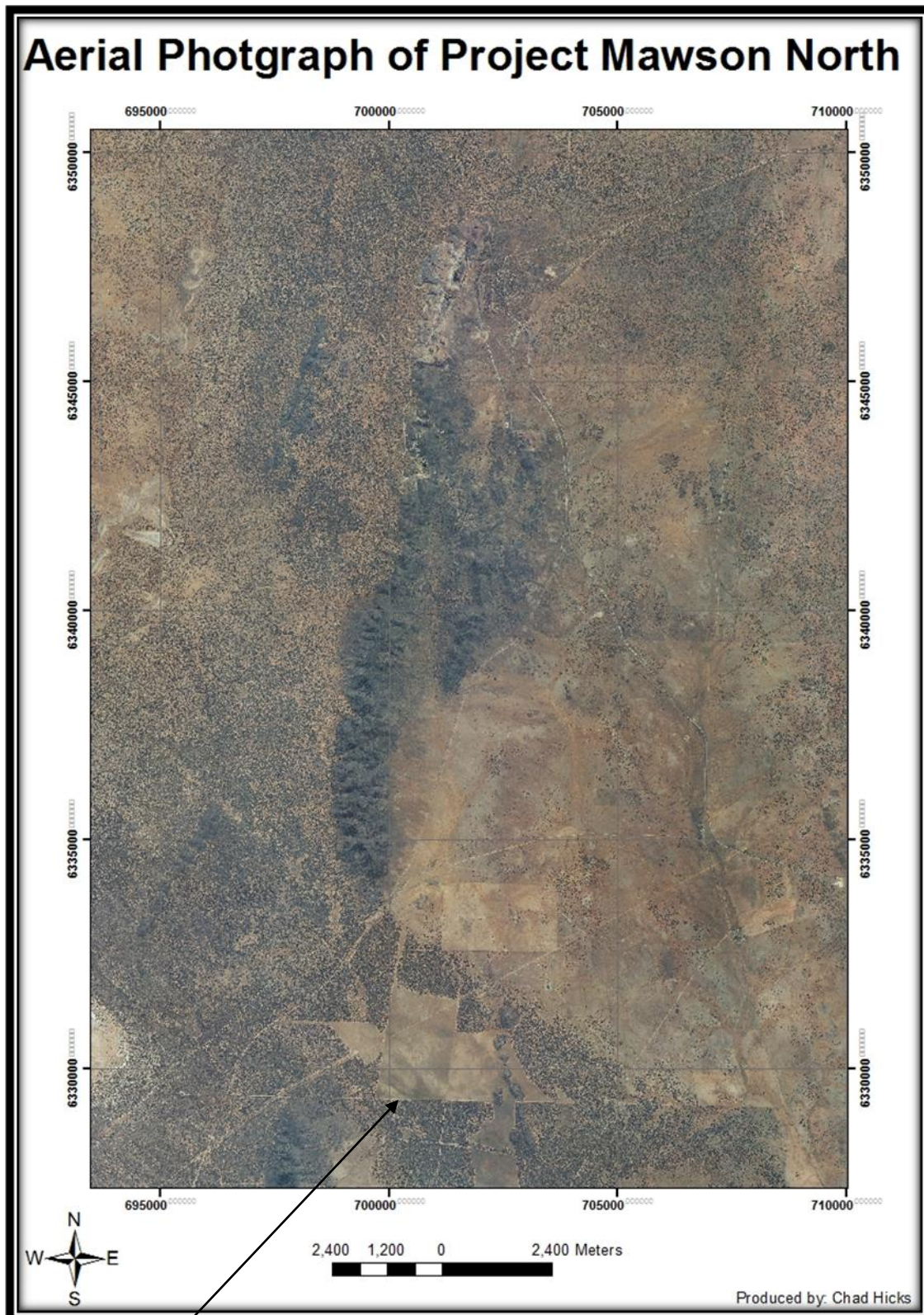












Figure 19.



Fence line illustrating a vegetation change, possibly an effect of overgrazing

Figure 20.

-  **Aed** – Small incised channels over areas of low topographic relief that are associated with contemporary drainage. Red-brown, fine sand-clay, with lag composed of; ± sub-angular to sub-rounded gravel – cobble, vein quartz, ironstone, quartzite, granite, calcrete, silcrete and ferruginous material. Chenopod shrub-land made up of *Casuarina pauper*, *Maireana sedifolia*, *Atriplex vesicaria* and many local shrubs and grasses.
-  **Afa<sub>1</sub>**- Red-brown, sandy-gravel, fine –sandy-clay located within outwash fans and channels, downstream from channel intersection points between channels and adjacent Alluvial Fans. Lag composed of; ± angular to sub-angular gravel-boulder, ironstone, calcrete, vein quartz and other lithic fragments. Chenopod shrub-land made up of *Casuarina pauper*, *Maireana sedifolia*, *Atriplex vesicaria* and many local shrubs and grasses
-  **Afa<sub>2</sub>** - Red-brown, fine sand-clay located within outwash fans and channels, downstream from channel intersection points between channels and adjacent Alluvial Fans. Lag composed of; ± angular to sub-angular gravel-cobble, ironstone, calcrete, vein quartz and other lithic fragments. Chenopod shrub-land made up of *Casuarina pauper*, *Maireana sedifolia*, *Atriplex vesicaria* and many local shrubs and grasses
-  **AOpd** - Low relief land-surfaces associated with flood areas of drainage depressions. Red-brown, fine sand-clay, with lag composed of; ± sub-angular to sub-rounded, gravel-pebble, vein quartz, ironstone, quartzite, granite, calcrete, silcrete. Chenopod shrub-land made up of *Casuarina pauper*, *Acacia papyrocarpa*, *Maireana sedifolia*, *Atriplex vesicaria* and many local shrubs and grasses.
-  **Apd** - Low relief land-surfaces associated with flood areas of drainage depressions. Red-brown, fine sand-clay, with lag composed of; ± sub-angular to sub-rounded, gravel –cobble, vein quartz, ironstone, quartzite, granite, calcrete, silcrete. Chenopod shrub-land made up of *Casuarina pauper*, *Acacia papyrocarpa*, *Maireana sedifolia*, *Atriplex vesicaria* and many local shrubs and grasses.
-  **Cer<sub>1</sub>** - Commonly occurring on regions of higher topographic relief, involving sediments predominantly transported by gravity. Red-brown, coarse sand, with lag composed of; large fragments > 1 m in diameter, of angular to sub-angular lithic fragments, with minor bedrock outcrop. Vegetation is generally sparse.
-  **CHep** – Areas of slight topographic relief consisting red-brown fine, sand-clay, with lag composed of;± sub-angular to sub-rounded, gravel –cobble, vein quartz, ironstone, quartzite, granite, calcrete, silcrete. Chenopod shrub-land made up of *Acacia papyrocarpa*, *Maireana sedifolia*, *Atriplex vesicaria* and many local shrubs and grasses
-  **CHfc** - Red-brown, fine sand-clay located within outwash fans and channels, downstream from channel intersection points, and often associated with areas of low and broad relief. Lag composed of; ± angular to sub-angular gravel-cobble, ironstone, calcrete, vein quartz and other lithic fragments. Chenopod shrub-land made up of *Casuarina pauper*, *Maireana sedifolia*, *Atriplex vesicaria* and many local shrubs and grasses



**Figure 20 Continued.**



**CHpd<sub>1</sub>** – Broad, low relief land-surfaces consisting of red-brown, fine sand-clay; ± sub-angular to sub-rounded, gravel-cobble, vein quartz, ironstone, quartzite, granite, calcrete, silcrete. Chenopod shrub-land of *Casuarina pauper*, *Acacia papyrocarpa*, *Maireana sedifolia*, *Atriplex vesicaria* and many local shrubs and grasses



**Fm<sub>1</sub>** – Urban areas commonly associated with a mine site. Surface lags are highly variable. Vegetation is variable with some exotic species also present



**ISps<sub>1</sub>** – Areas of slight topographic relief associated with dune margins. Red-brown, fine to medium, sub-rounded to rounded, moderately sorted quartzose sand and clay ± ironstone, lithic fragments and calcrete nodules. Chenopod shrub-land made up of *Acacia papyrocarpa*, *Maireana sedifolia*, *Atriplex vesicaria* and many local shrubs and grasses



**ISul<sub>1</sub>** – Dune-field of NW-SE linear dunes, consisting of red-brown, fine to medium, sub-rounded to rounded, moderately sorted quartzose sand and clay ± ironstone, lithic fragments and calcrete nodules. Chenopod shrub-land made up of *Acacia papyrocarpa*, *Maireana sedifolia*, *Atriplex vesicaria* and many local shrubs and grasses



**Lpd<sub>1</sub>** – Paleo-ephemeral lakes associated with areas of low topographic relief, consisting of fine, sand-clay, with lithic fragments ranging from rounded to sub-angular gravel to cobbles. The unit is generally sparsely vegetated, and dominated by *Maireana sedifolia* and *Atriplex vesicaria*.



**SMep<sub>1</sub>** – Exposures of the Middleback subgroup along regions of slight topographic relief, lag consists of gravel-boulder, ironstone, vein quartz ± lithic fragments and red-brown, fine sand. Chenopod shrub-land composed of *Acacia papyrocarpa*, *Maireana sedifolia*, *Atriplex vesicaria* and many local shrubs and grasses



**SMep<sub>2</sub>** – Exposures of Myola Volcanics along regions of slight topographic relief, lag consists of gravel-boulder, Myola Volcanics, ironstone, vein quartz ± lithic fragments and red-brown, fine sand. Chenopod shrub-land, of *Acacia papyrocarpa*, *Maireana sedifolia*, *Atriplex vesicaria* and many local shrubs and grasses



**SMep<sub>3</sub>** - Exposures of Broadview Schist along regions of slight topographic relief, lag consists of gravel-boulder, schist, ironstone, vein quartz ± lithic fragments and red-brown, fine sand. Chenopod shrub-land composed of *Acacia papyrocarpa*, *Maireana sedifolia*, *Atriplex vesicaria* and many local shrubs and grasses



**SMep<sub>4</sub>** - Exposure of silcrete along regions of slight topographic relief, lag consists of gravel-boulder, silcrete, vein quartz, ironstone, ± lithic fragments and red-brown, fine, sand. Chenopod shrub-land composed of *Acacia papyrocarpa*, *Maireana sedifolia*, *Atriplex vesicaria* and local shrubs and grasses



**SMep<sub>5</sub>** – Exposures of outcropping bedrock along regions of slight topographic relief, lag consists of gravel-boulder, vein quartz, ironstone, ± lithic fragments and red-brown, fine, sand. Chenopod shrub-land composed of *Acacia papyrocarpa*, *Maireana sedifolia*, *Atriplex vesicaria* and many local shrubs and grasses



**SMer<sub>1</sub>** - Exposures of the Middleback subgroup along regions of moderate topographic relief, lag consists of gravel-boulder, ironstone, vein quartz ± lithic fragments and red-brown, fine sand. Chenopod shrub-land composed of *Acacia papyrocarpa*, *Maireana sedifolia*, *Atriplex vesicaria* and many local shrubs and grasses



**SMer<sub>2</sub>** - Exposures of Myola Volcanics along regions of moderate topographic relief, lag consists of gravel-boulder, Myola Volcanics, ironstone, vein quartz ± lithic fragments and red-brown, fine sand. Chenopod shrub-land, of *Acacia papyrocarpa*, *Maireana sedifolia*, *Atriplex vesicaria* and local shrubs and grasses



**SMer<sub>3</sub>** – Exposures of Broadview Schist along regions of moderate topographic relief, lag consists of gravel-boulder, schist, ironstone, vein quartz ± lithic fragments and red-brown, fine sand. Chenopod shrub-land composed of *Acacia papyrocarpa*, *Maireana sedifolia*, *Atriplex vesicaria* and many local shrubs and grasses



**SMer<sub>4</sub>** – Exposures of undifferentiated granite along regions of moderate topographic relief, lag consists of gravel-boulder, undifferentiated granite, ironstone, vein quartz ± lithic fragments and red-brown, fine sand. Chenopod shrub-land composed of *Acacia papyrocarpa*, *Maireana sedifolia*, *Atriplex vesicaria* and many local shrubs and grasses



**SMer<sub>5</sub>** – Exposures of quartz along known structures with moderate topographic relief, lag consists of gravel- boulder quartz, ironstone ± lithic fragments and red-brown, fine, sand. Chenopod shrub-land composed of *Acacia papyrocarpa*, *Maireana sedifolia*, *Atriplex vesicaria* and many local shrubs and grasses



**SMer<sub>6</sub>** – Exposure of silcrete within a region of moderate topographic relief, lag consists of gravel-boulder, silcrete, vein quartz, ironstone, and red-brown, fine, sand. Chenopod shrub-land composed of *Acacia papyrocarpa*, *Maireana sedifolia*, *Atriplex vesicaria* and many local shrubs and grasses



**SMer<sub>7</sub>** – Exposures of ferricreted conglomerate and sandstone within a region of moderate topographic relief, lag consists of gravel-boulder, silcrete, vein quartz, ironstone, and red-brown, fine, sand. Chenopod shrub-land composed of *Acacia papyrocarpa*, *Maireana sedifolia*, *Atriplex vesicaria* and many local shrubs and grasses



**SMer<sub>8</sub>** – Exposures of undifferentiated bedrock along regions of moderate topographic relief, lag consists of gravel-boulder, ironstone, vein quartz ± lithic fragments and red-brown, fine sand. Chenopod shrub-land of *Acacia papyrocarpa*, *Maireana sedifolia*, *Atriplex vesicaria* and many local shrubs and grasses



**SSel<sub>1</sub>** - Exposures of the Middleback subgroup along regions of significant topographic relief, lag consists of gravel-boulder, ironstone, vein quartz ± lithic fragments and red-brown, fine sand. Chenopod shrub-land of *Acacia papyrocarpa*, *Maireana sedifolia*, *Atriplex vesicaria* and many local shrubs and grasses

**Figure 20 continued.**



**SSer<sub>1</sub>** - Exposures of the Middleback subgroup along regions of moderate topographic relief, lag consists of gravel-boulder, ironstone, vein quartz ± lithic fragments and red-brown, fine sand. Chenopod shrub-land of *Acacia papyrocarpa*, *Maireana sedifolia*, *Atriplex vesicaria* and many local shrubs and grasses



**SSer<sub>2</sub>** - Exposures of quartz along known structures with moderate topographic relief, lag consists of gravel- boulder quartz, ironstone ± lithic fragments and red-brown, fine, sand. Chenopod shrub-land of *Acacia papyrocarpa*, *Maireana sedifolia*, *Atriplex vesicaria* and many local shrubs and grasses

Figure 21.

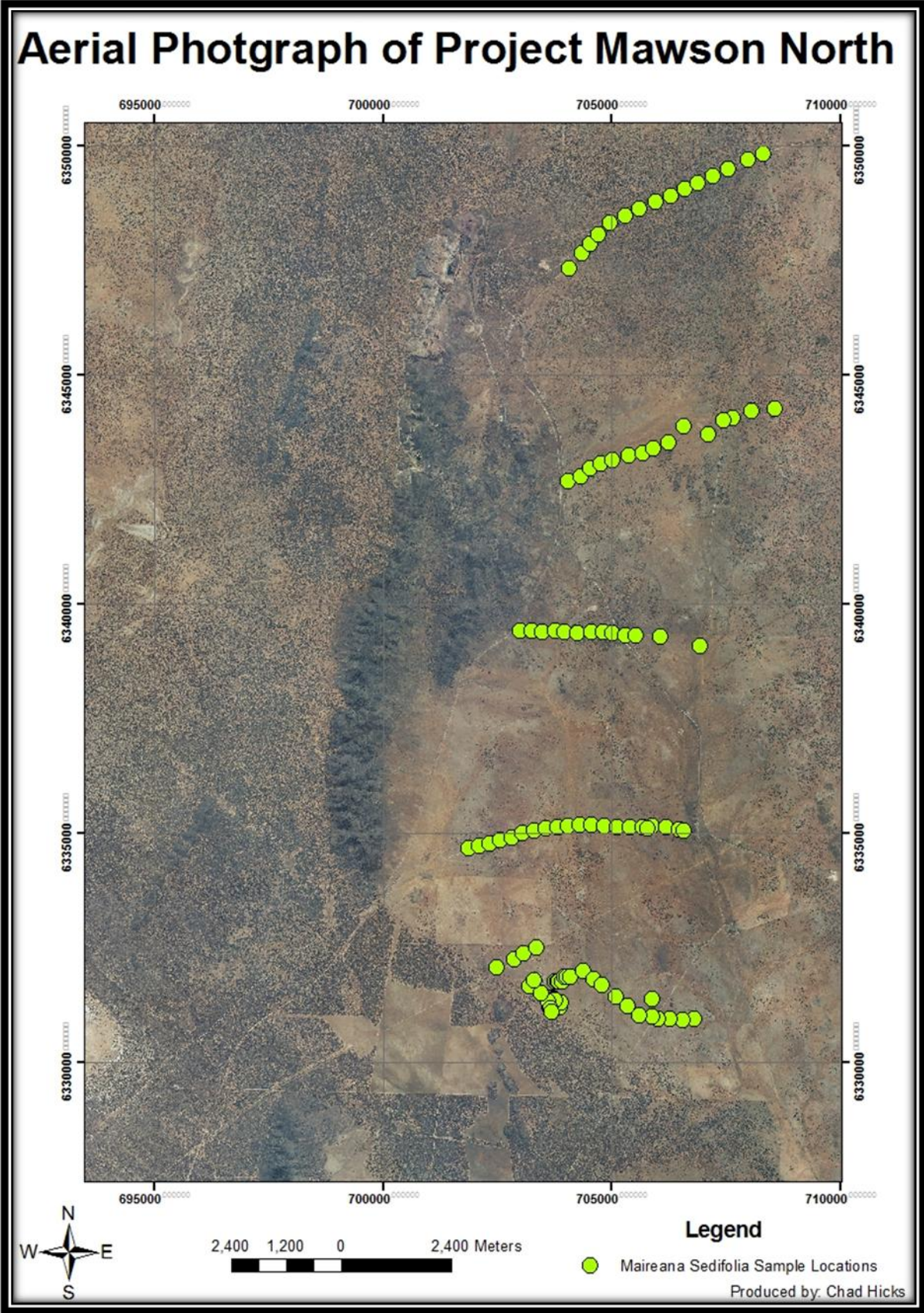
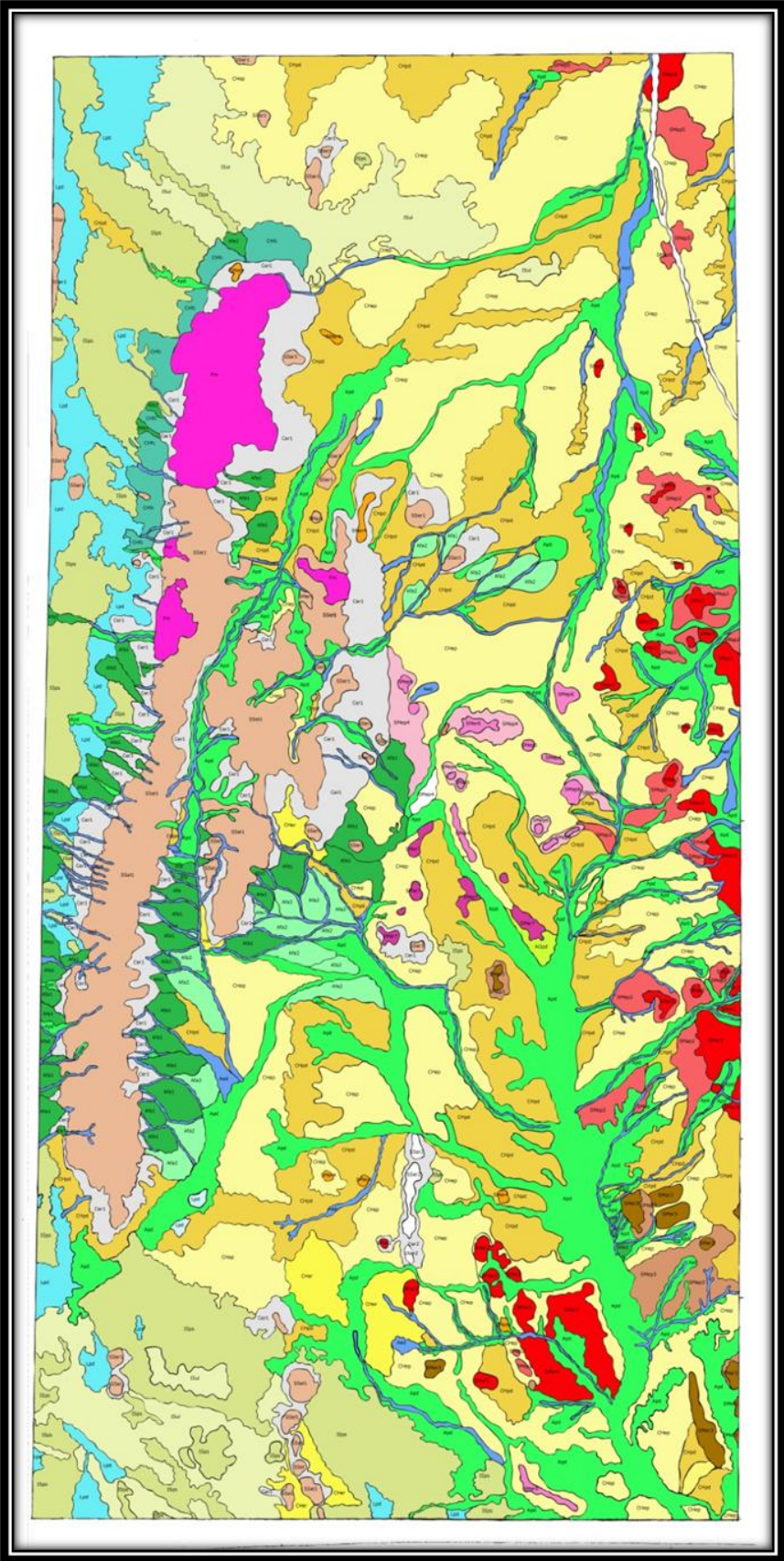




Figure 22.



**Figure 23.**





Figure 24.

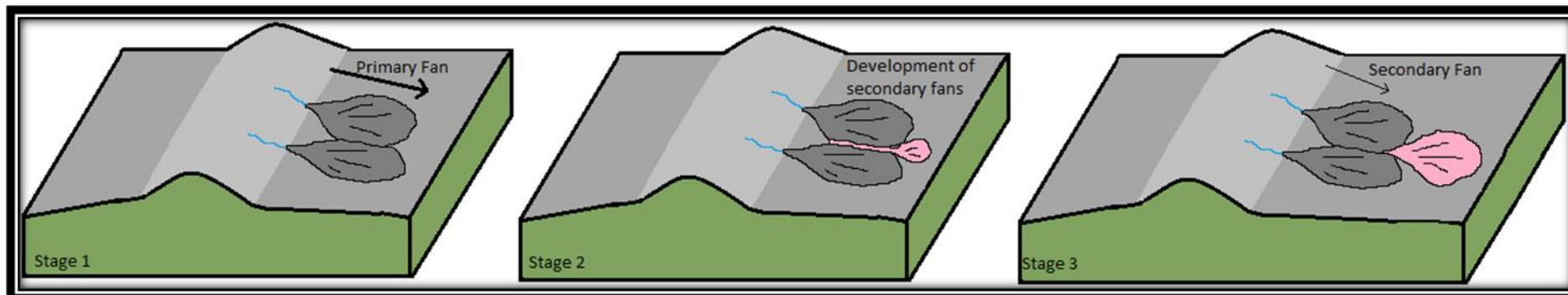
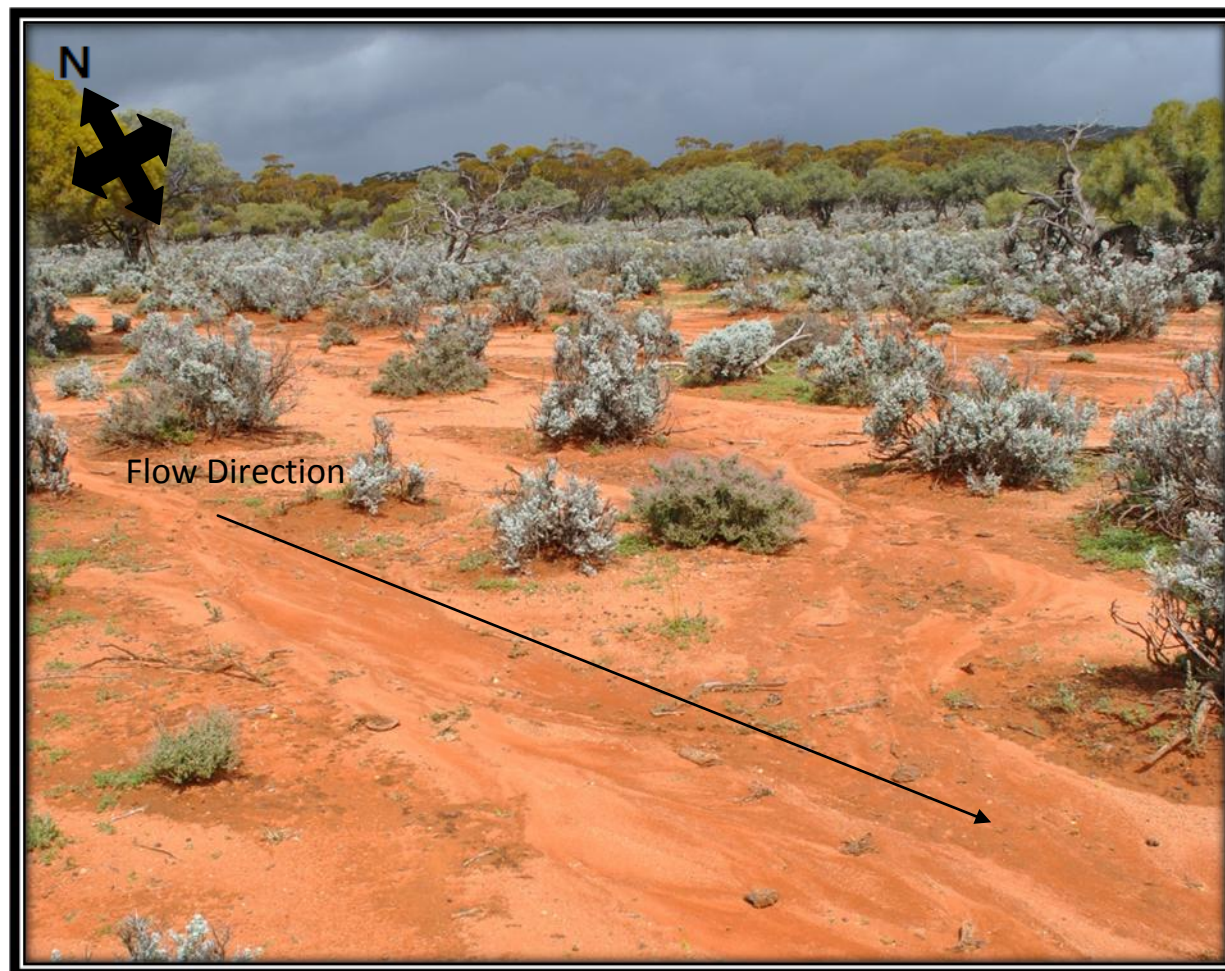


Figure 25.





**Figure 26.**



Figure 27.

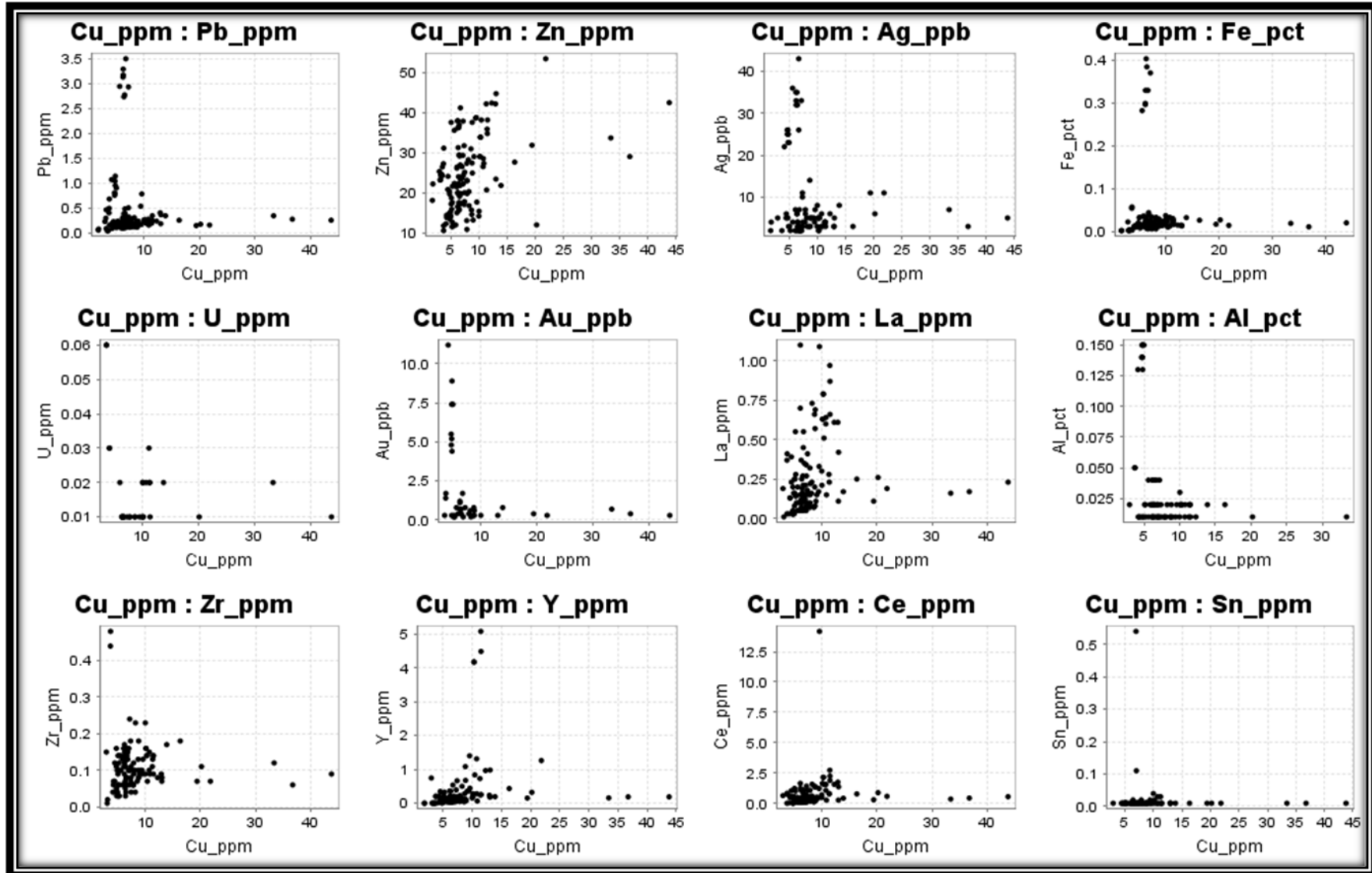


Figure 28.

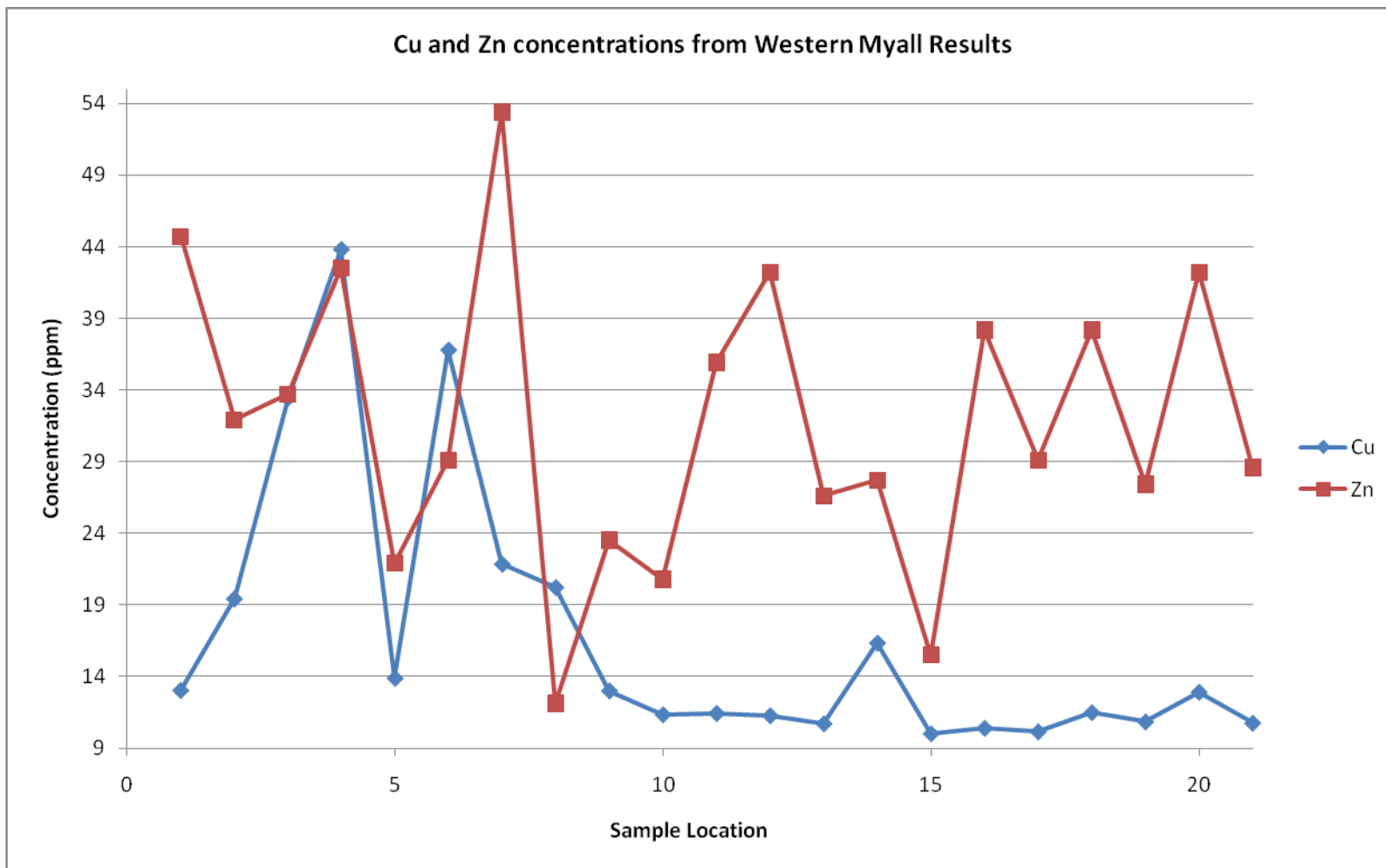


Figure 29.

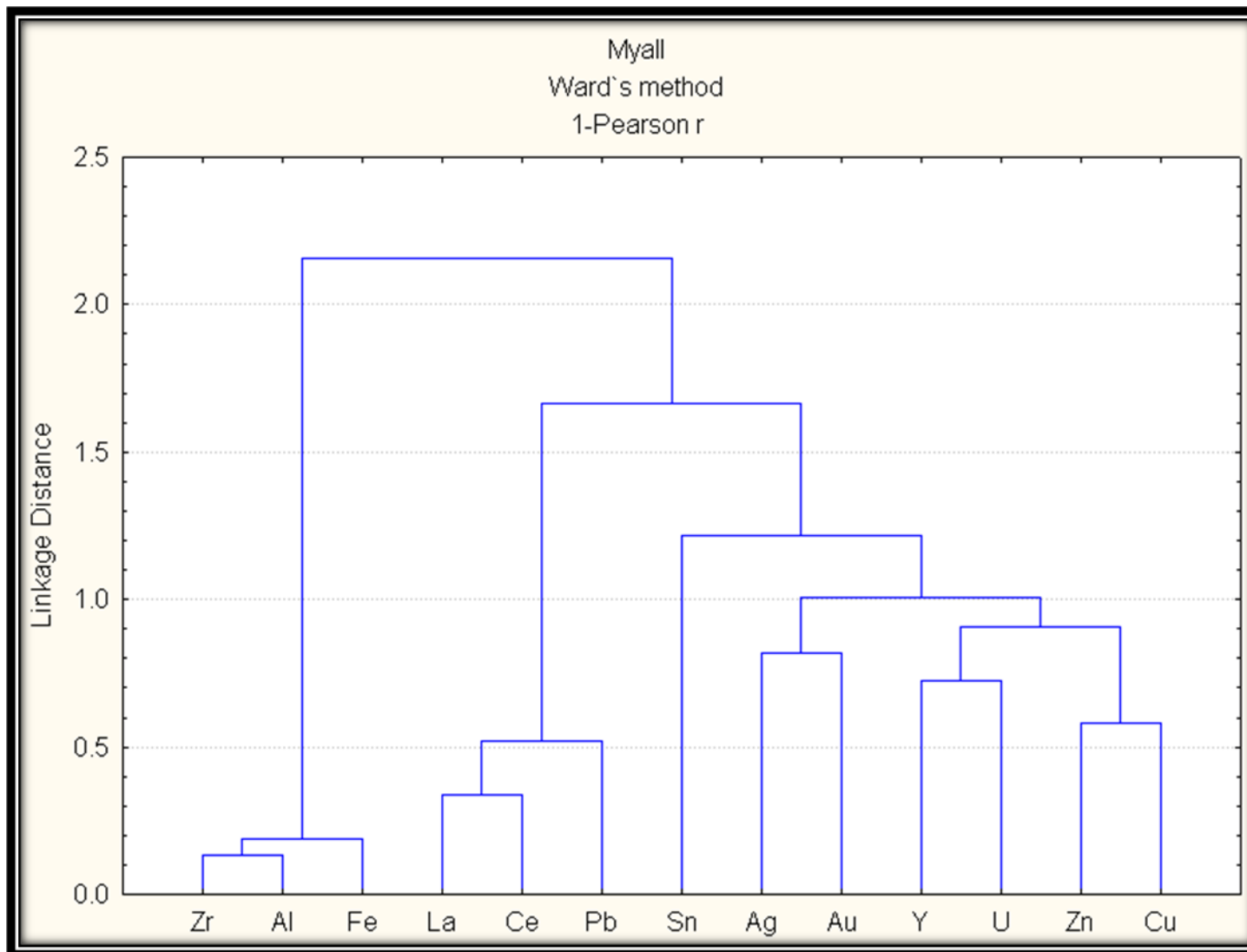


Figure 30.

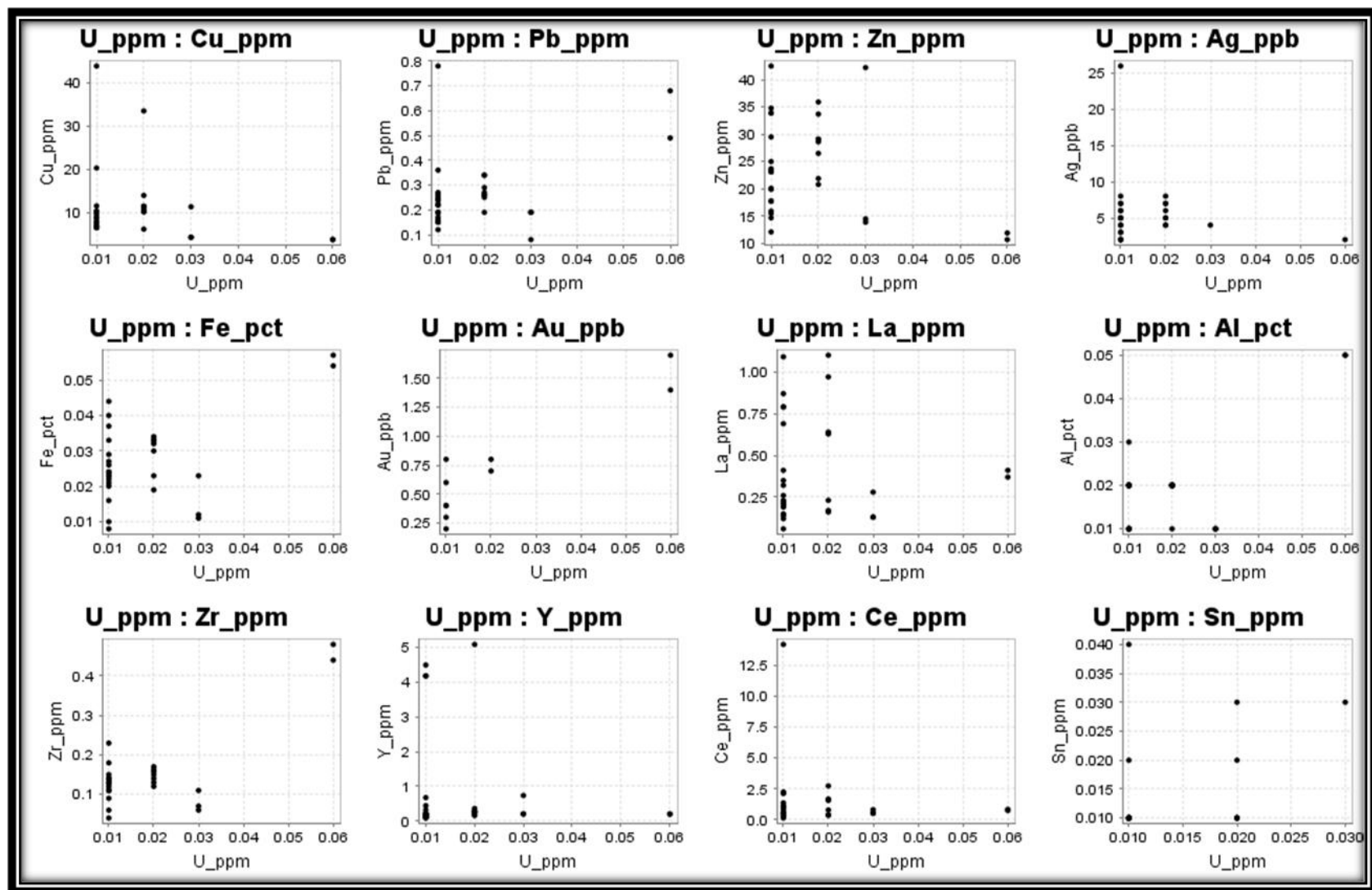


Figure 31.

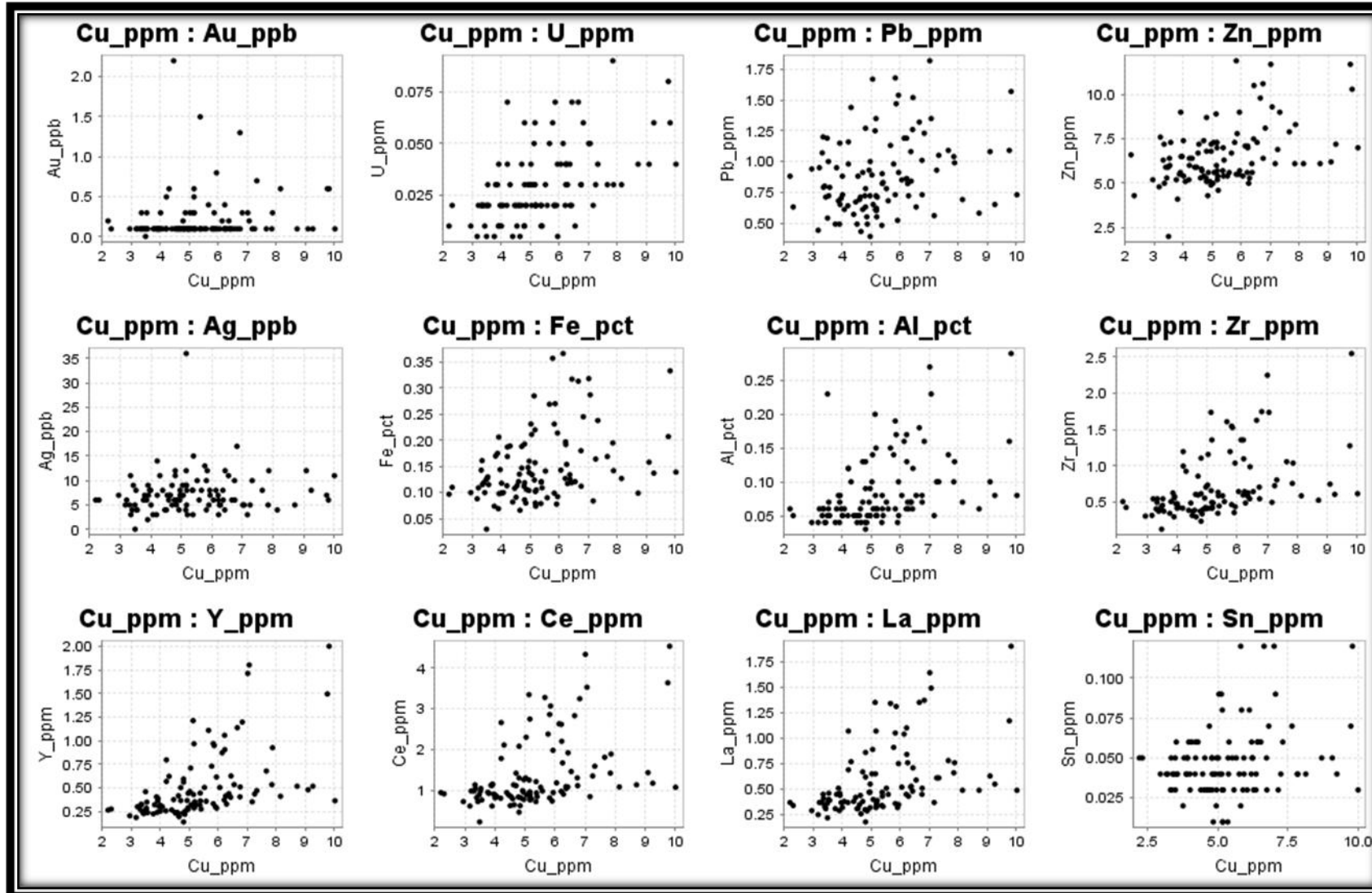


Figure 32.

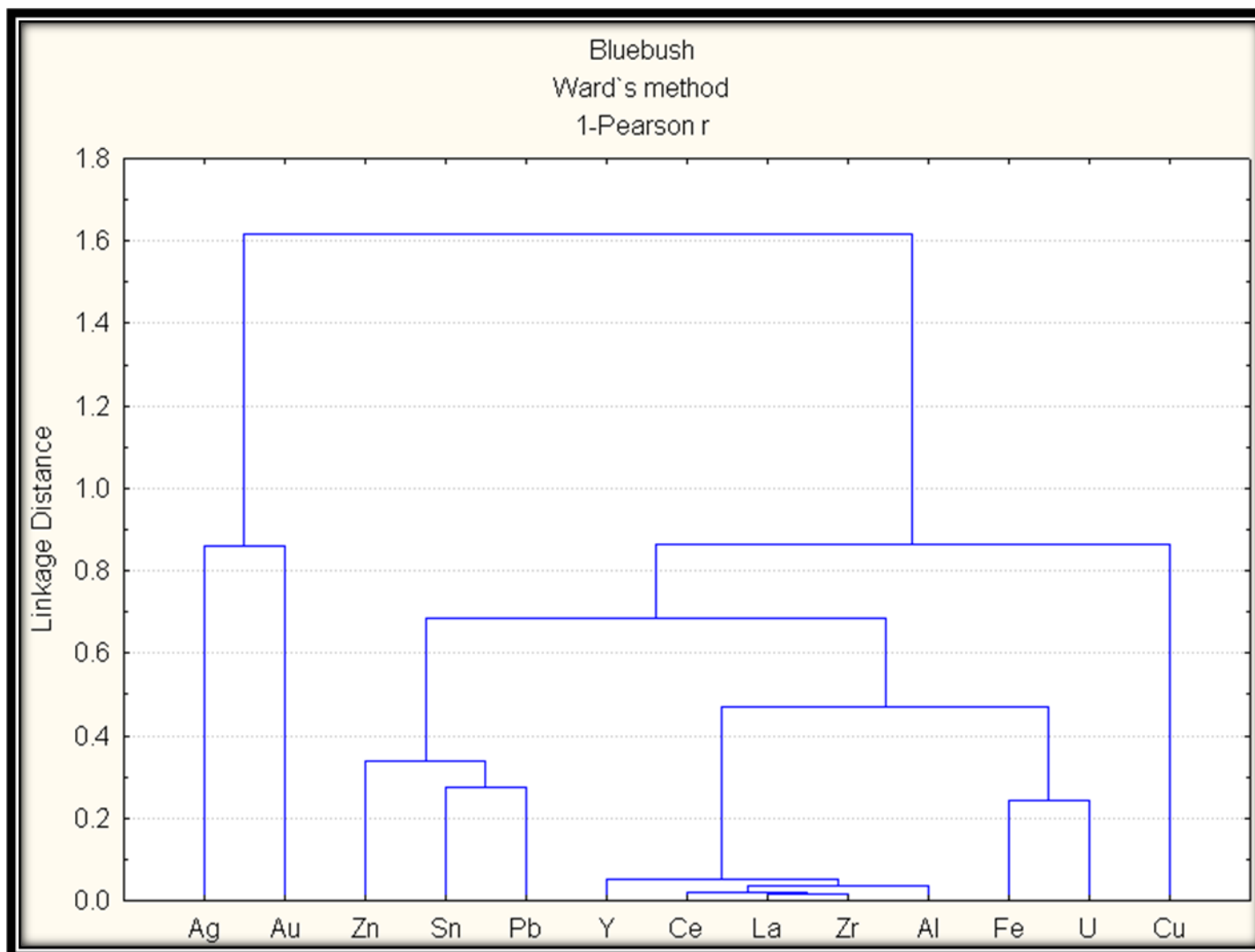




Figure 33.

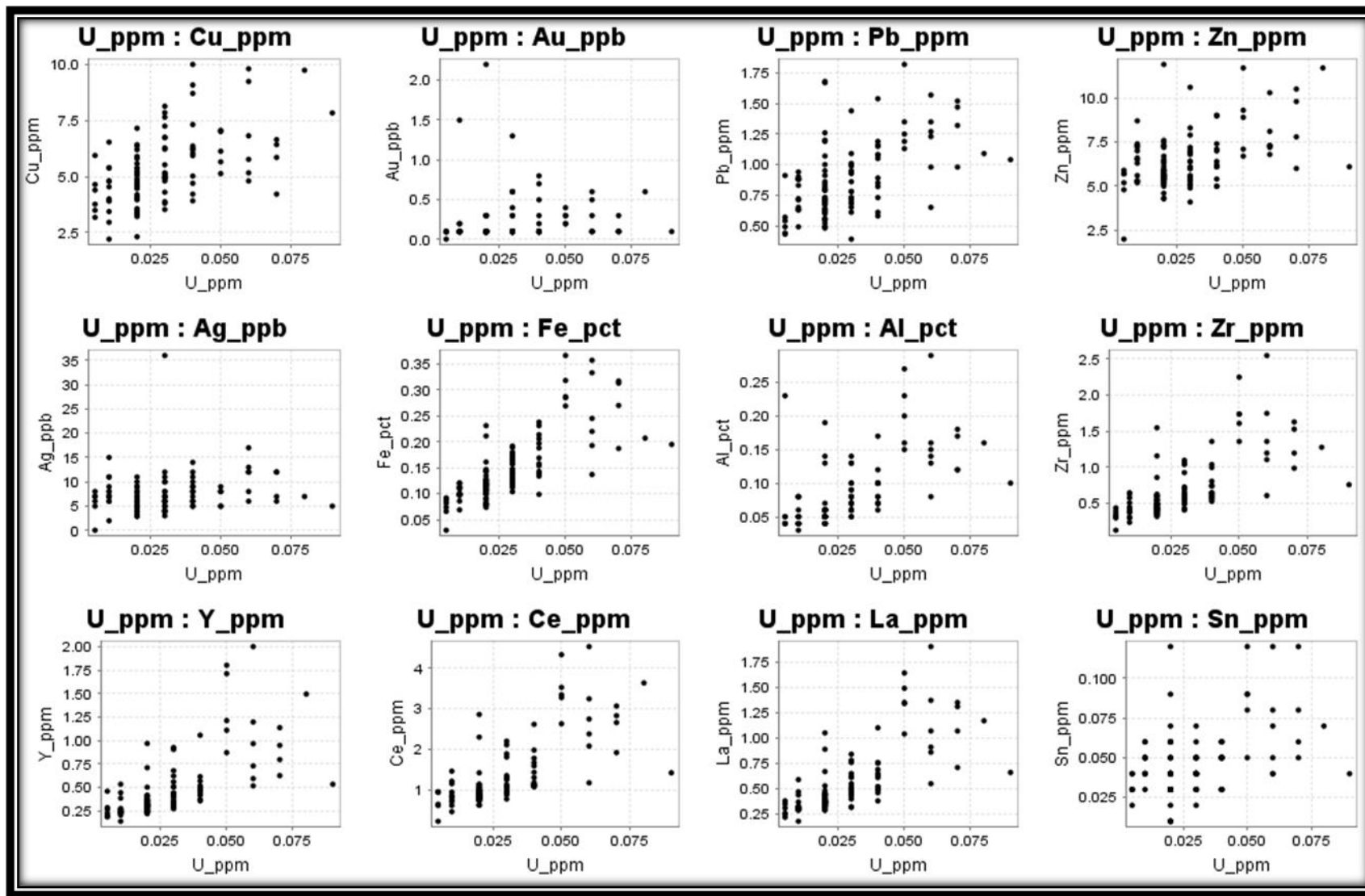




Figure 34.

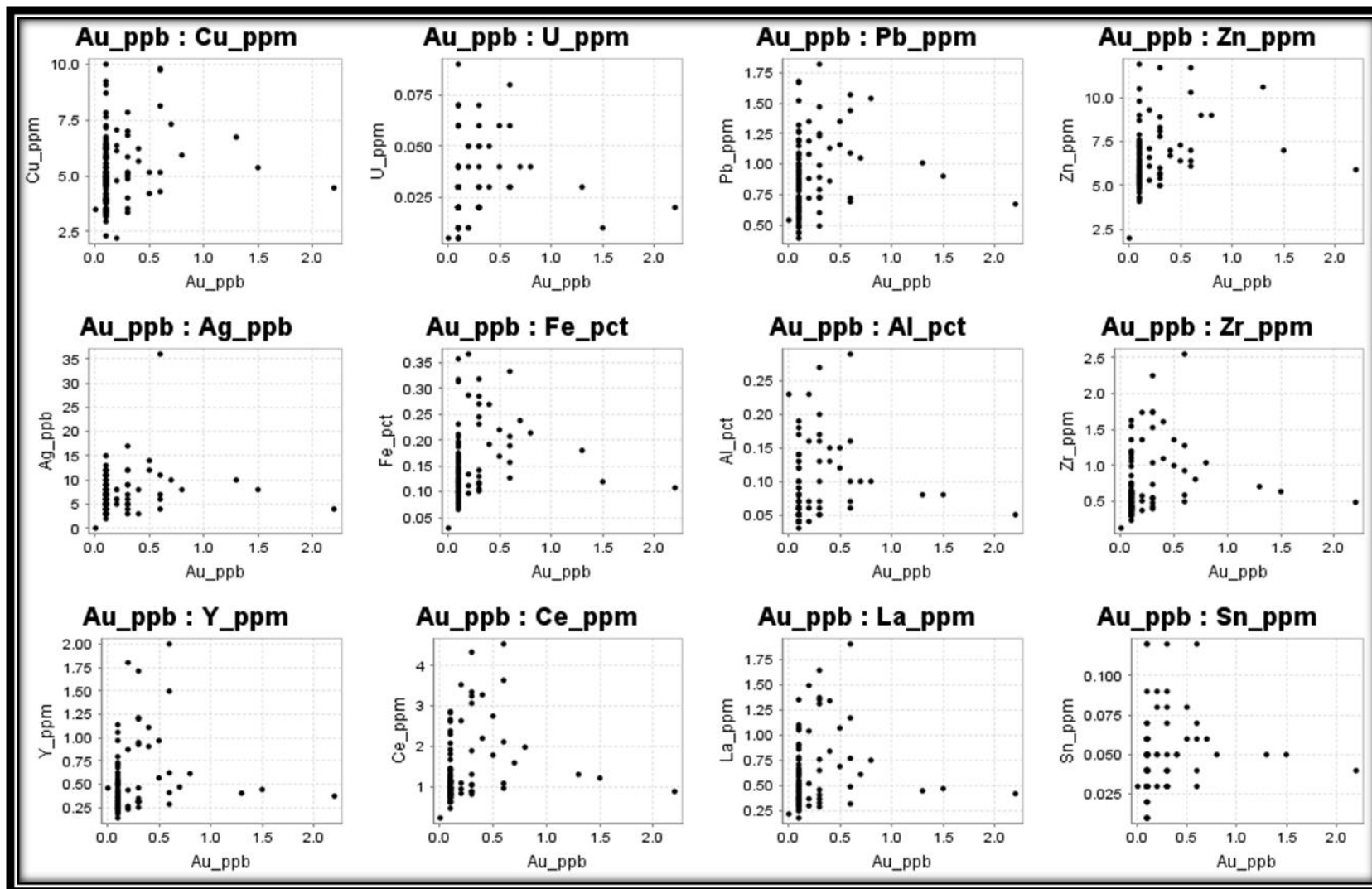


Figure 35.

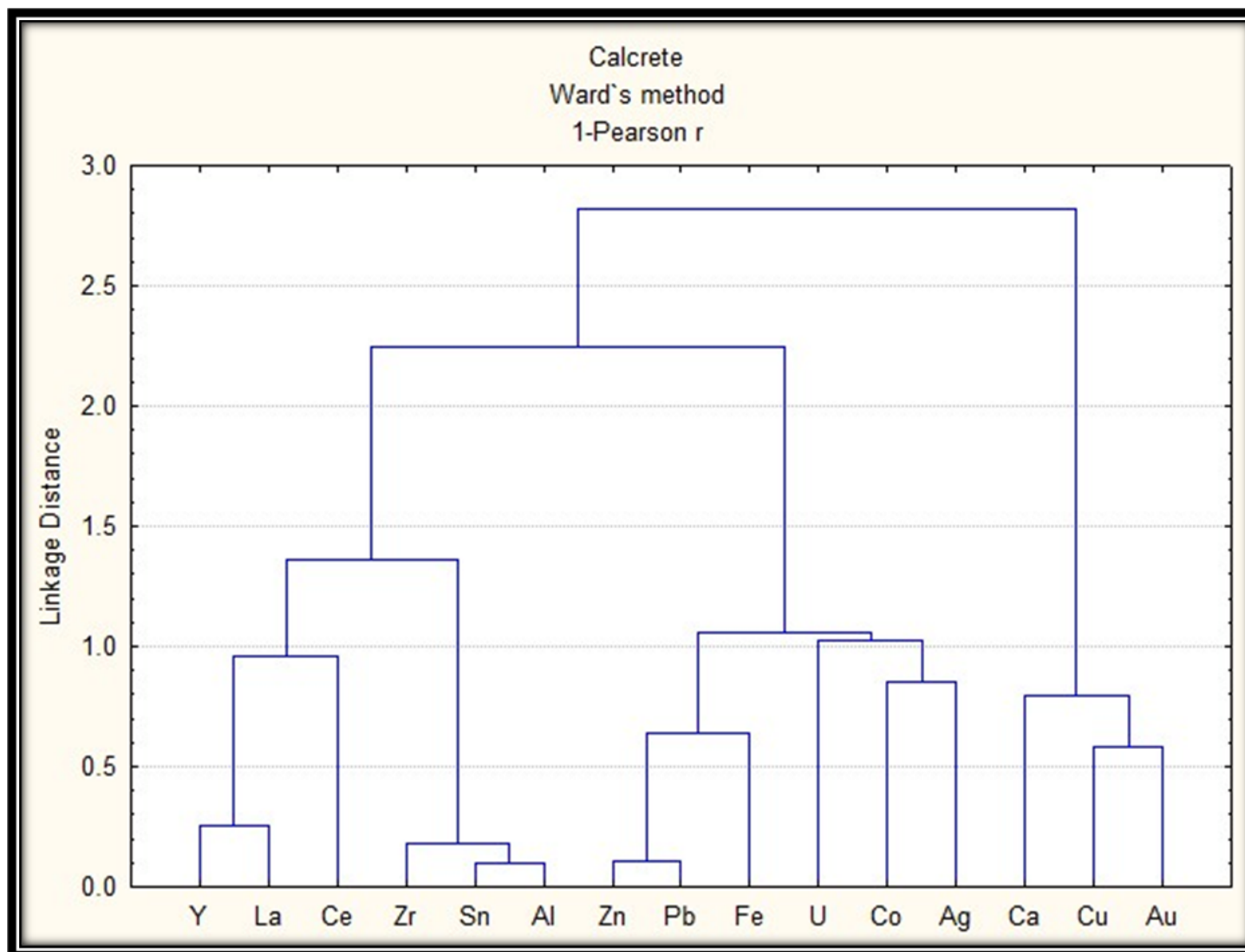


Figure 36.

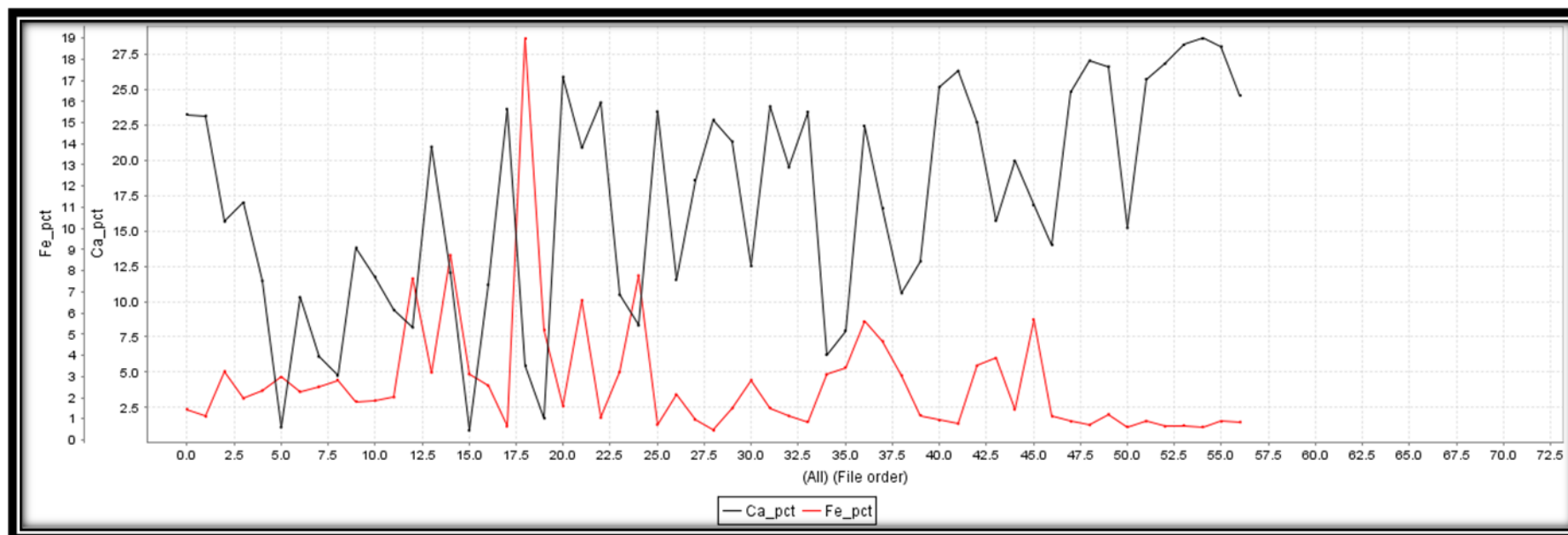


Figure 37.

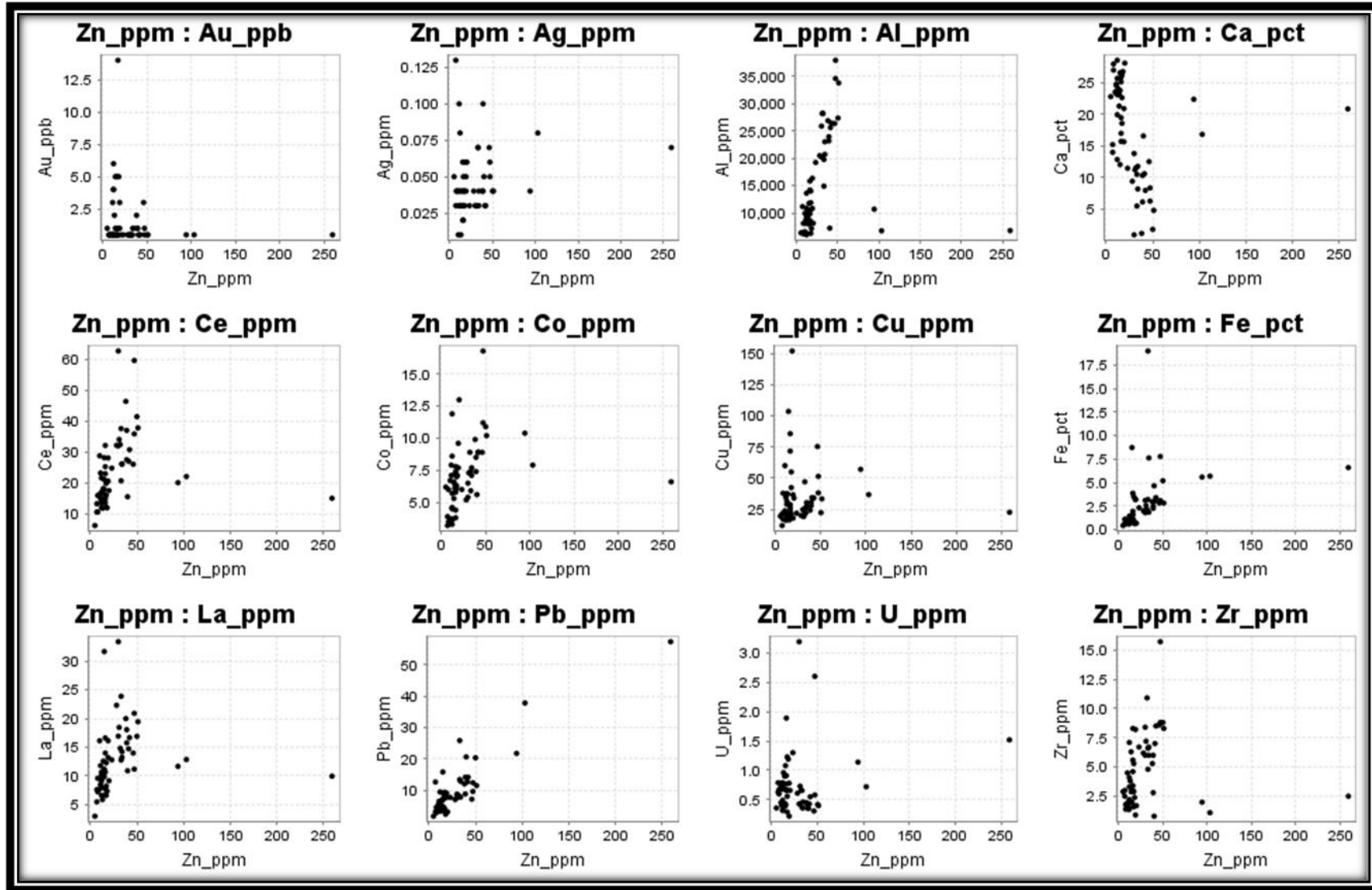


Figure 38.

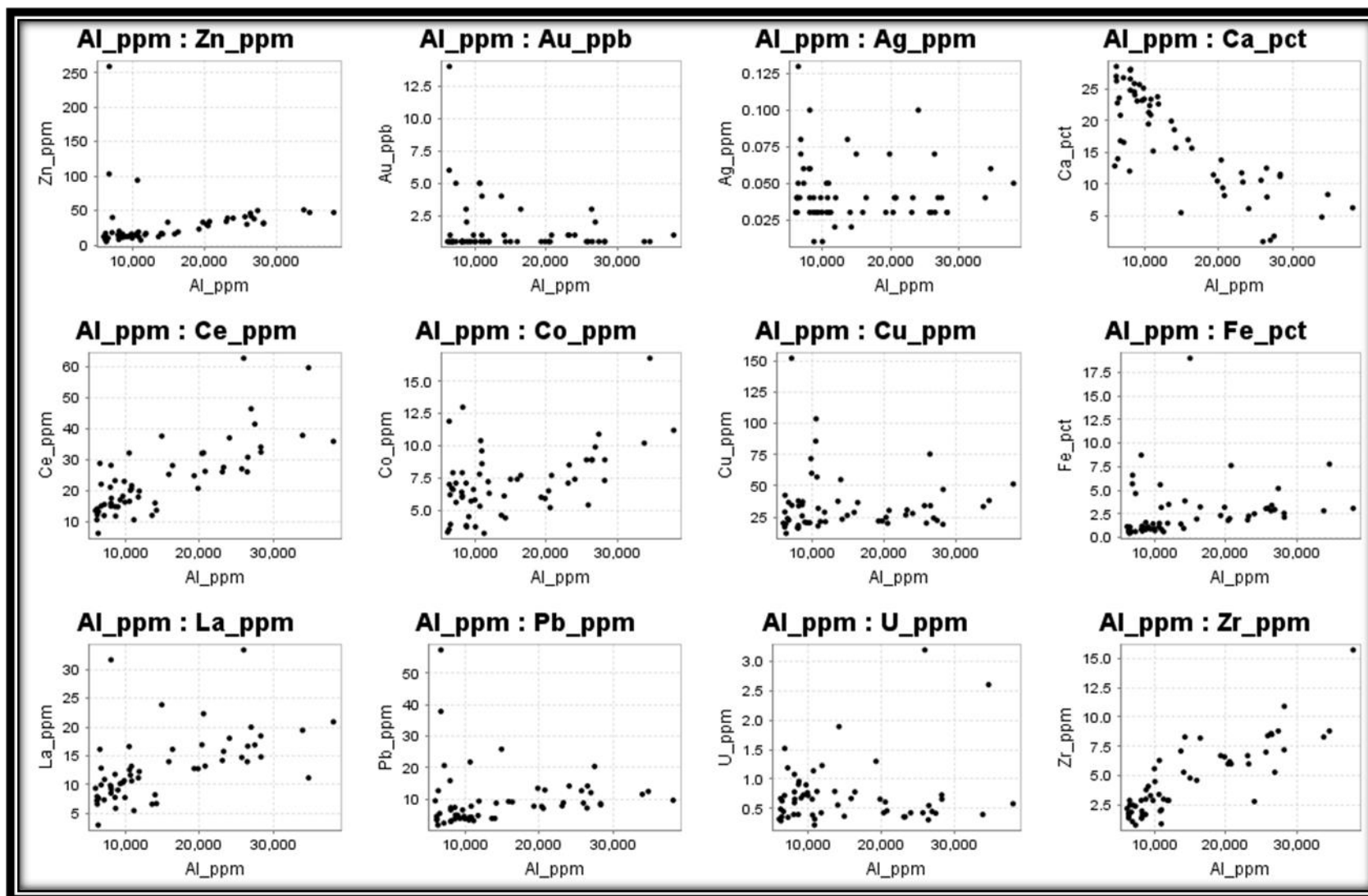




Figure 39.

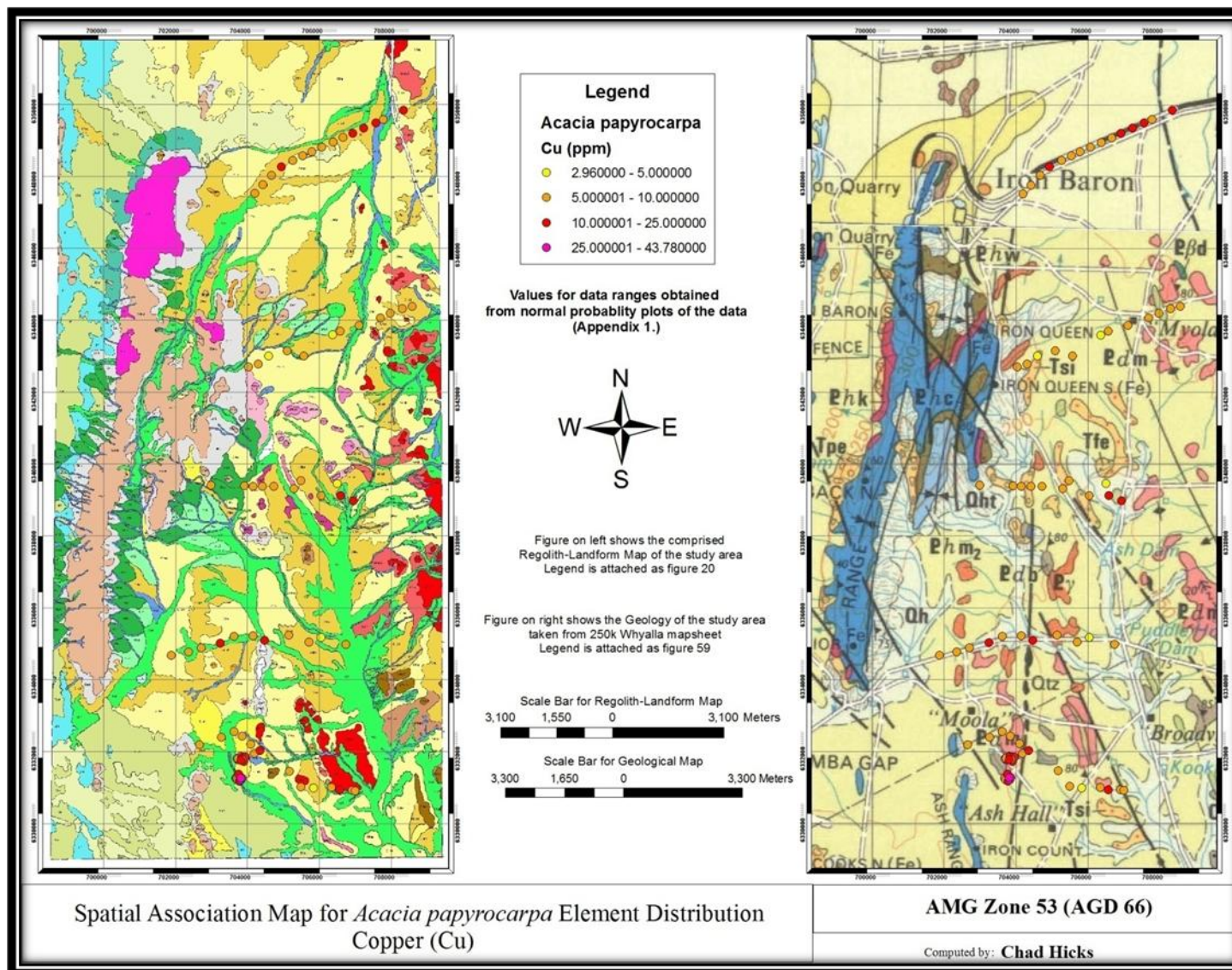




Figure 40.

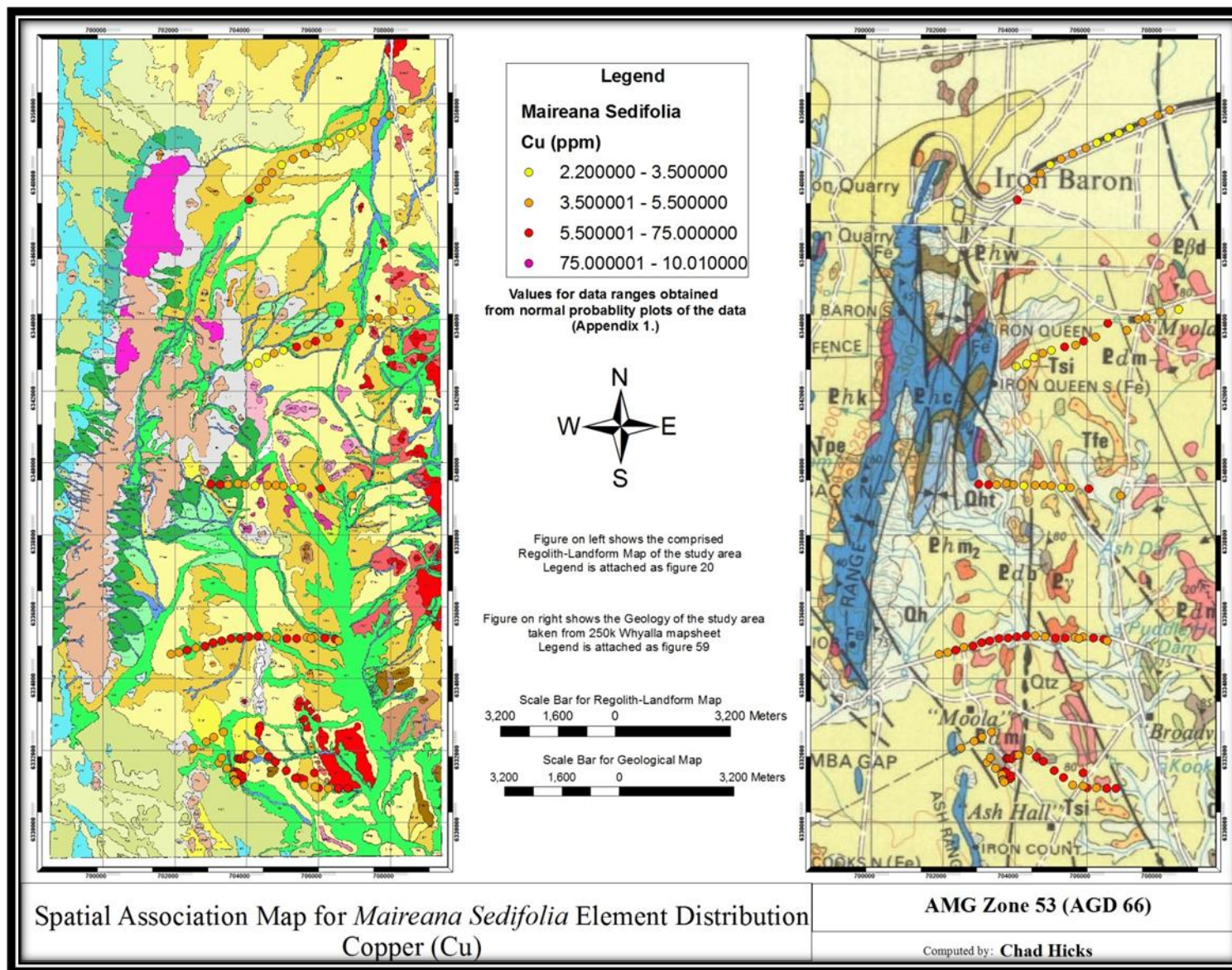




Figure 41.

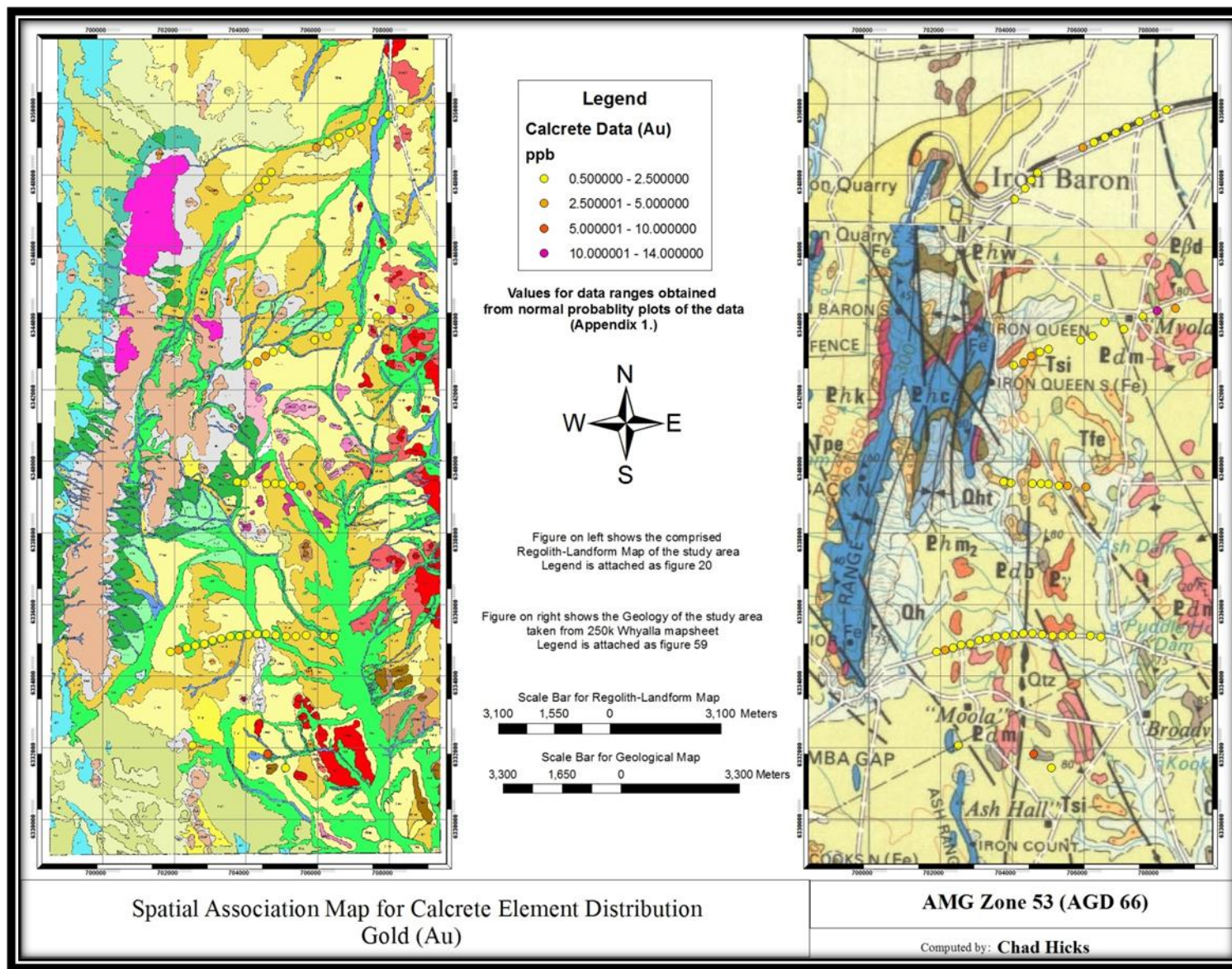




Figure 42.

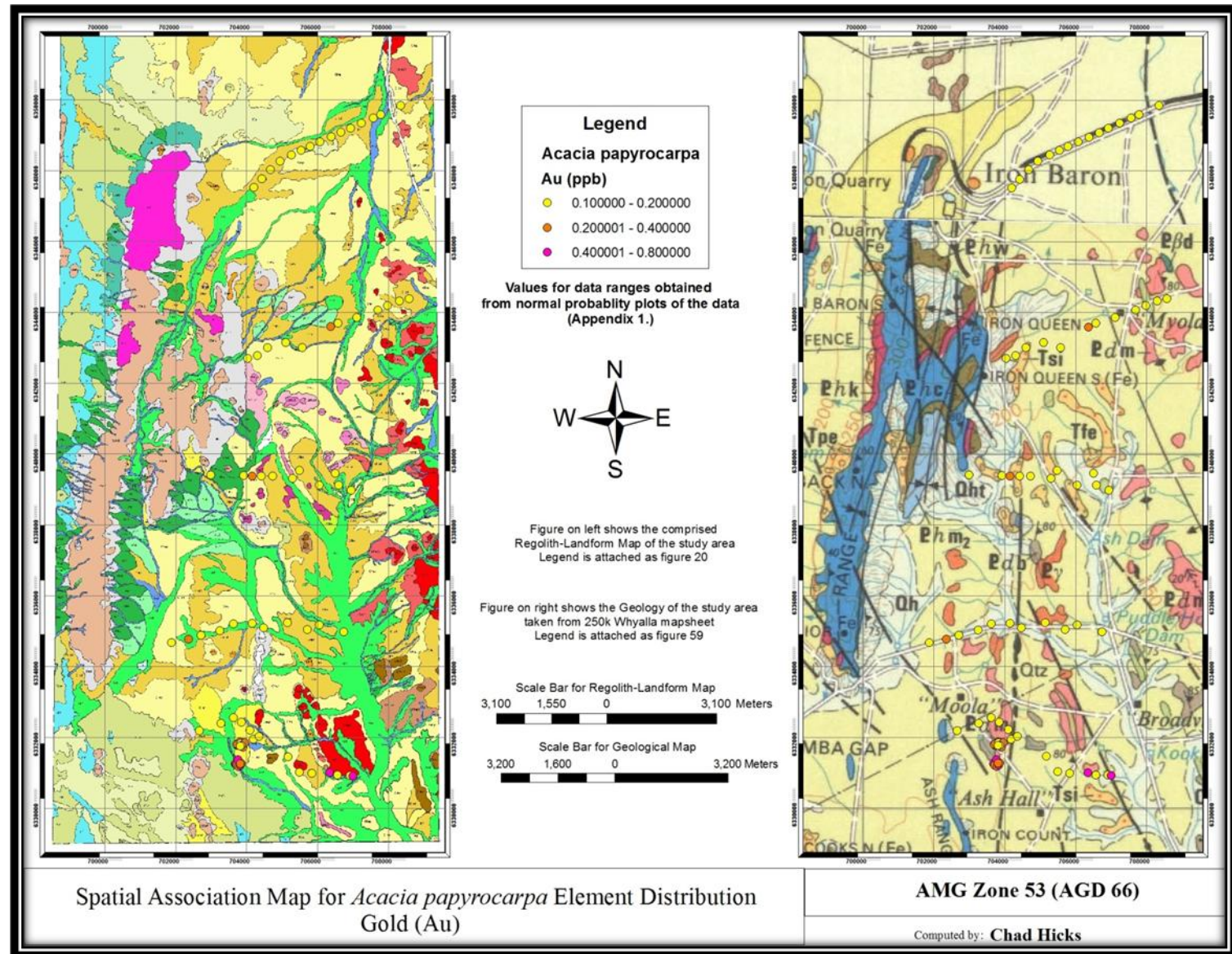




Figure 43.

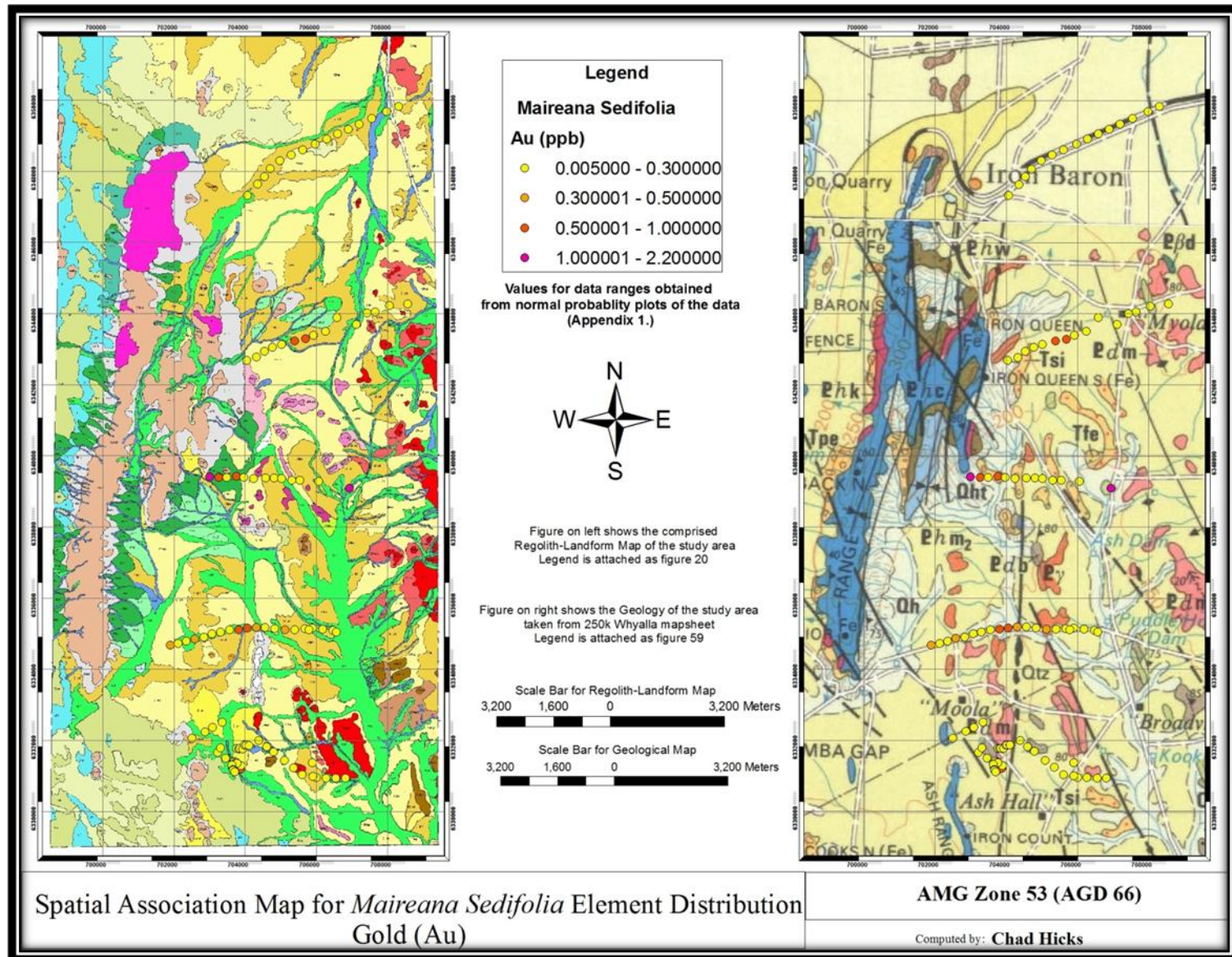




Figure 44.

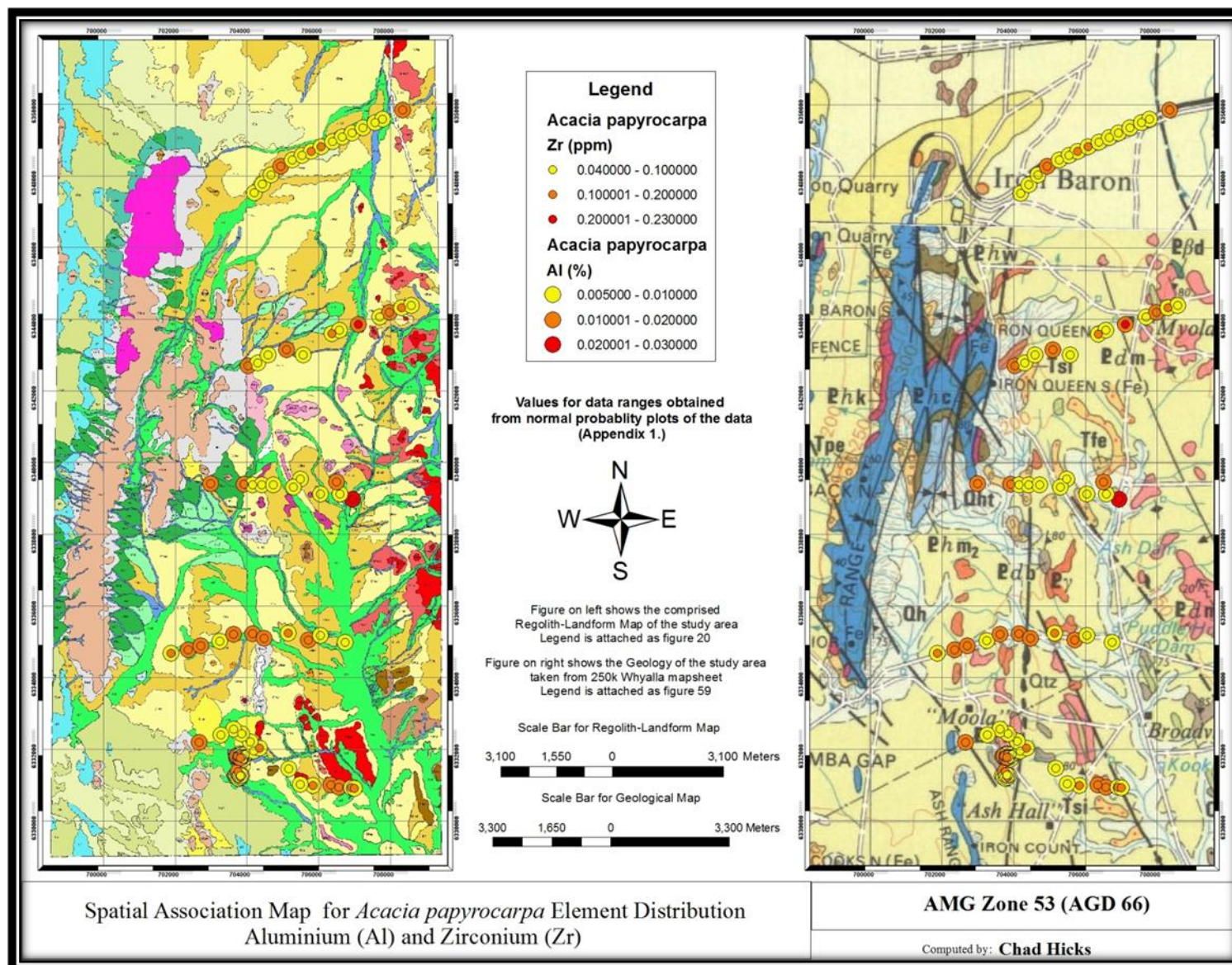




Figure 45.

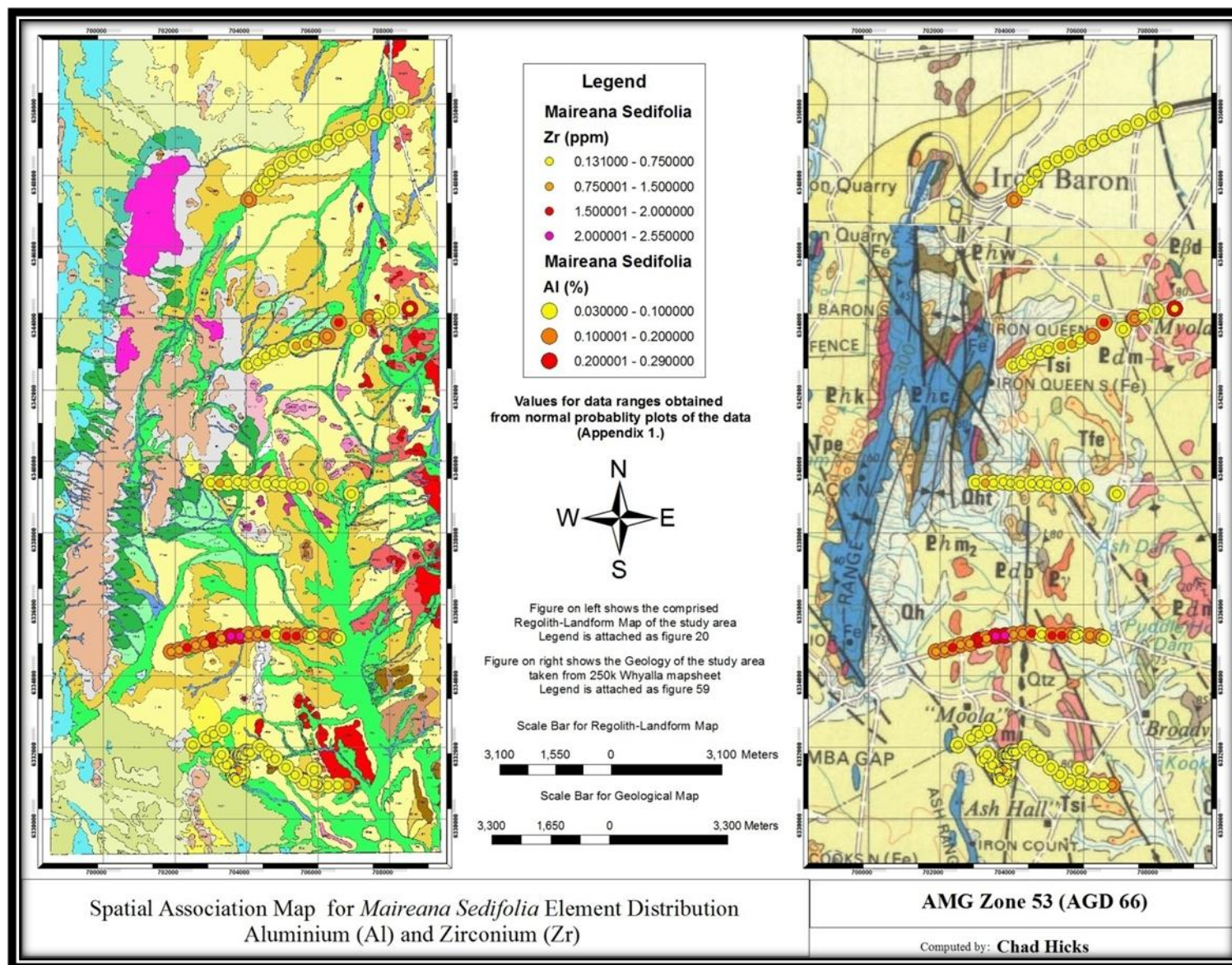




Figure 46.

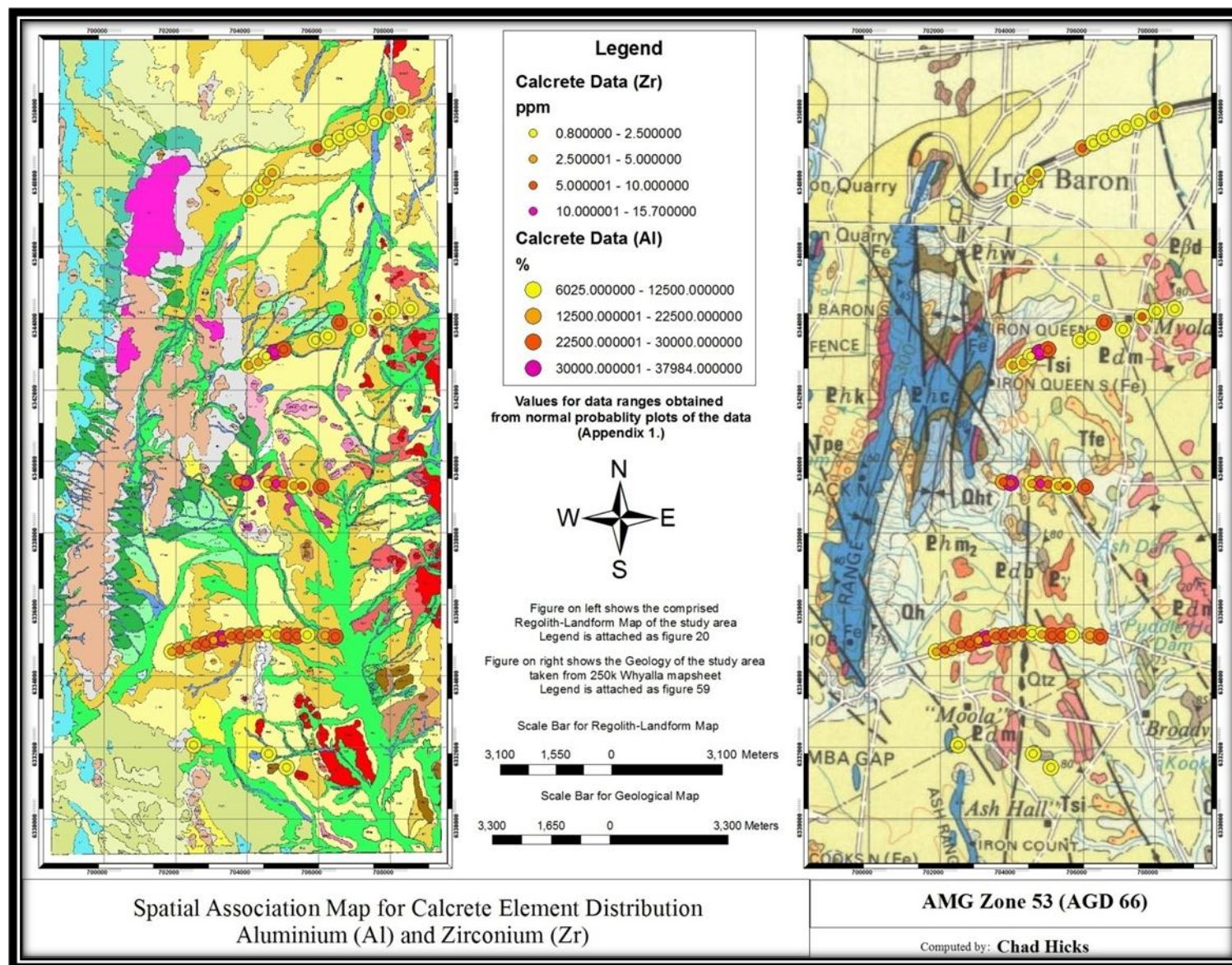




Figure 47.

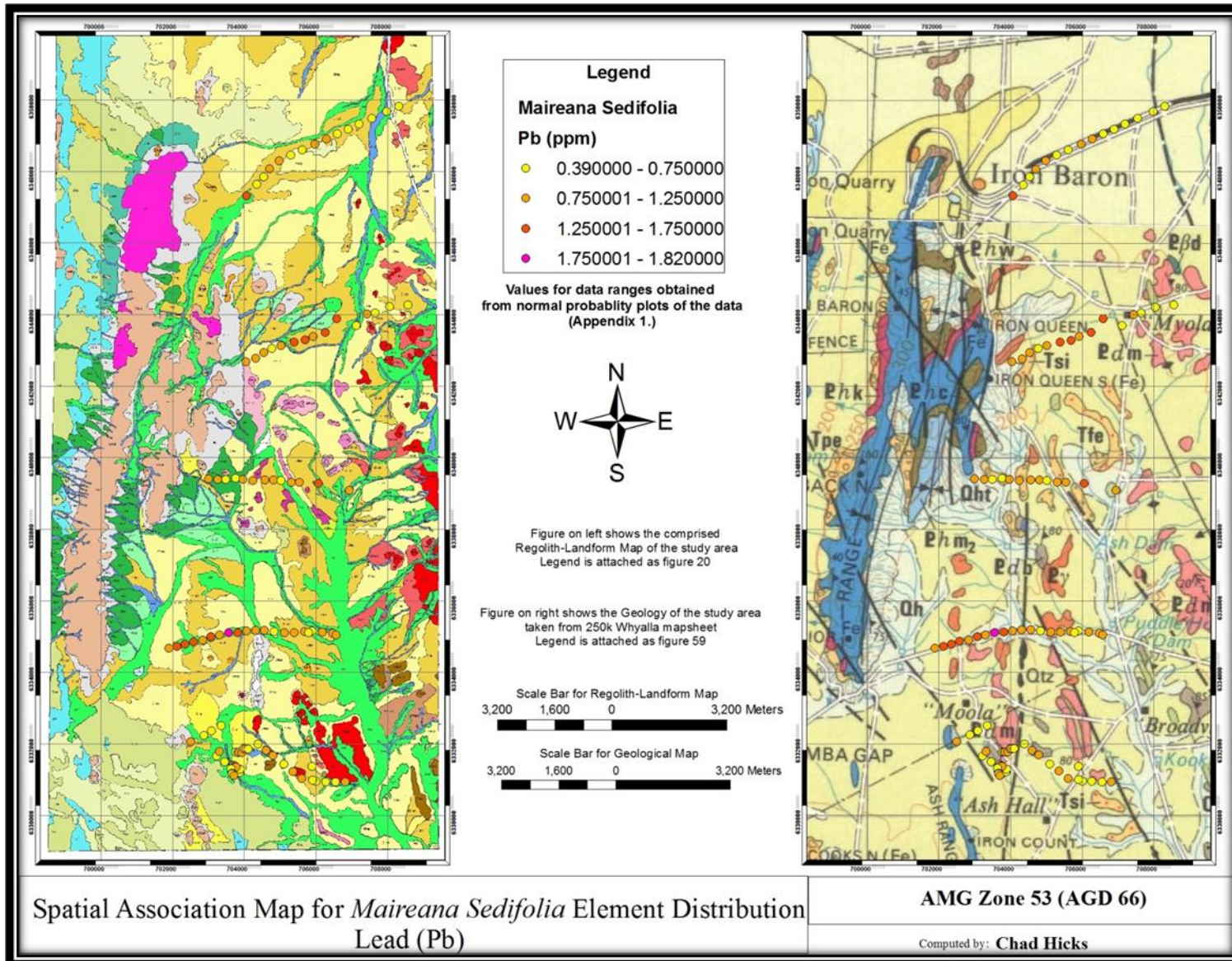




Figure 48.

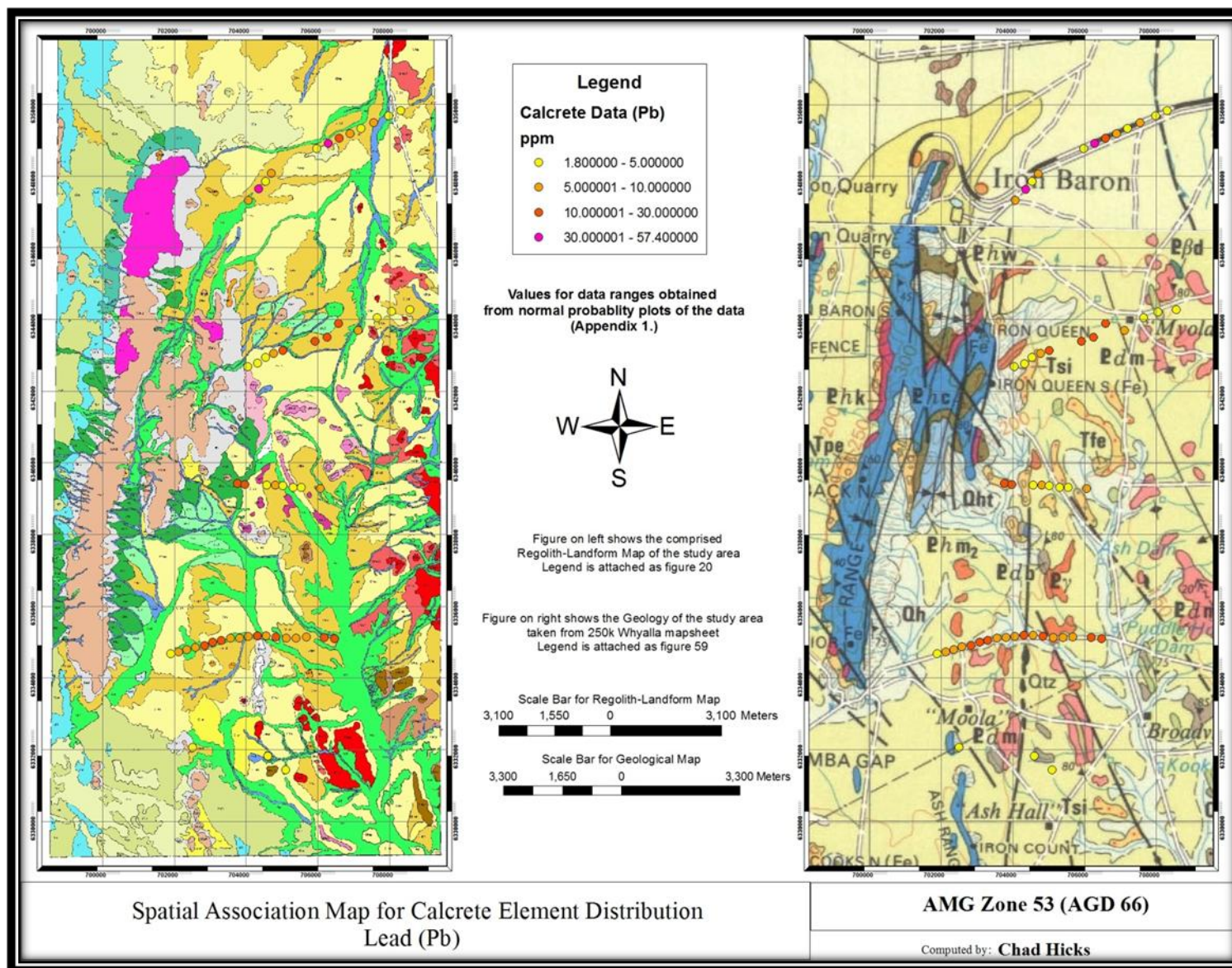




Figure 49.

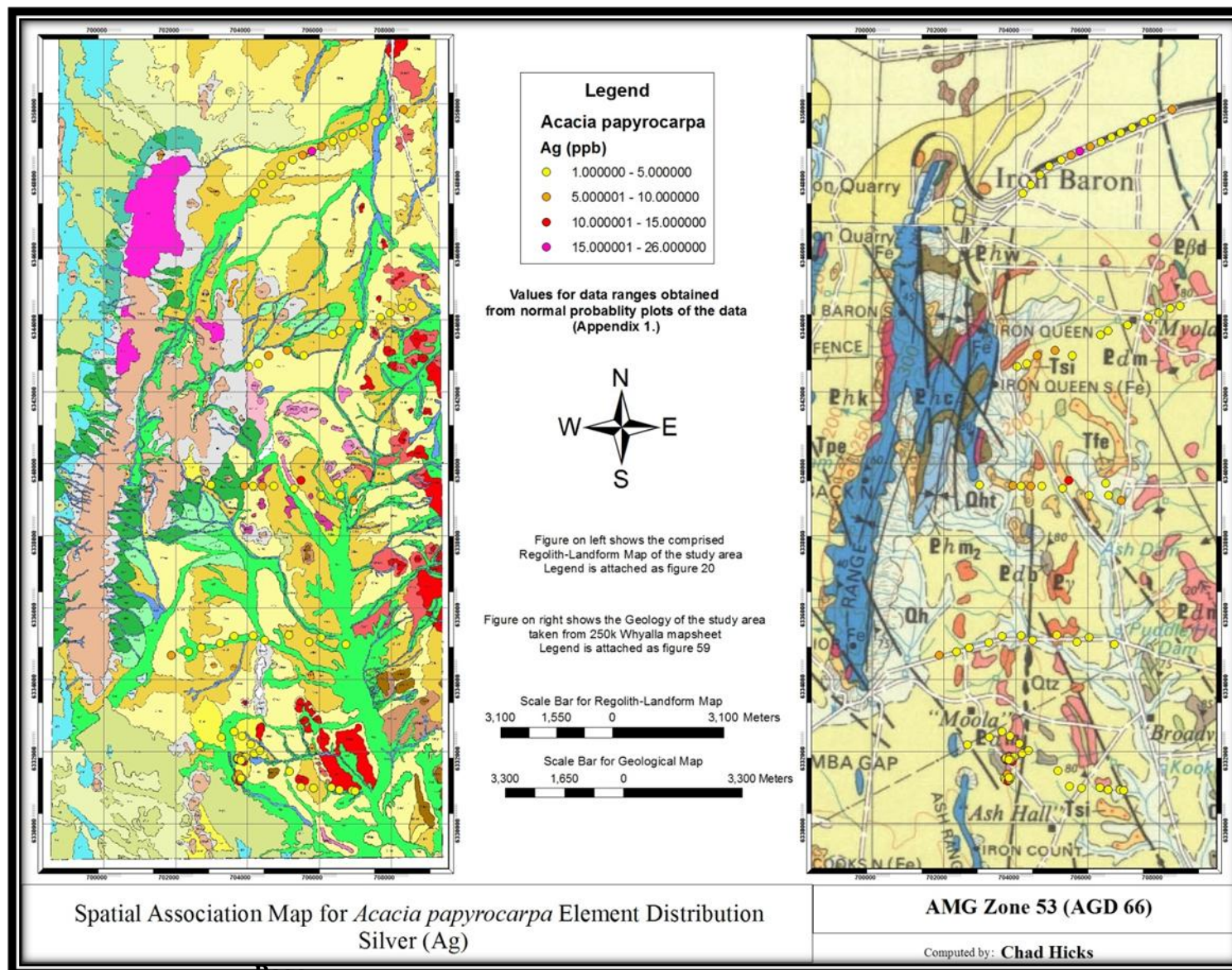




Figure 50.

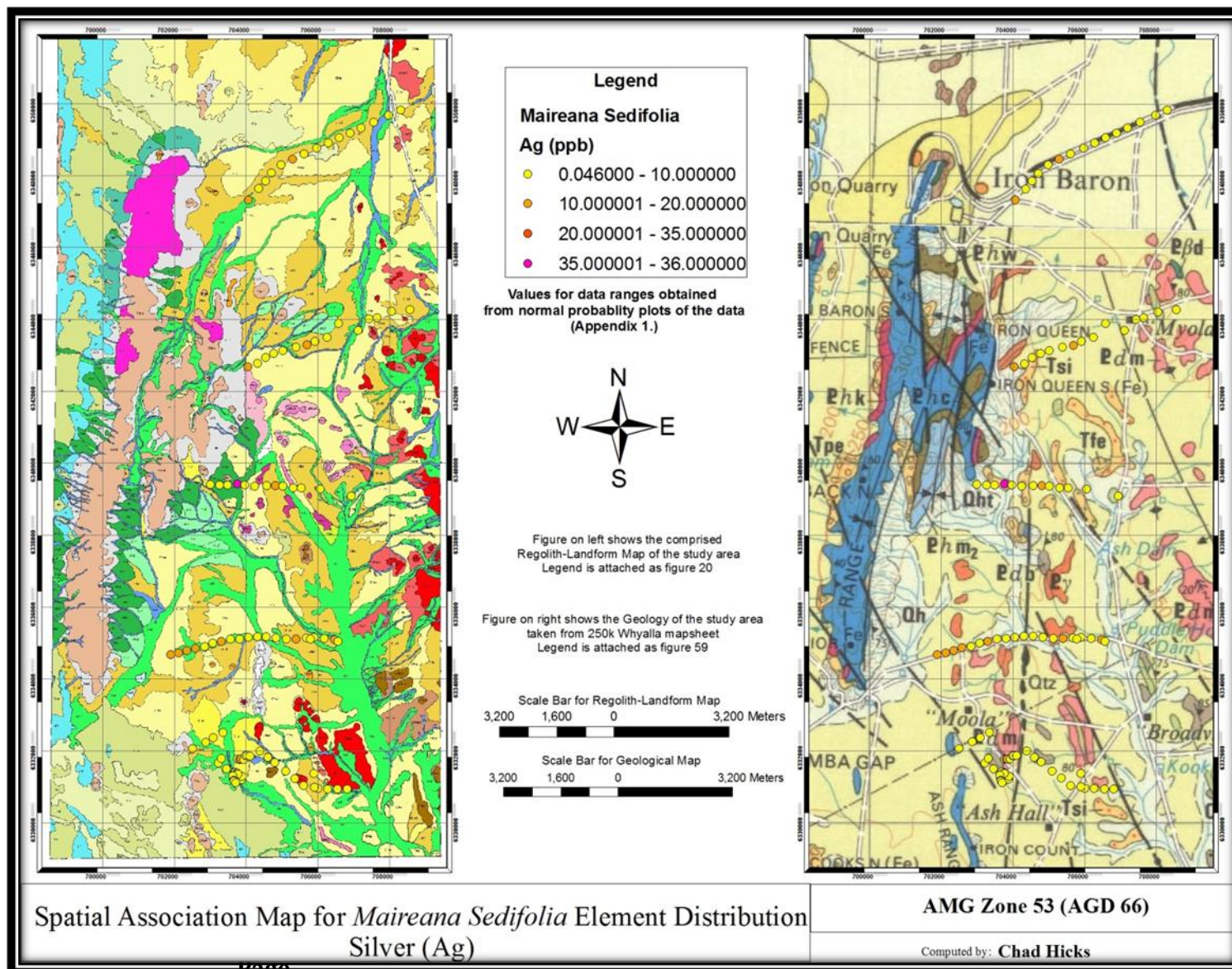




Figure 51.

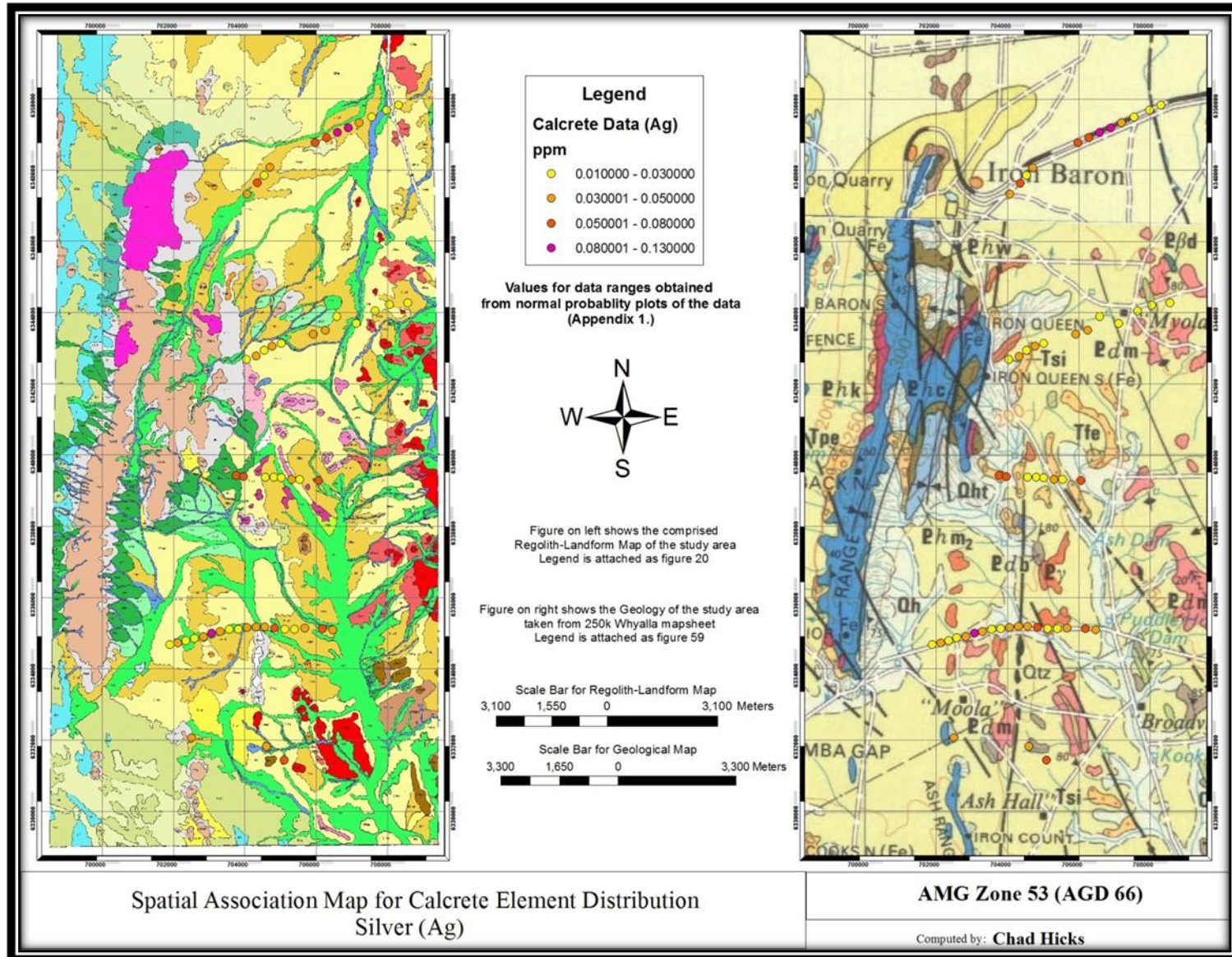




Figure 52.

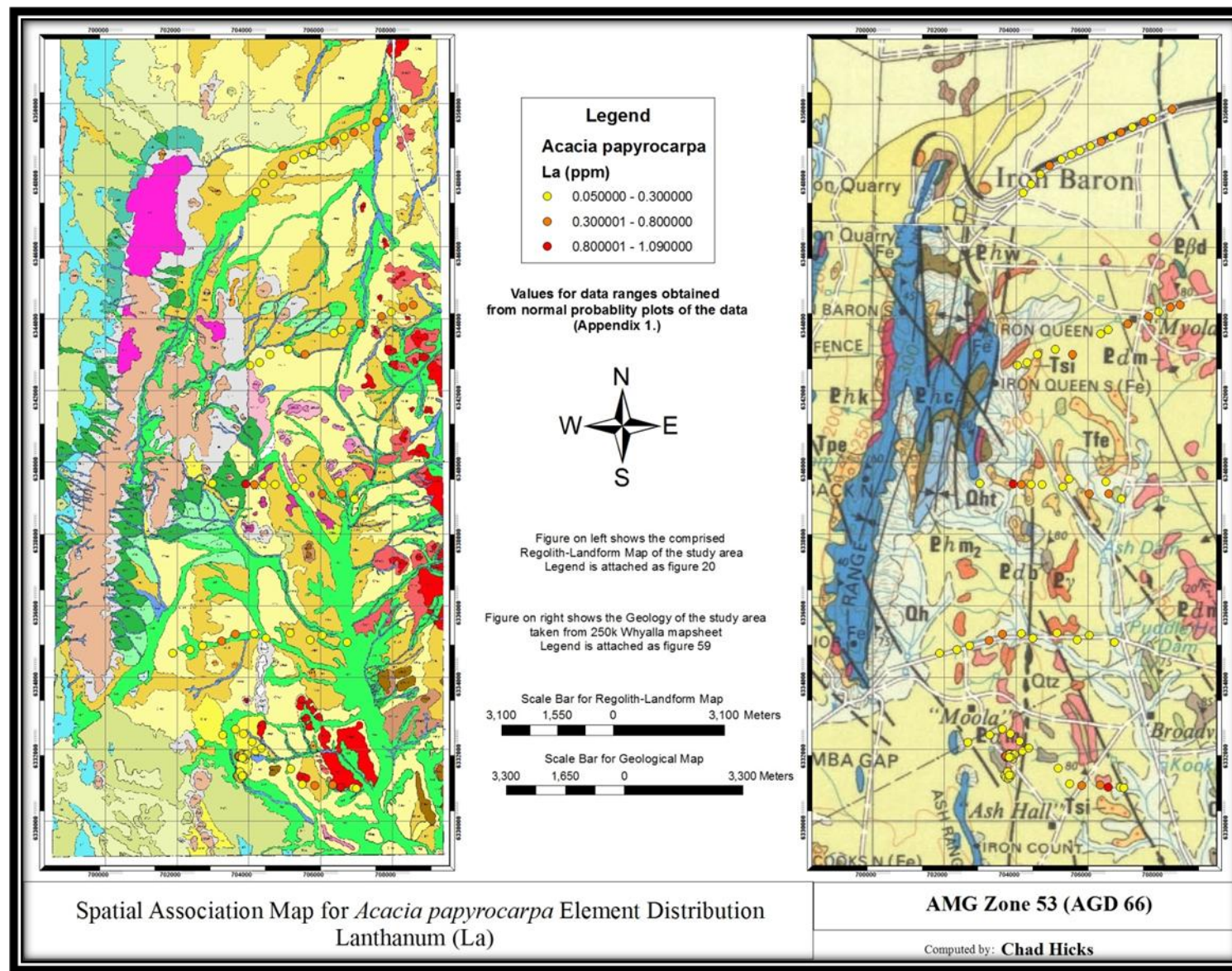




Figure 53.

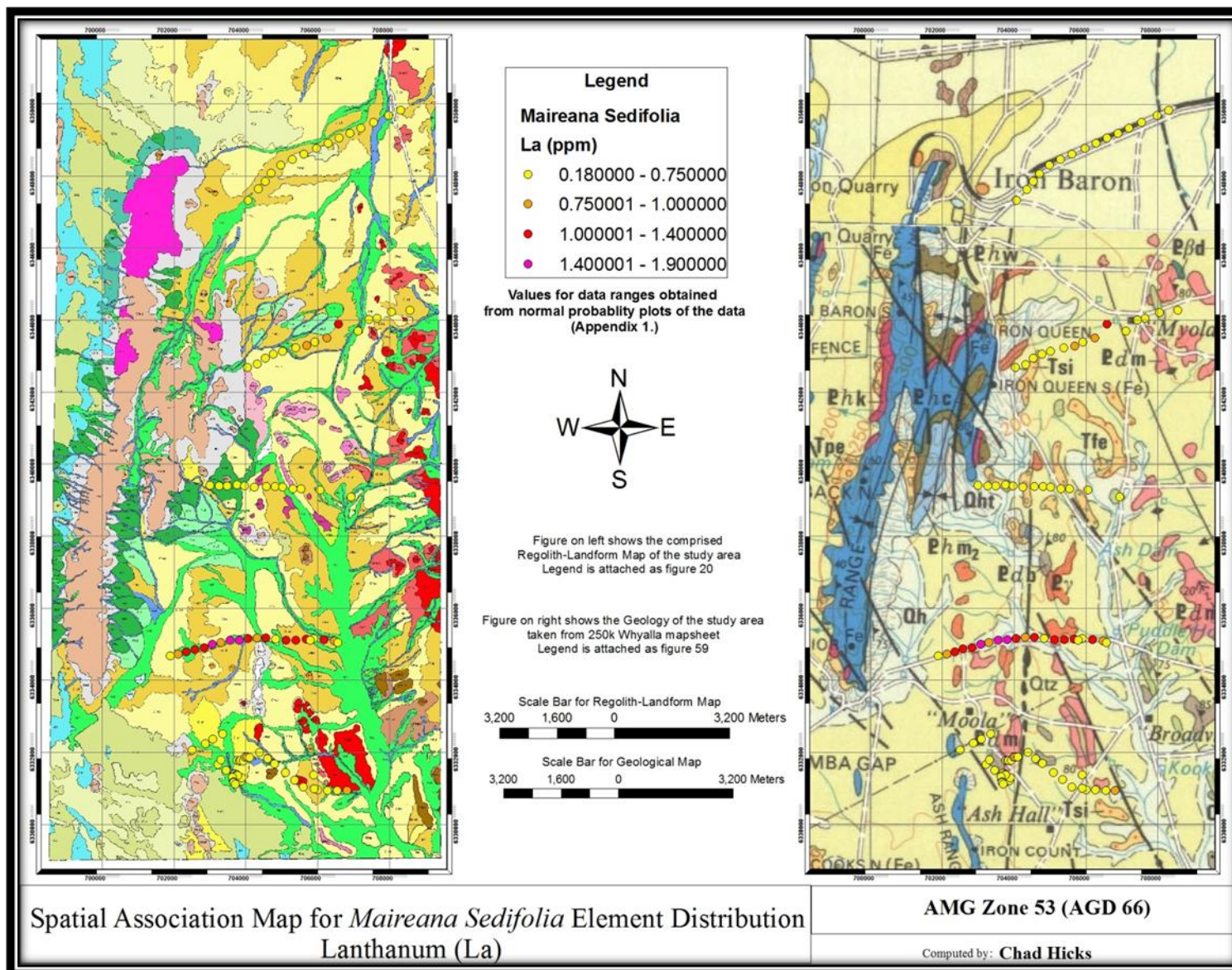




Figure 54.



Figure 55.

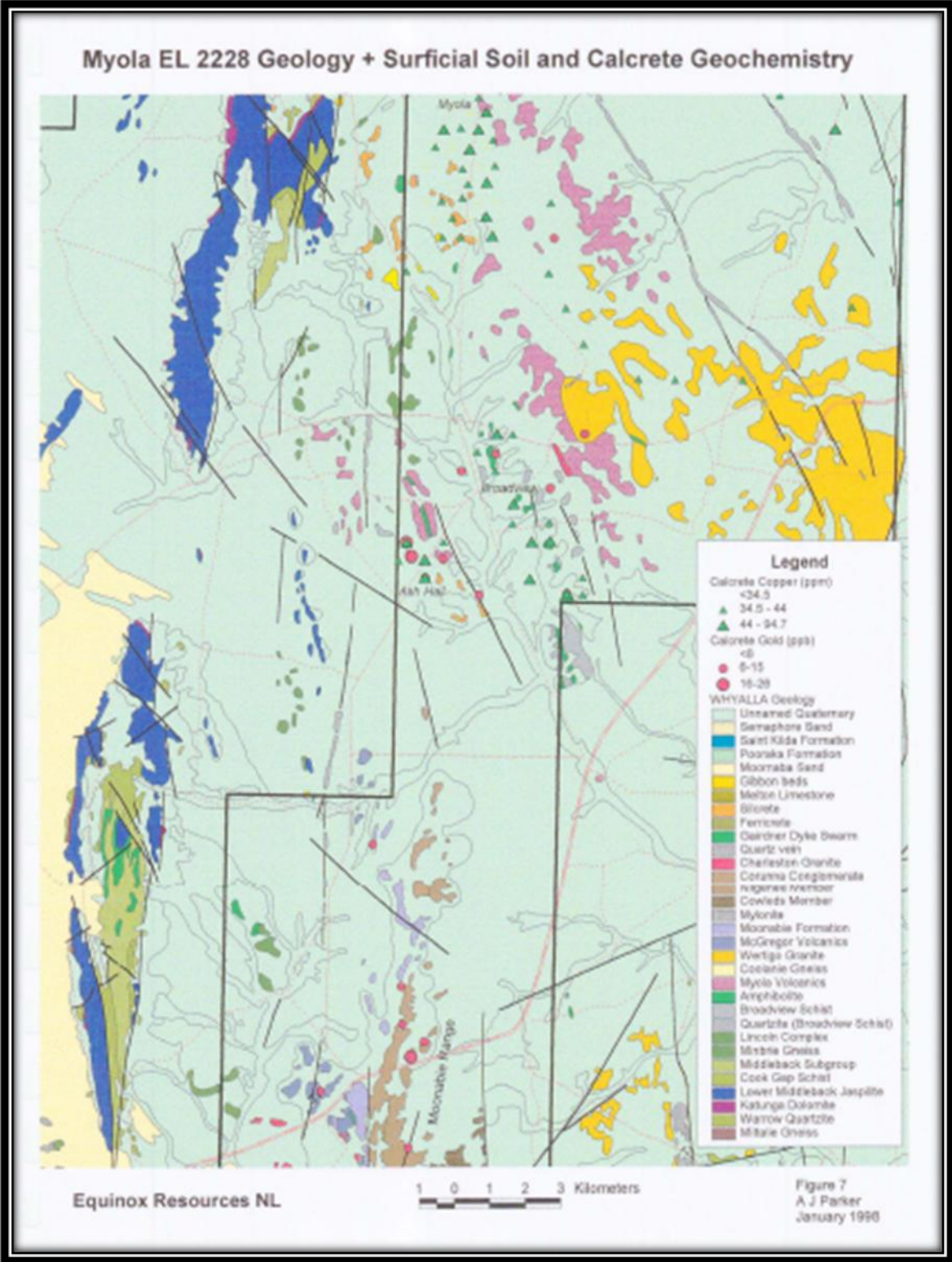




Figure 56.



Figure 57.





Figure 58.

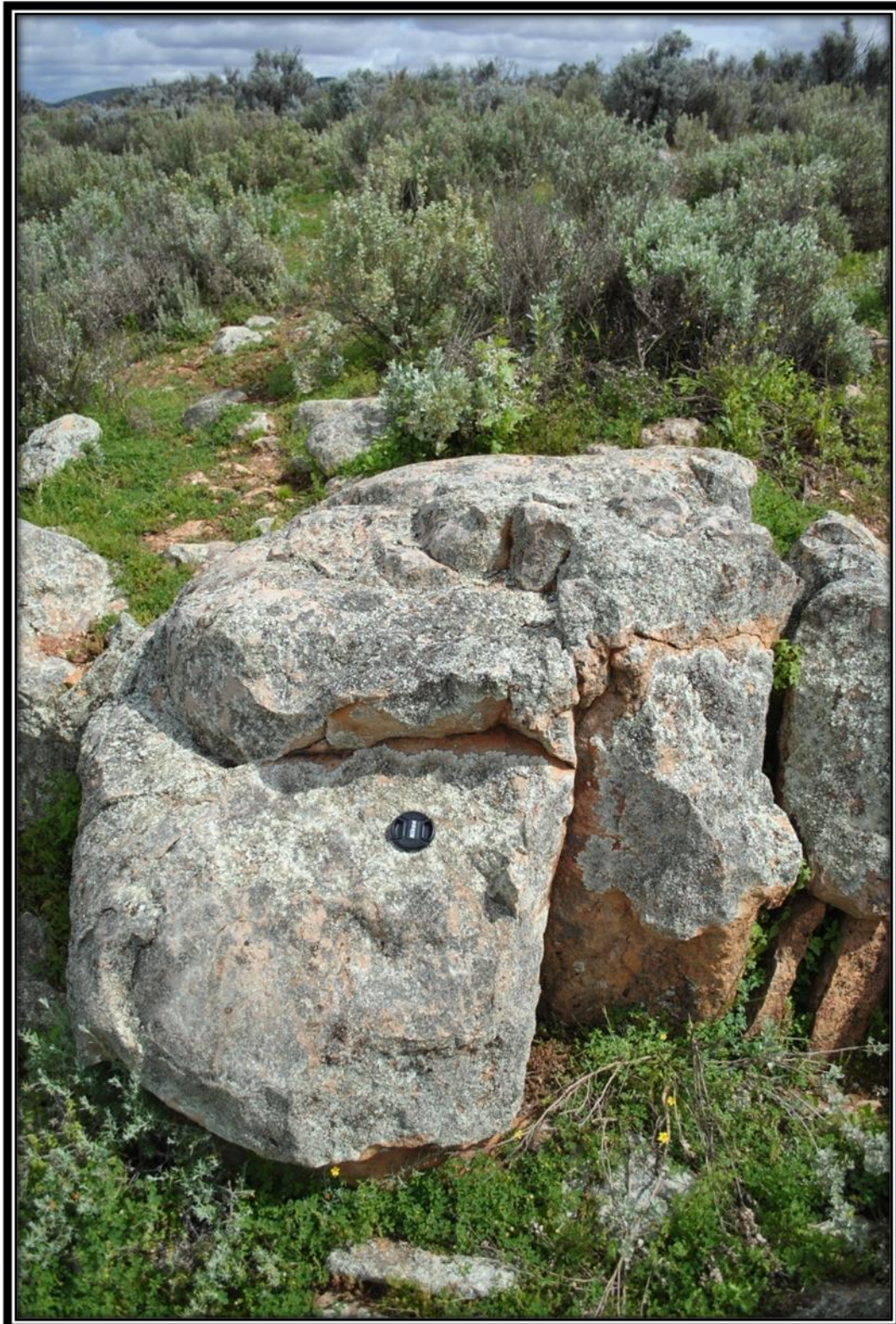




Figure 59.

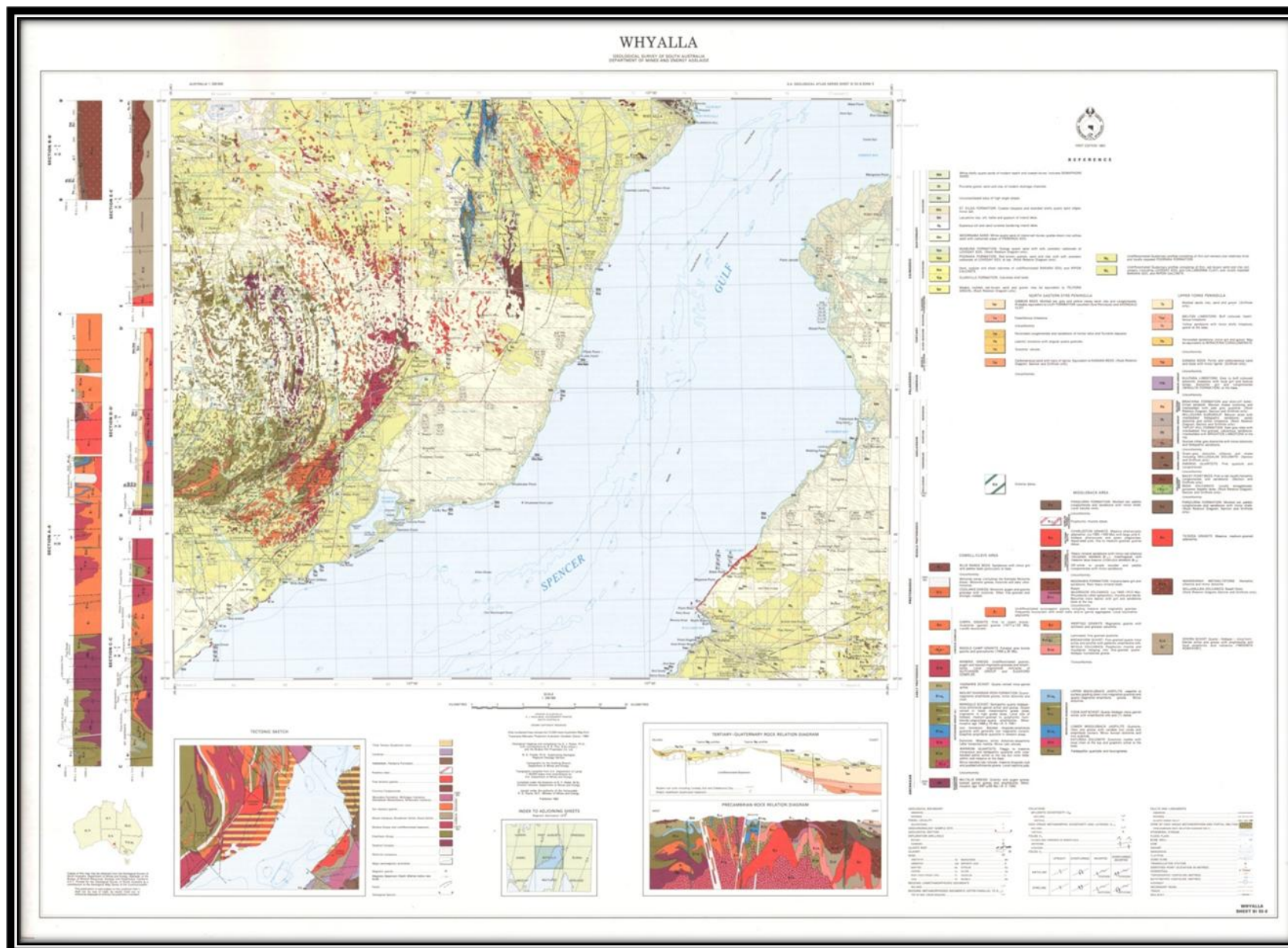


Figure 60.

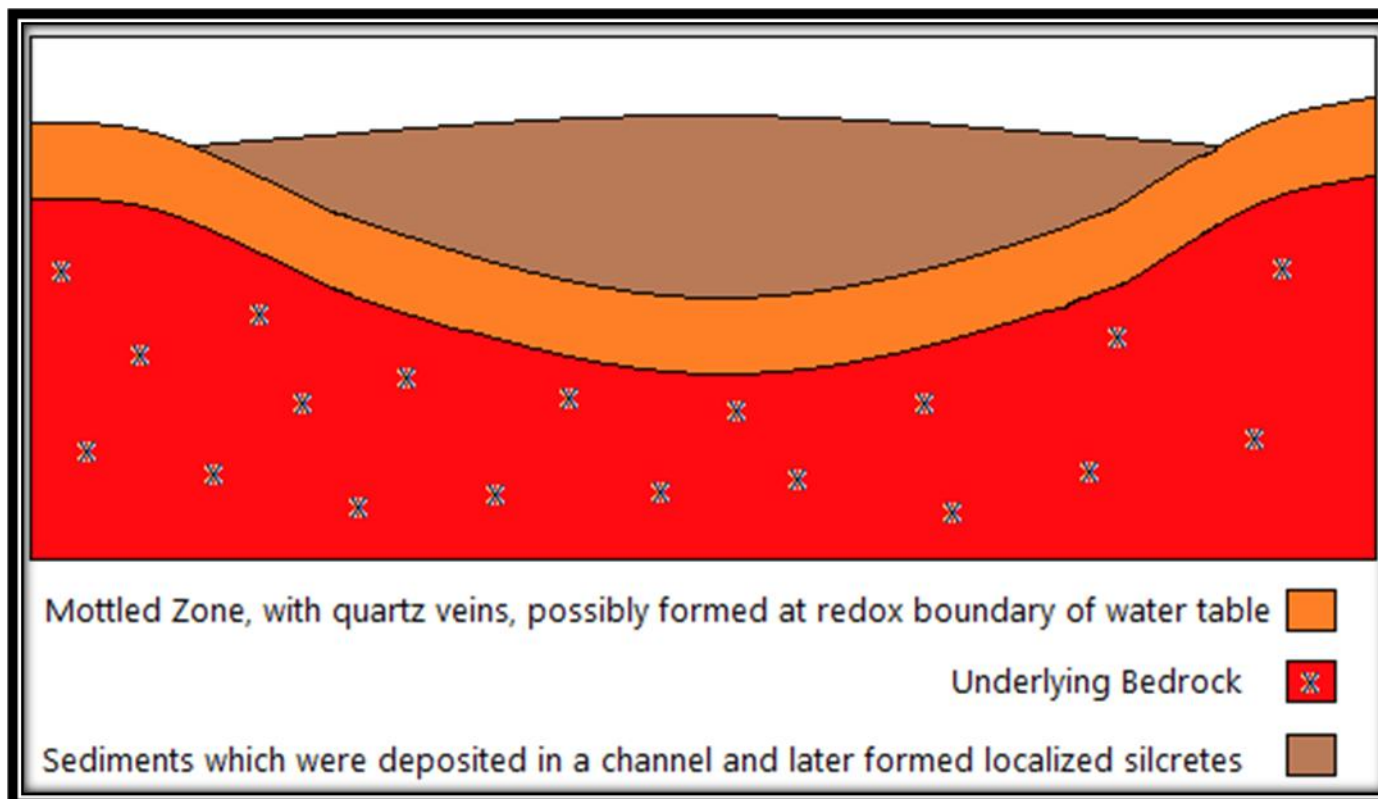


Figure 61.

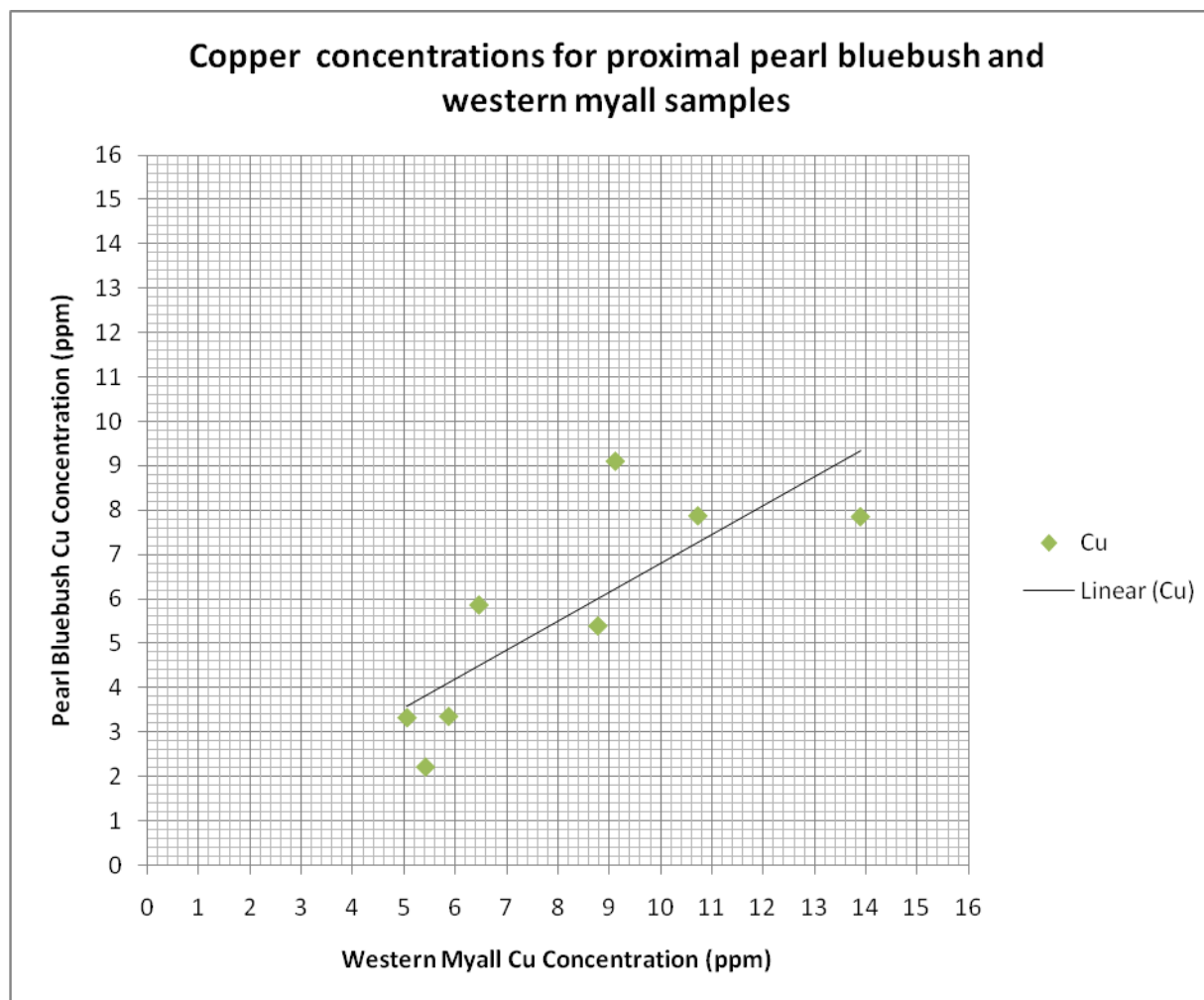


Figure 62.

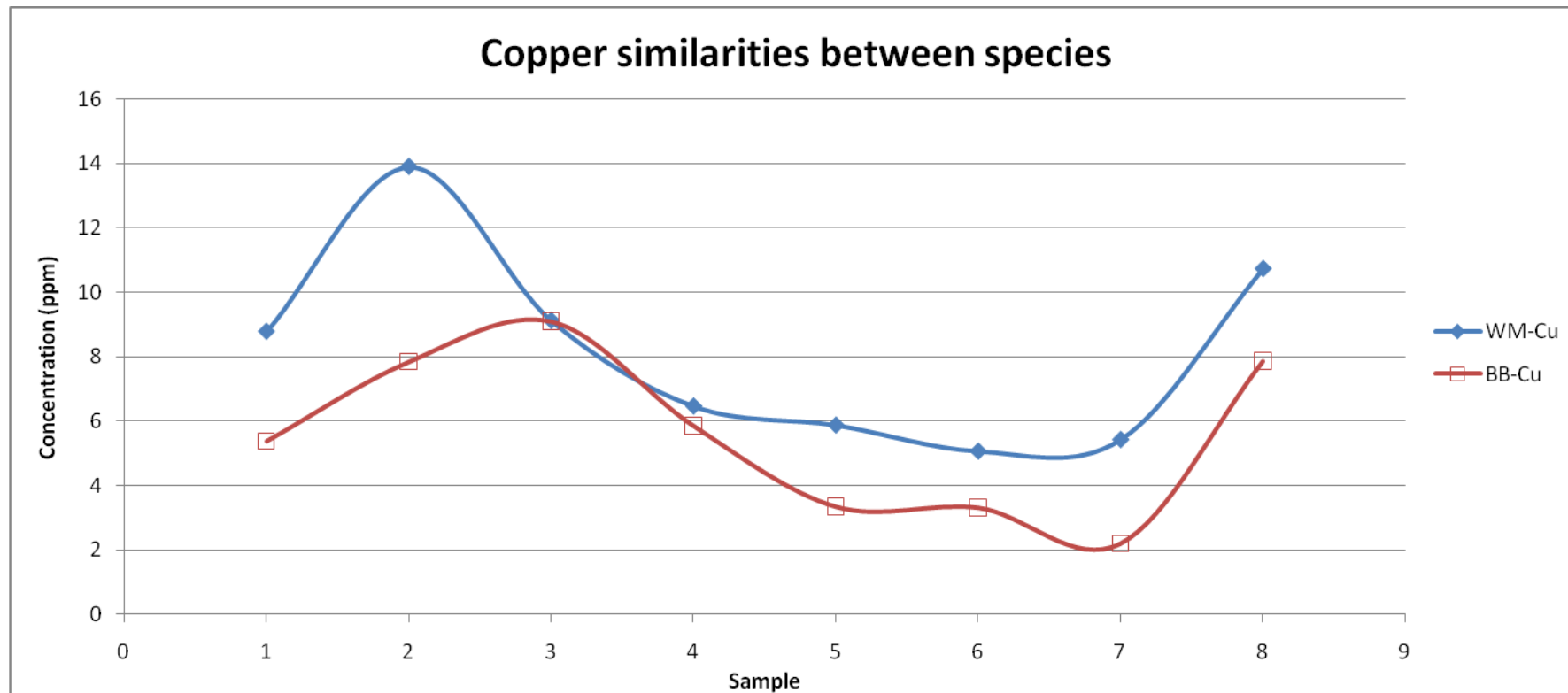




Figure 63.

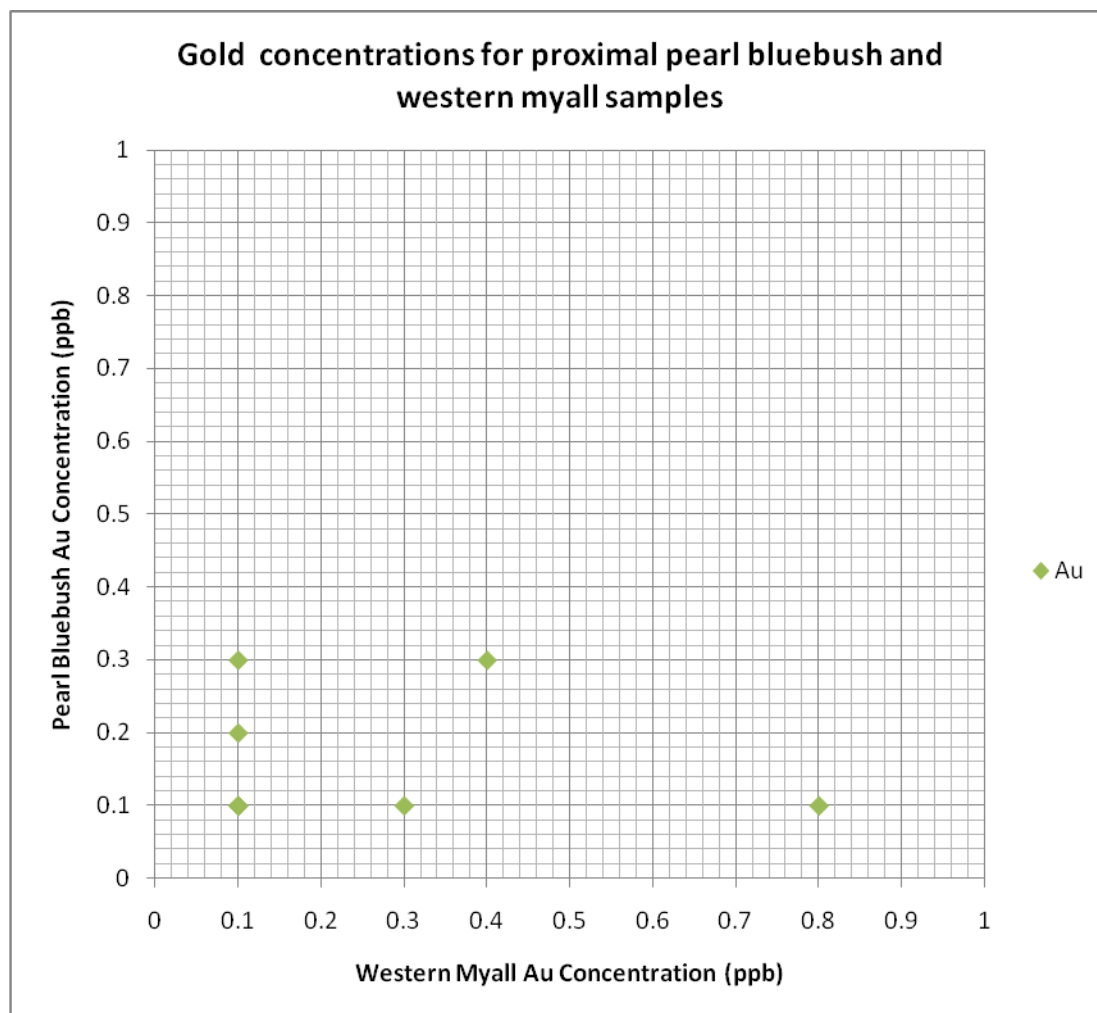


Figure 64.

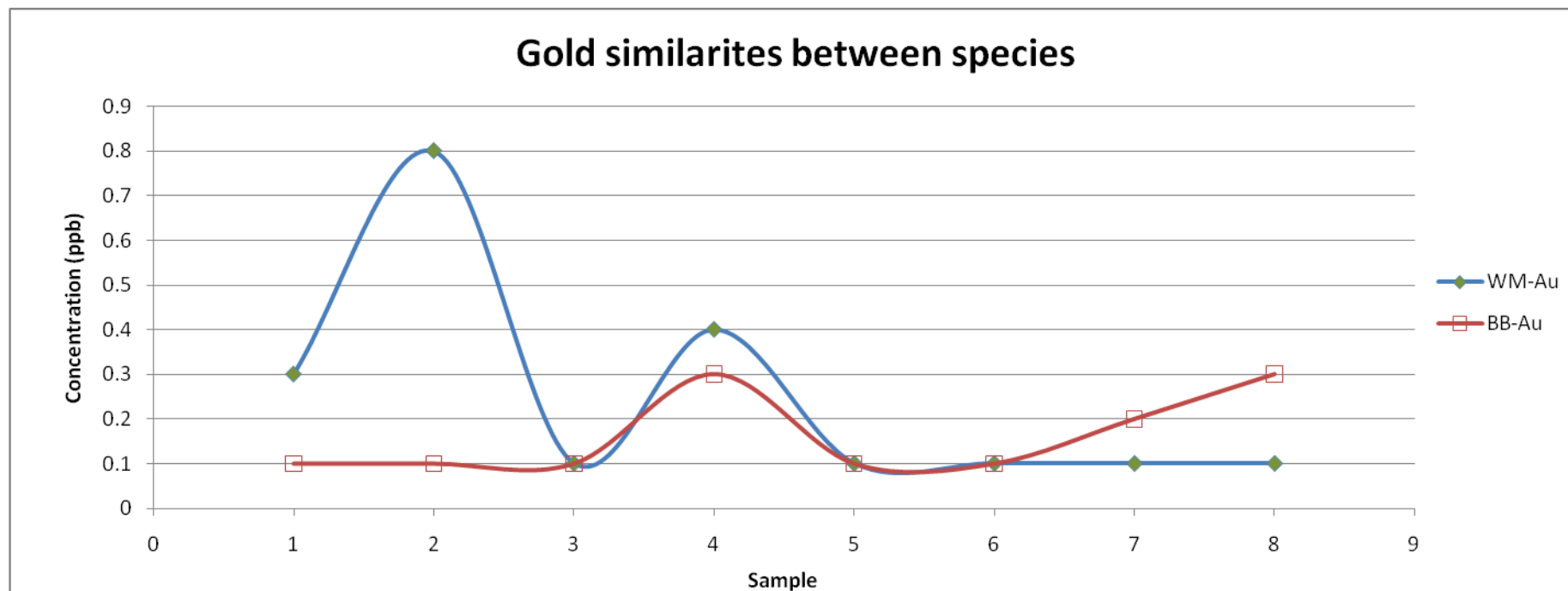


Figure 65.

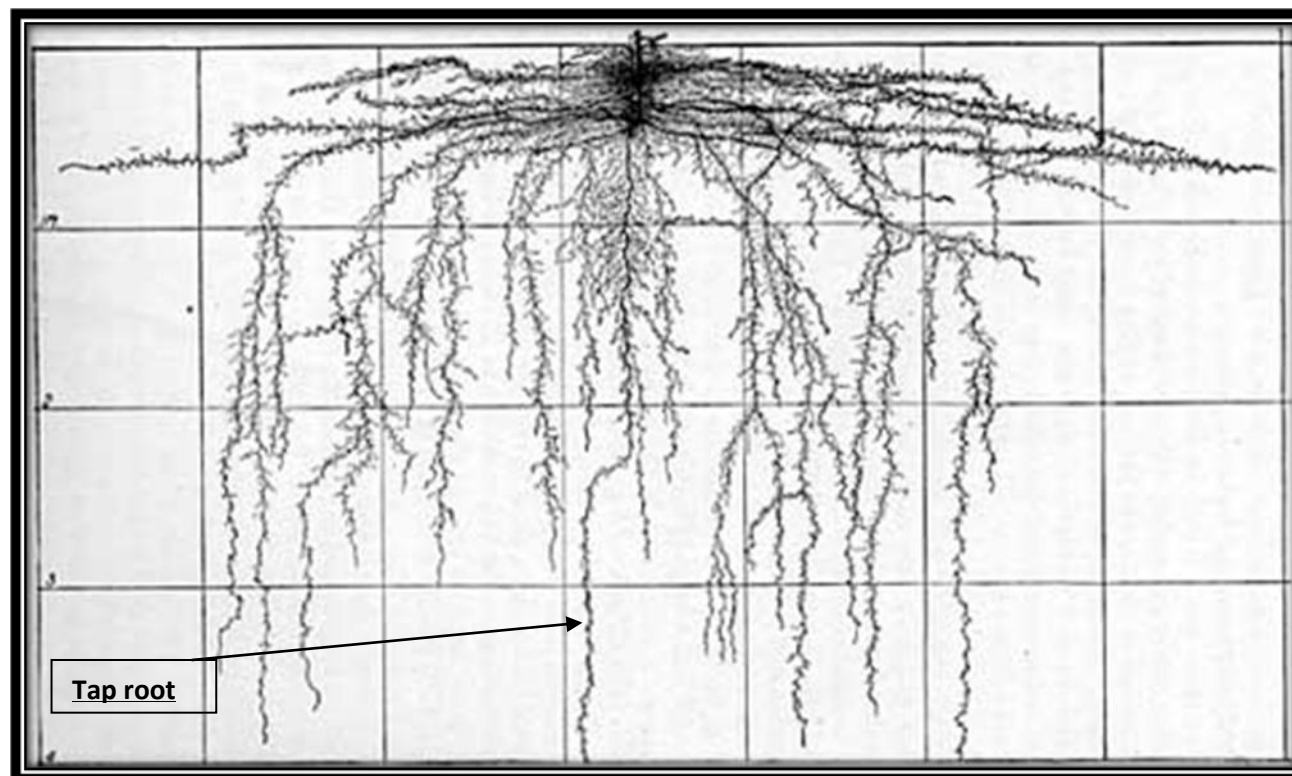


Figure 66.

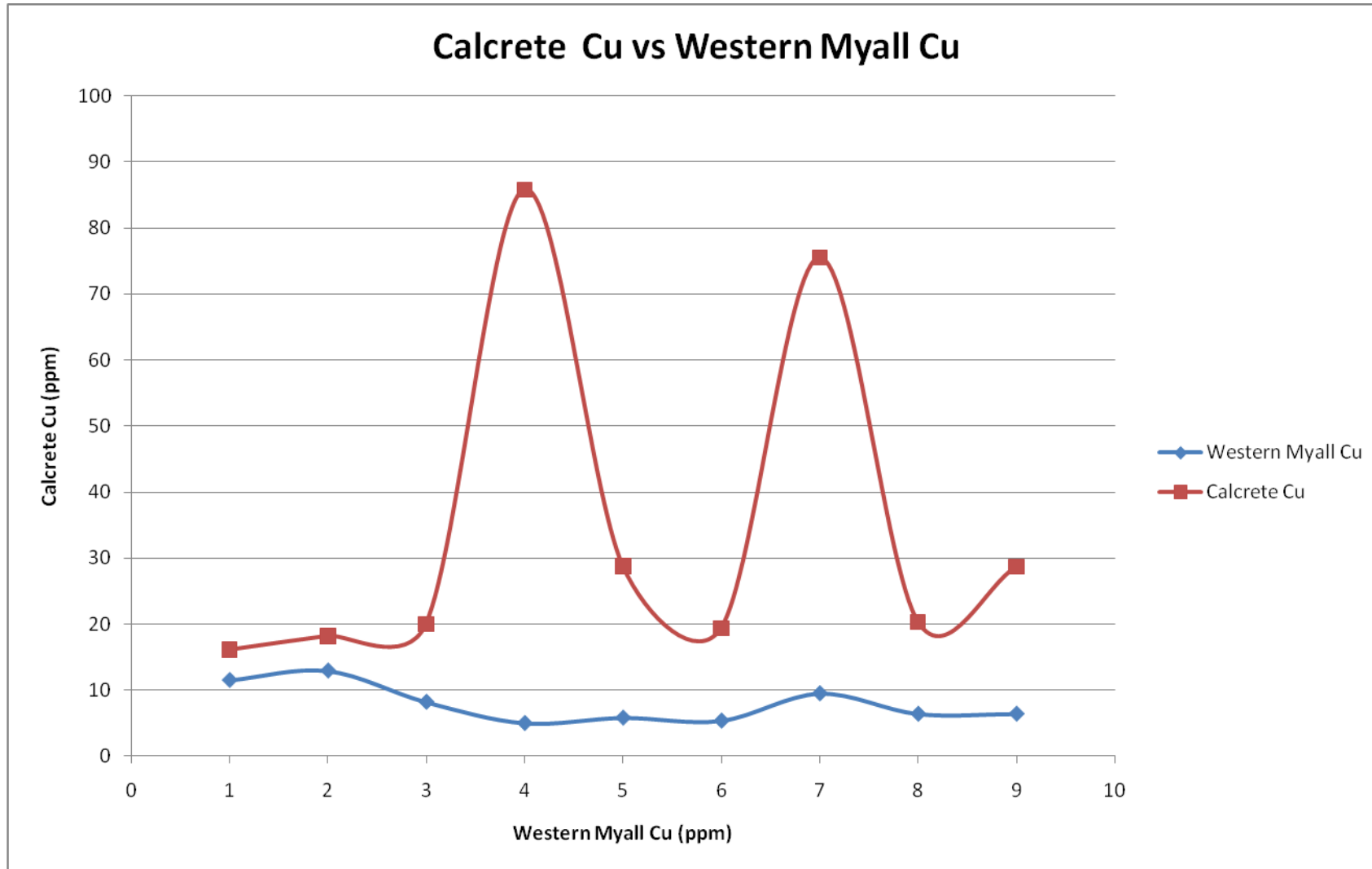




Figure 67.

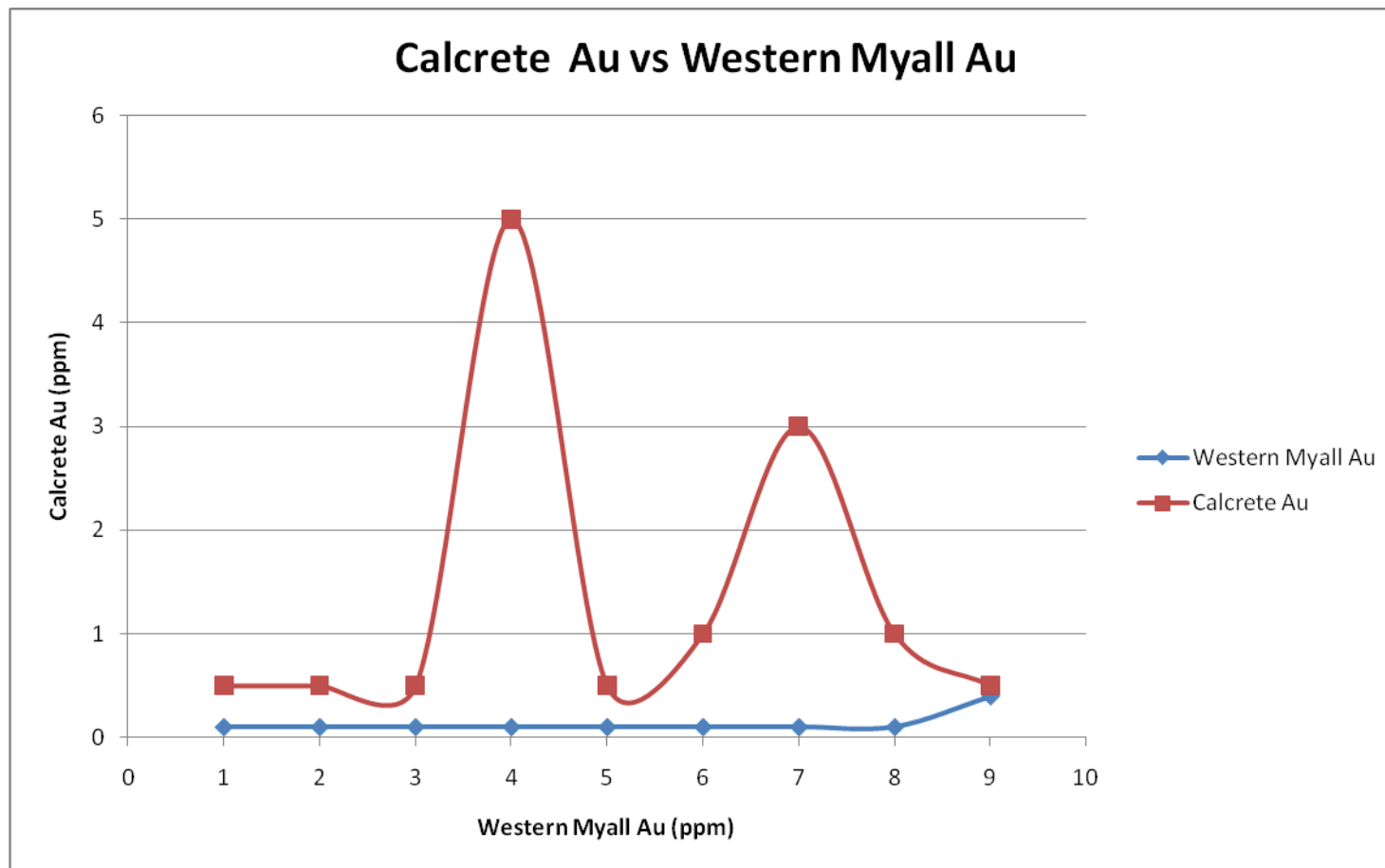


Figure 68.

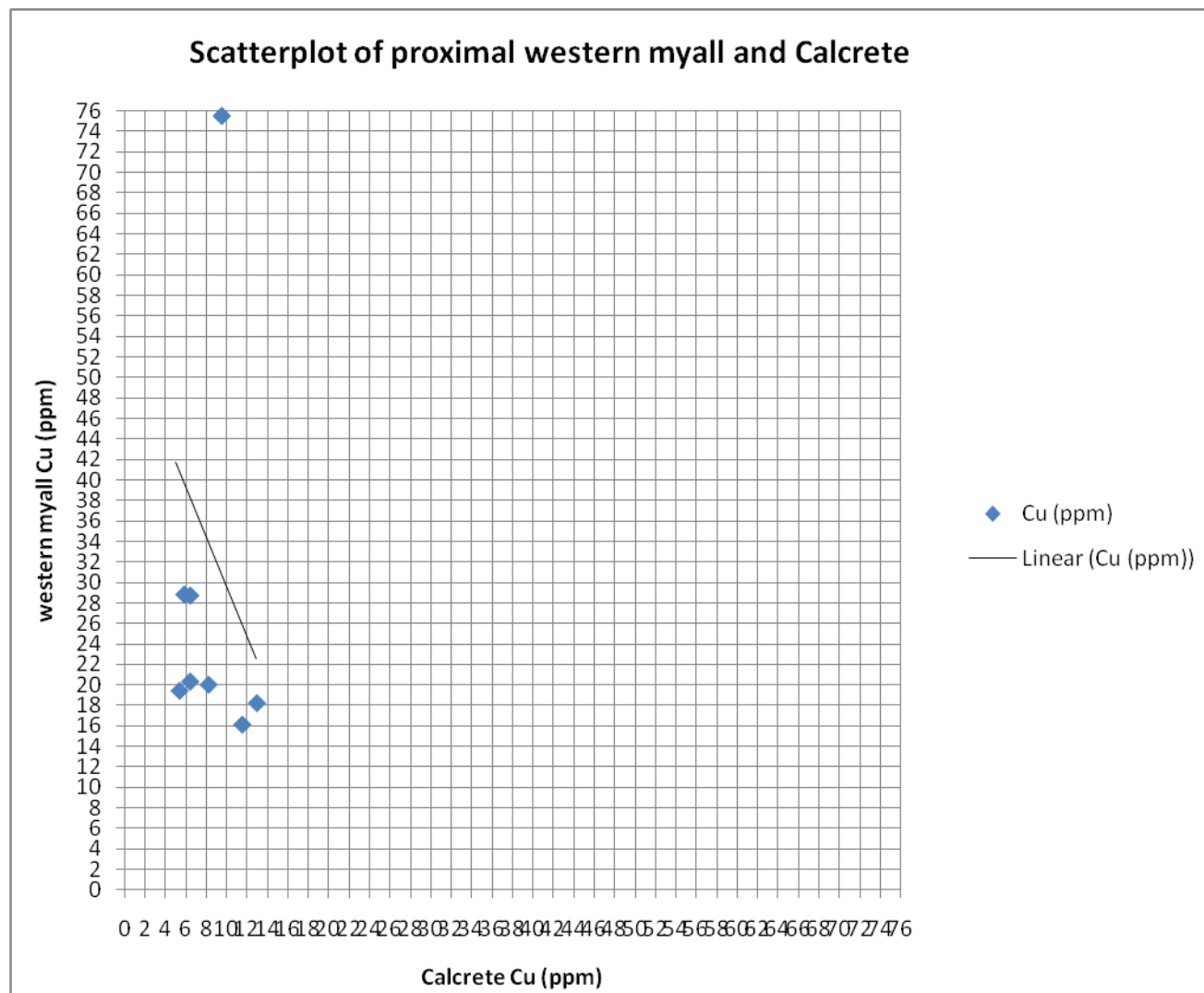


Figure 69.

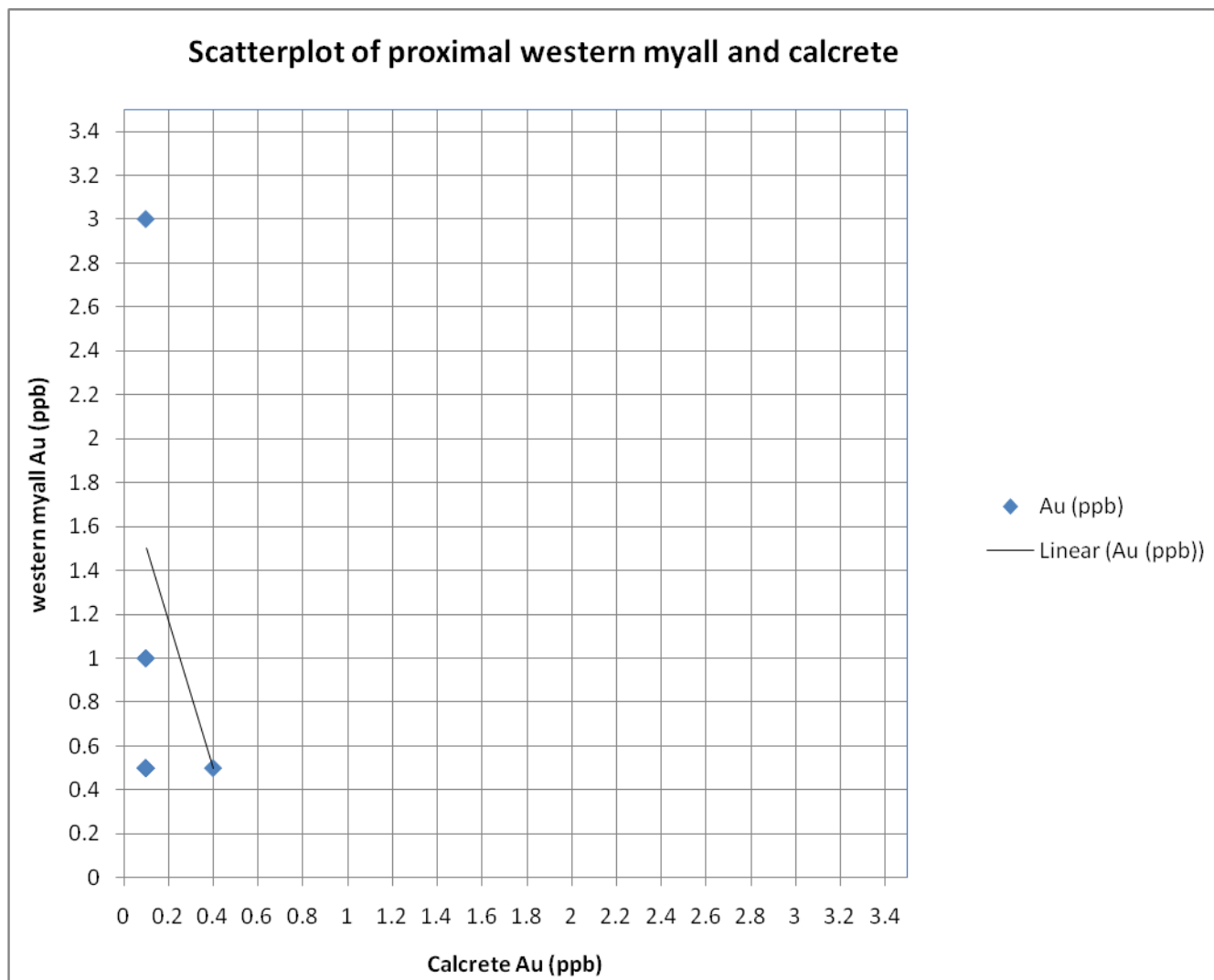


Figure 70.

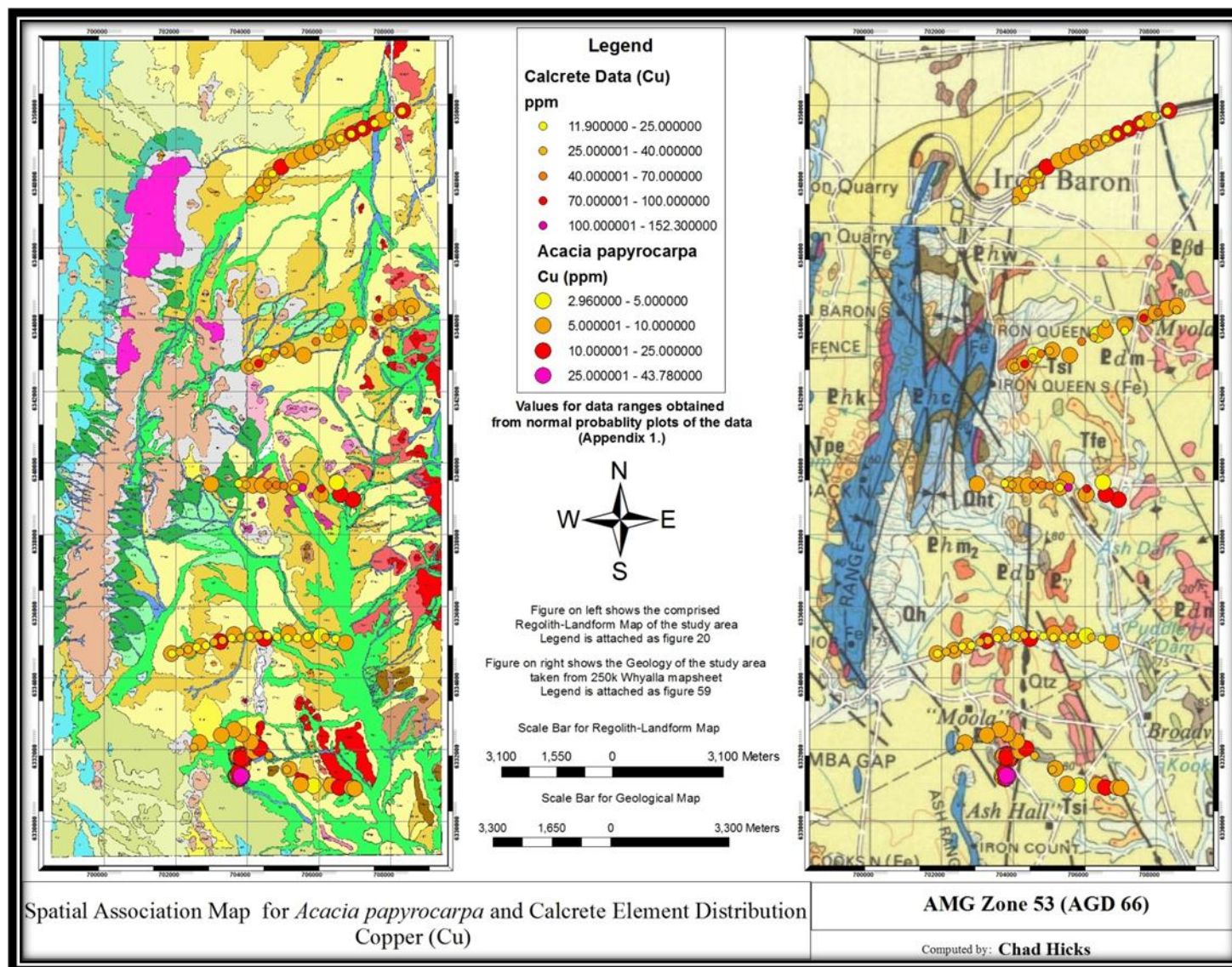




Figure 71.

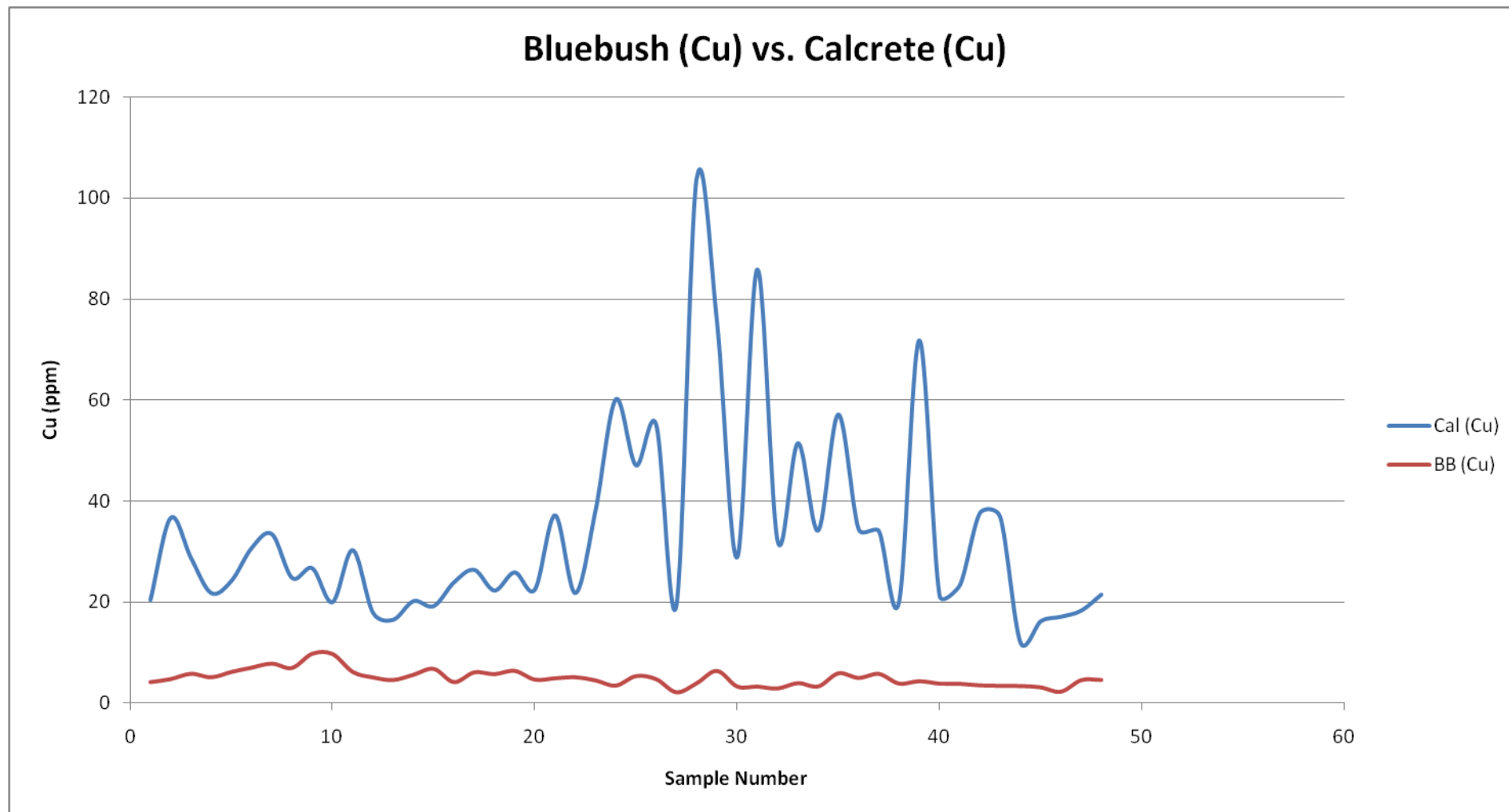


Figure 72.

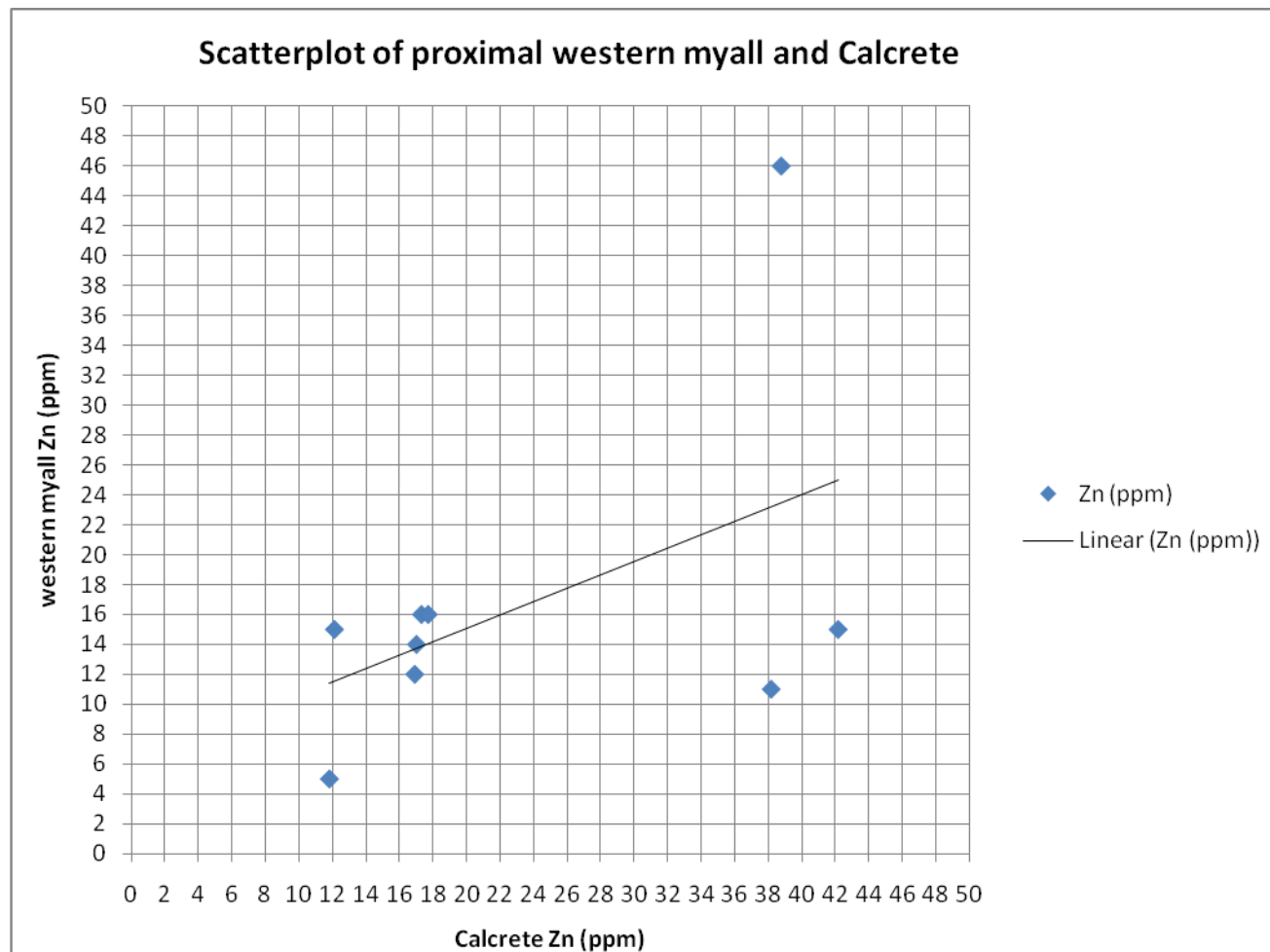


Figure 73.

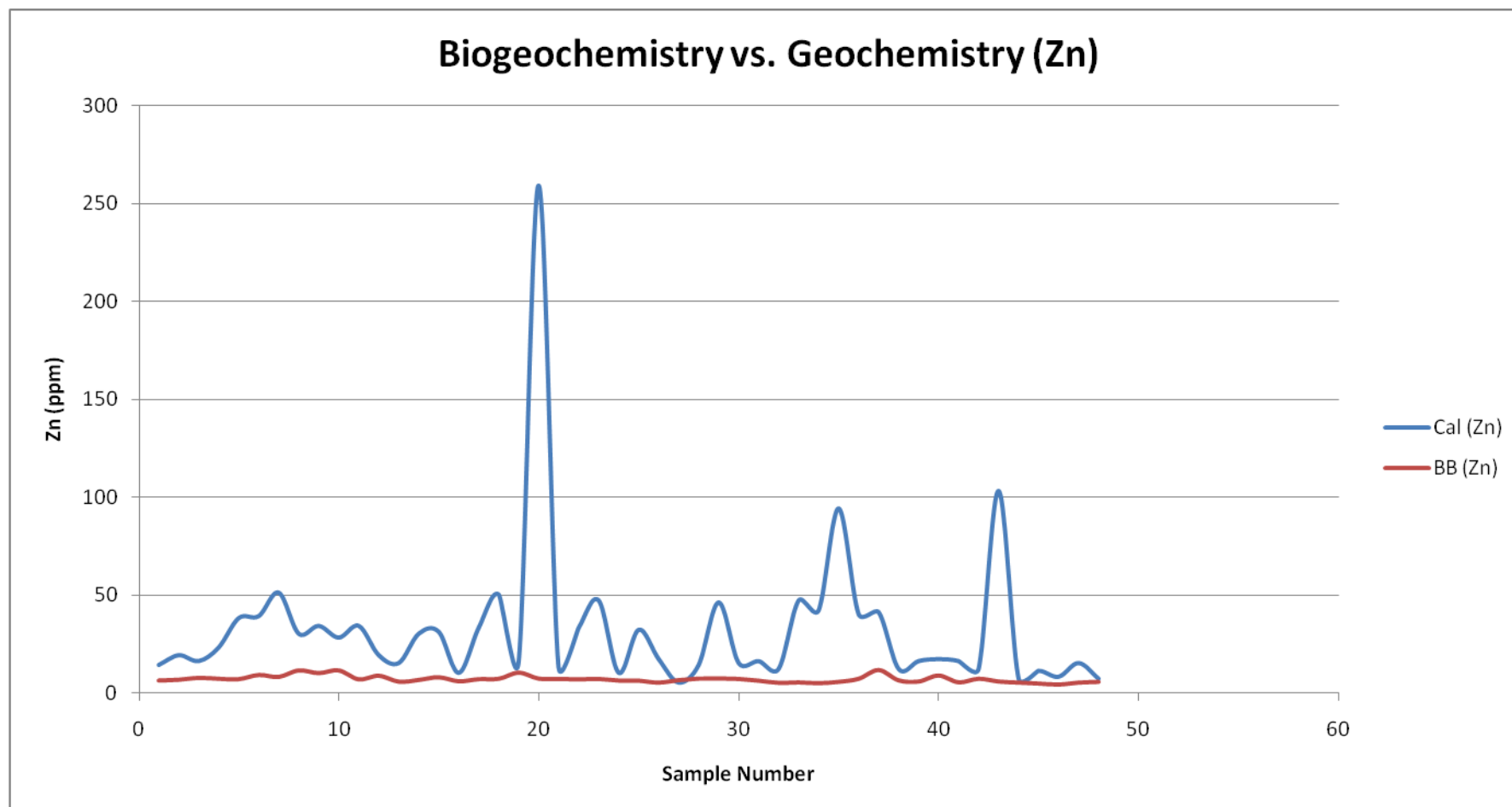


Figure 74.

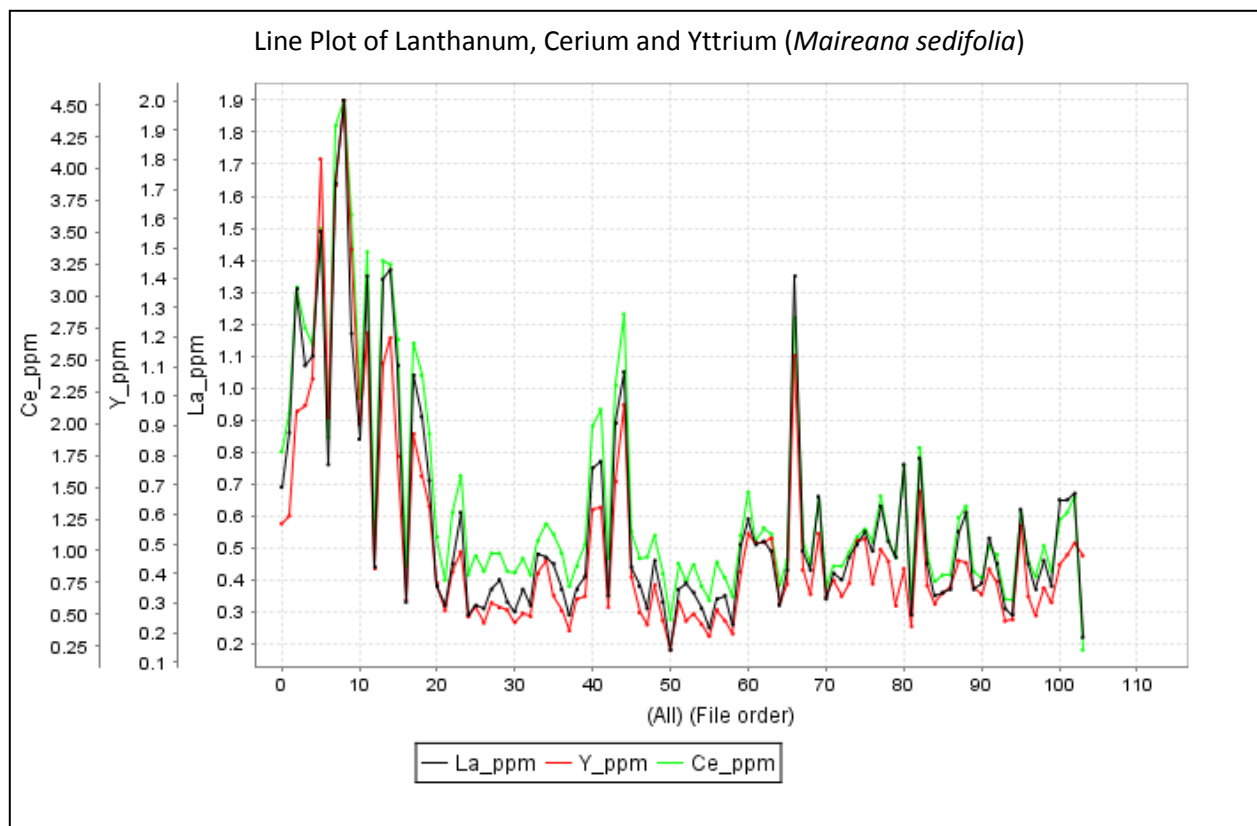


Figure 75.

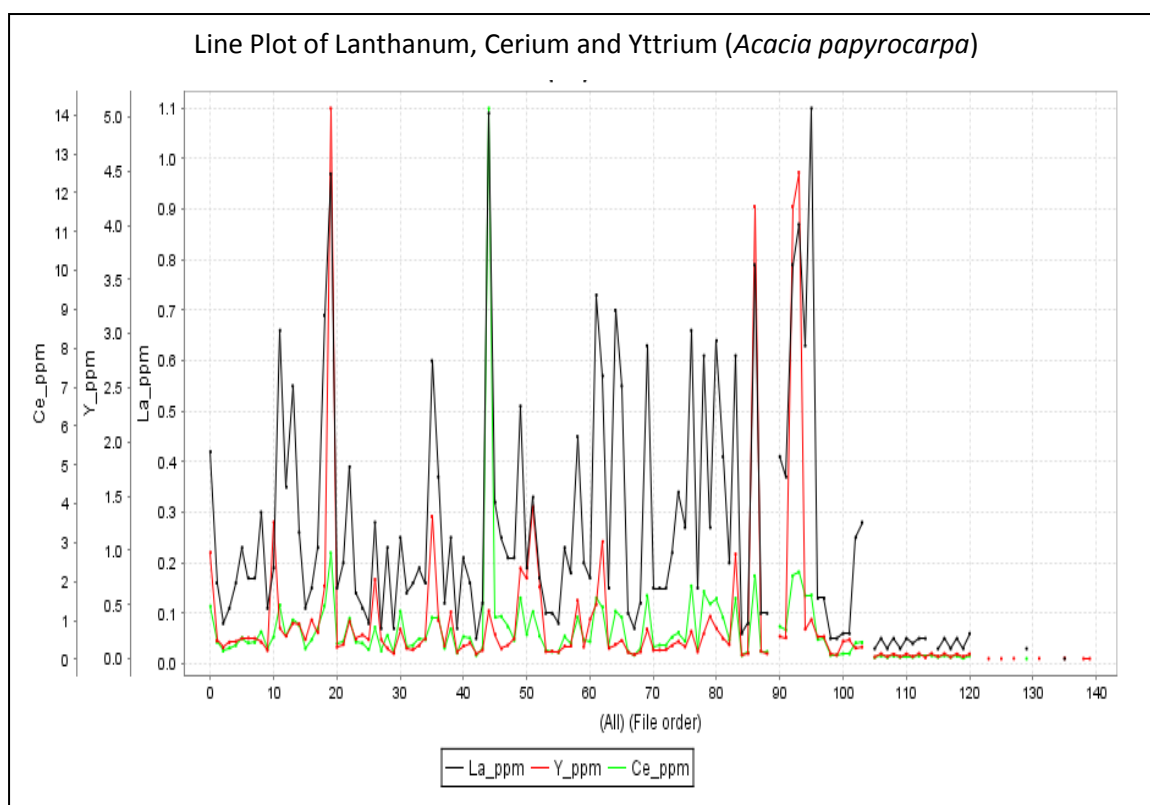




Figure 76.

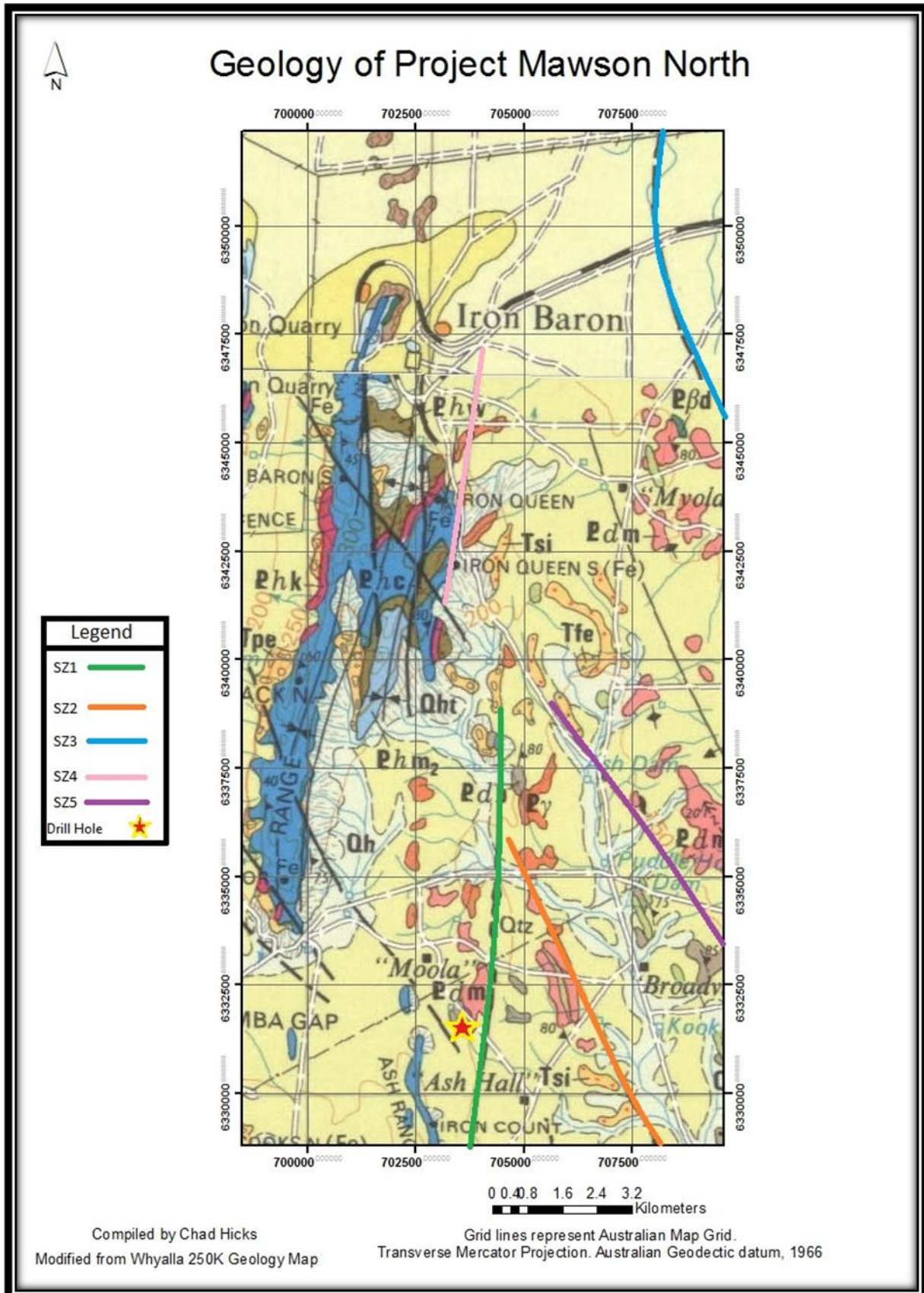


Figure 77.

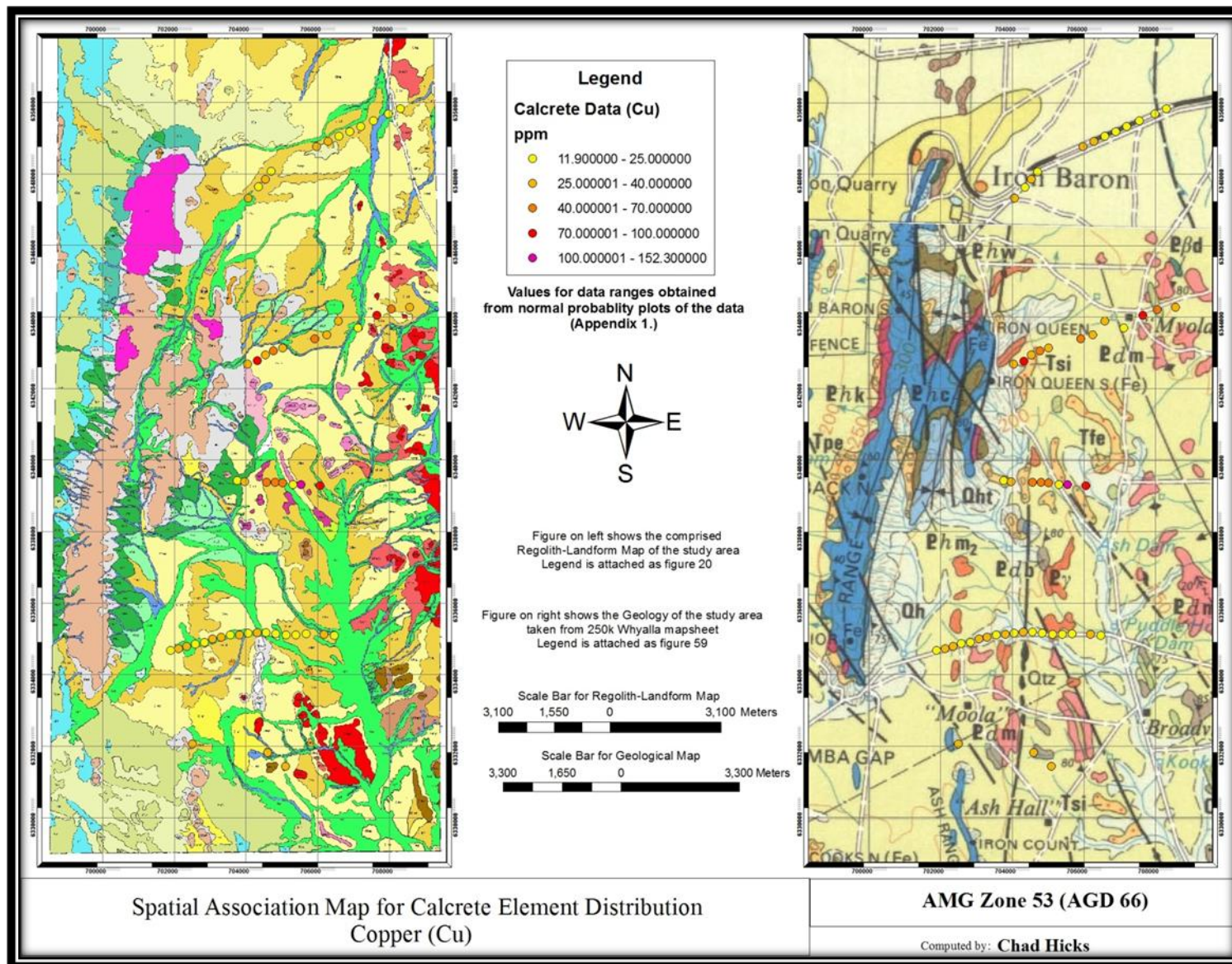
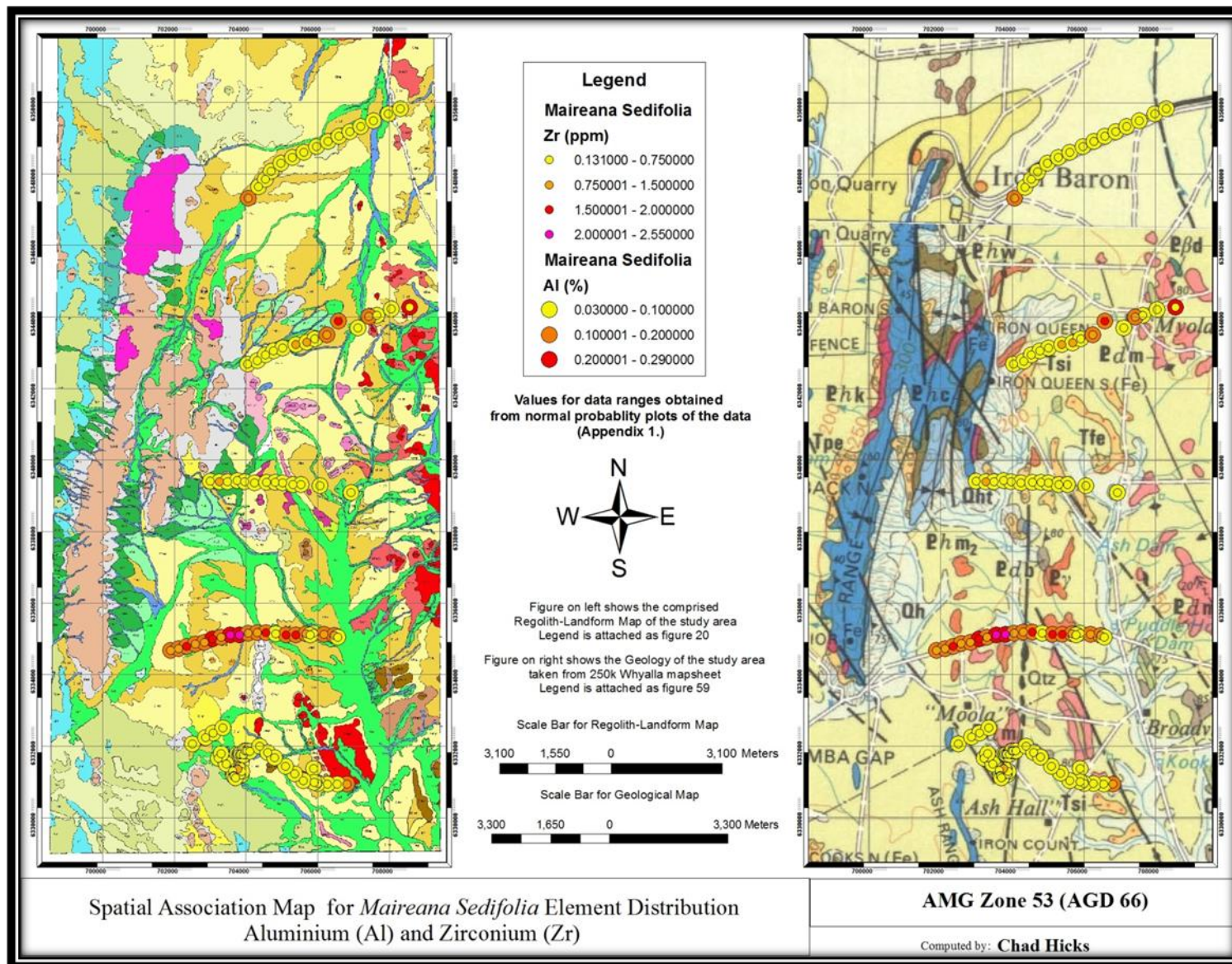




Figure 78.





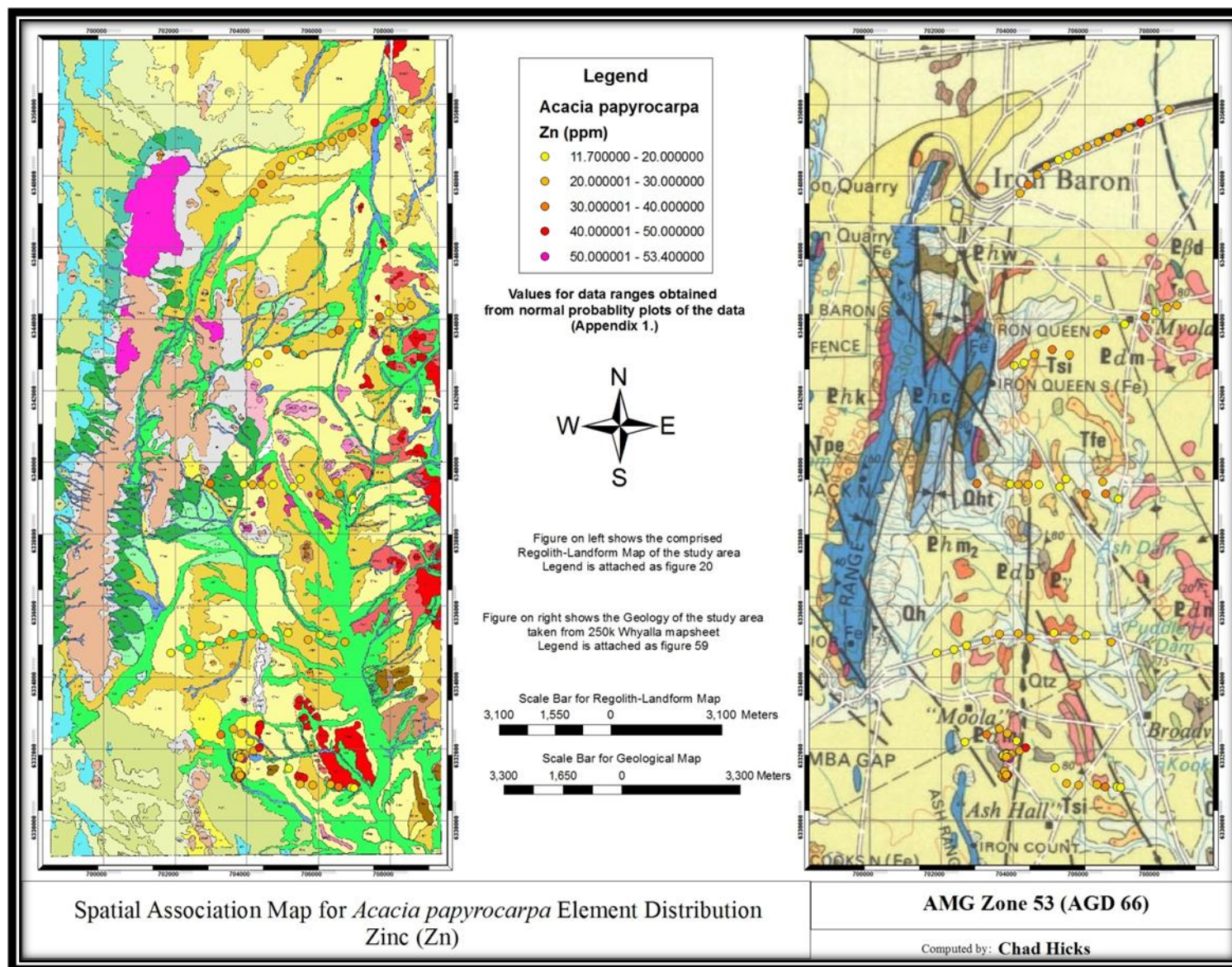


Figure 79.



Figure 80.

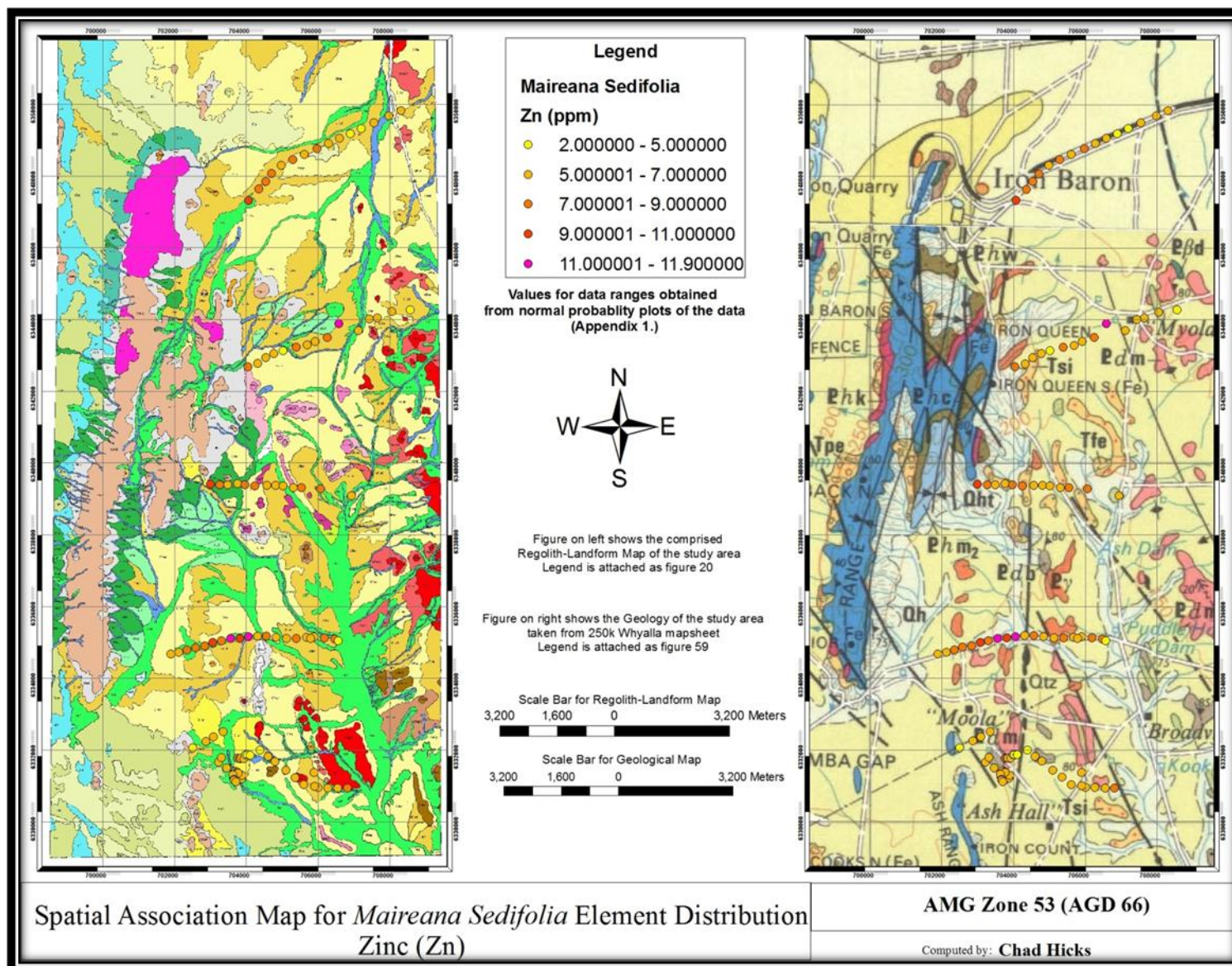




Figure 81.

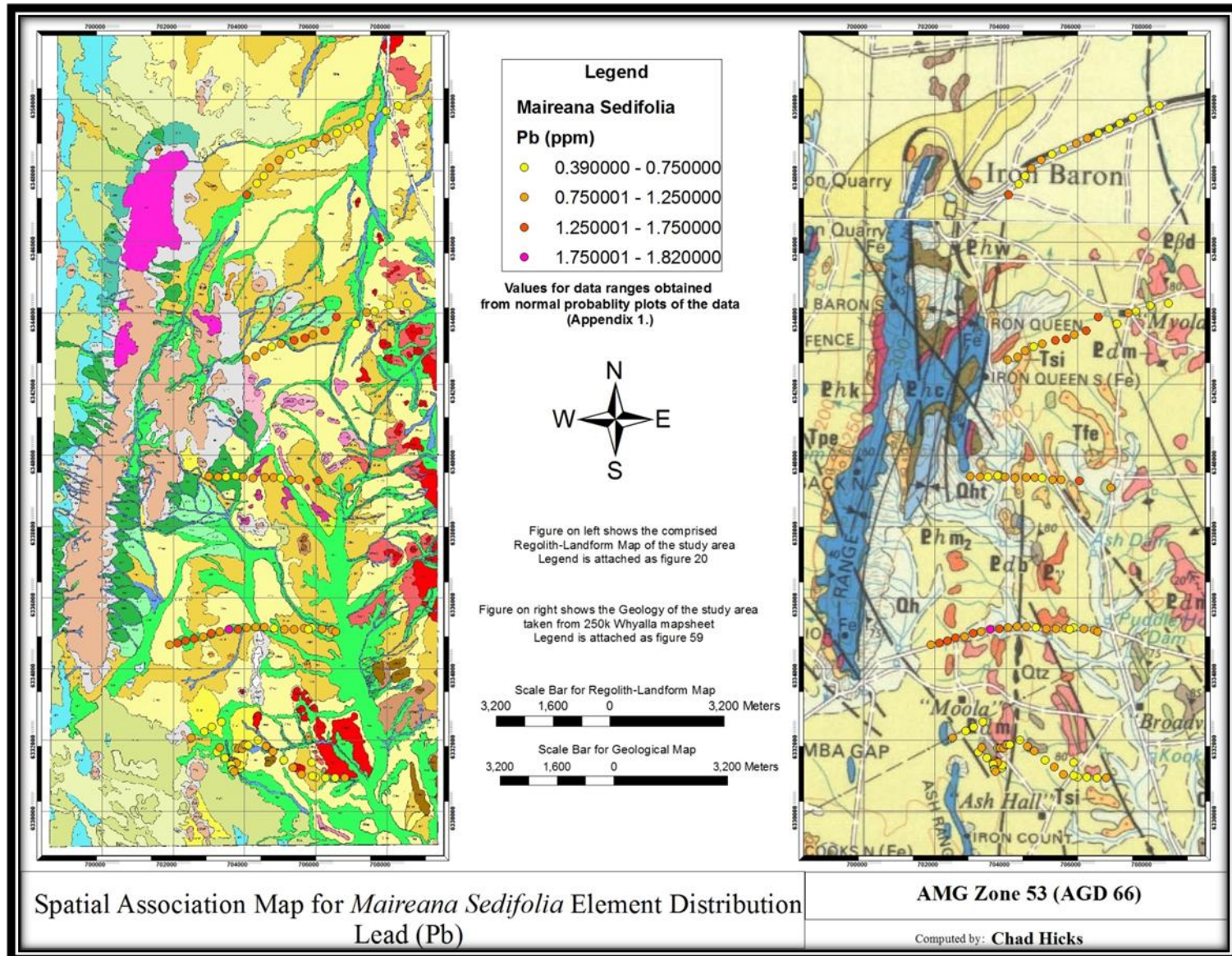




Figure 82.

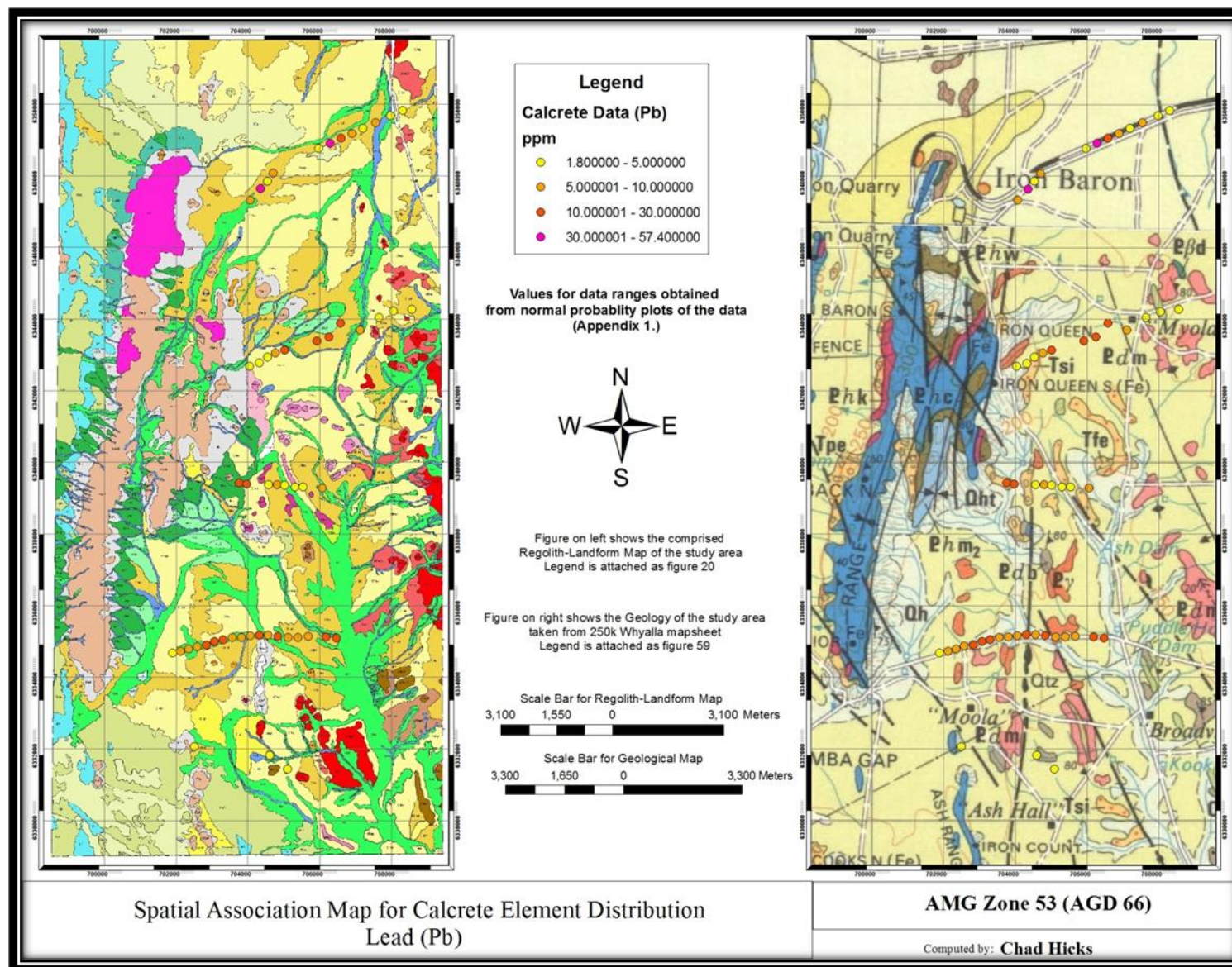


Figure 83.

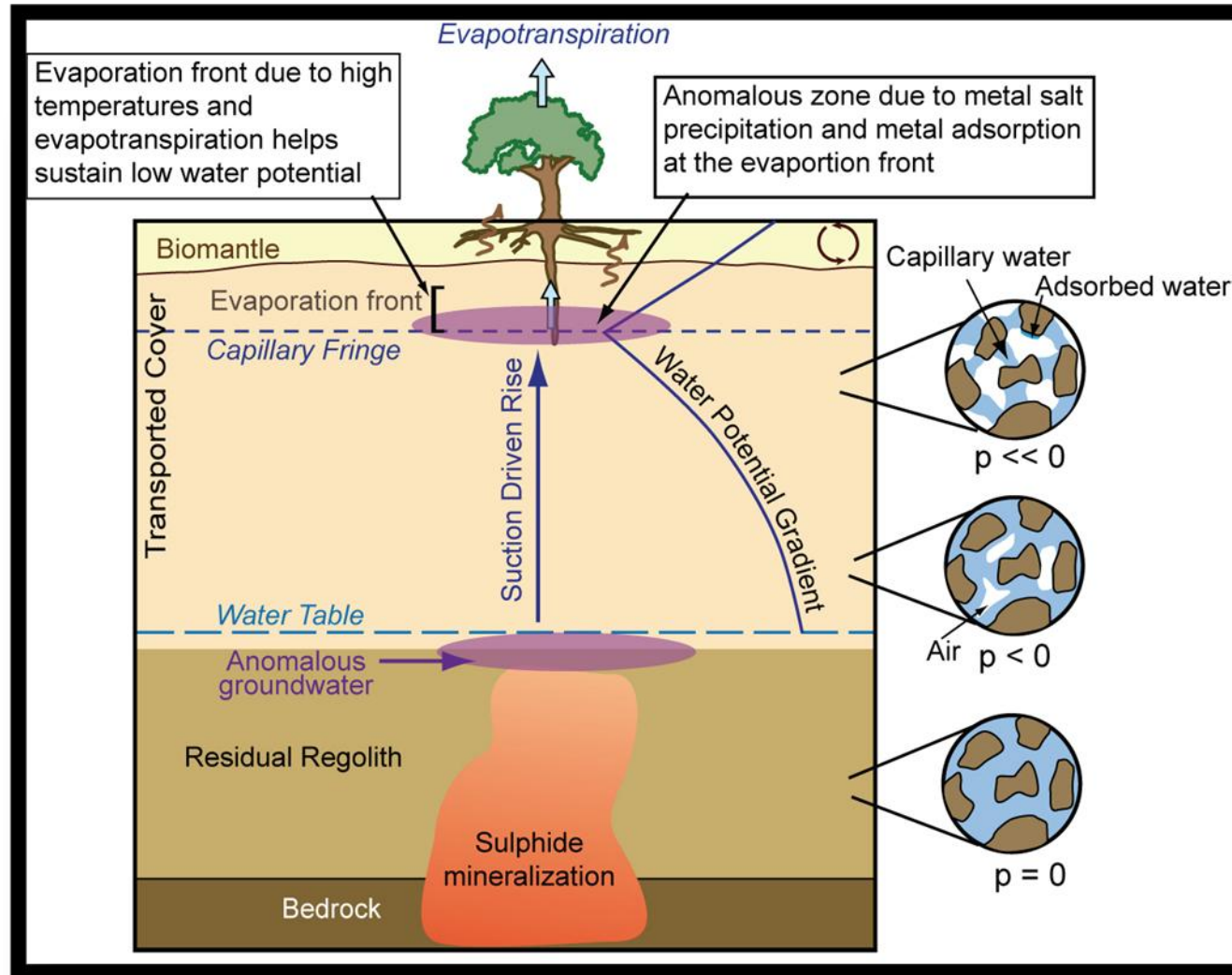




Figure 84.

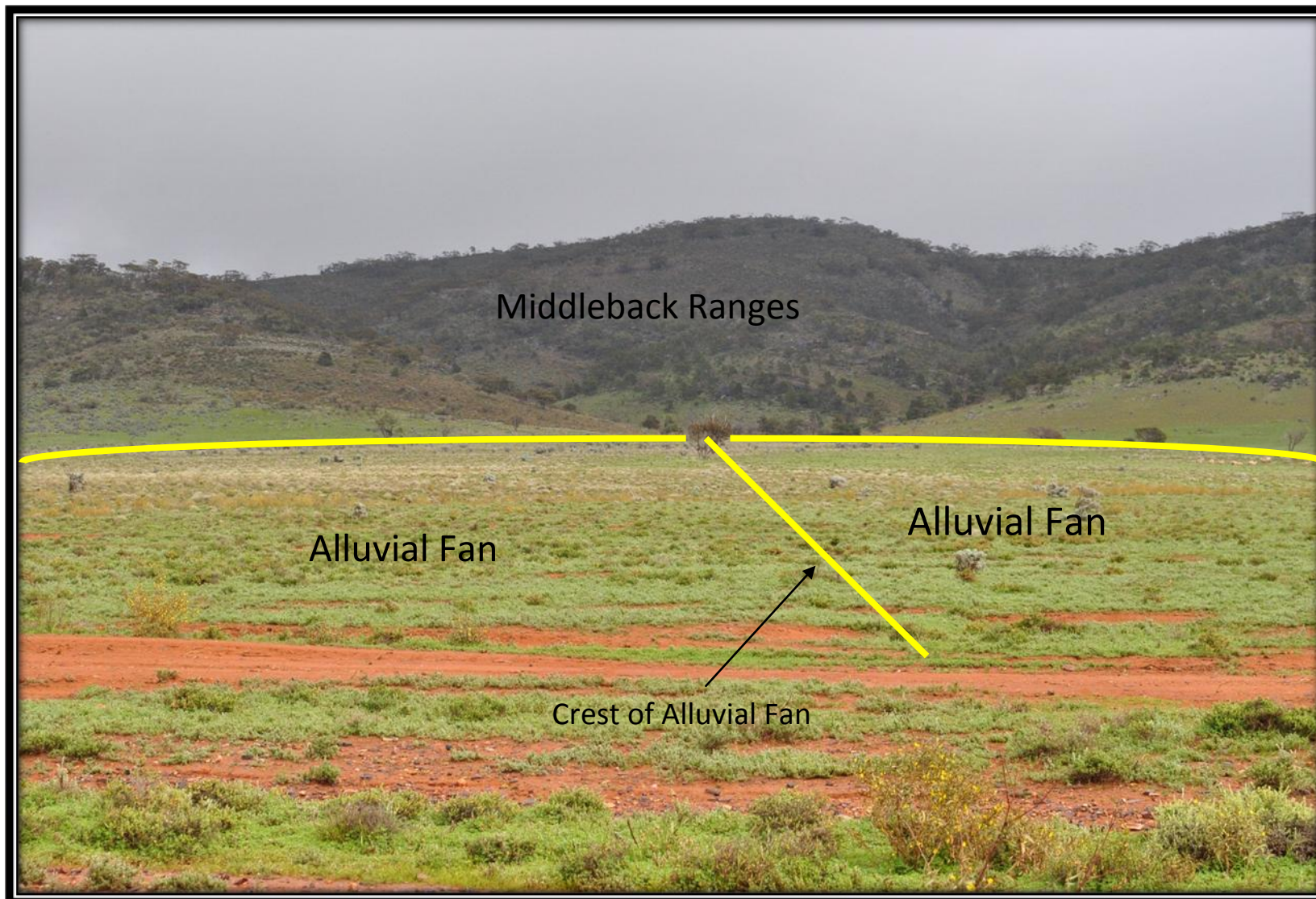
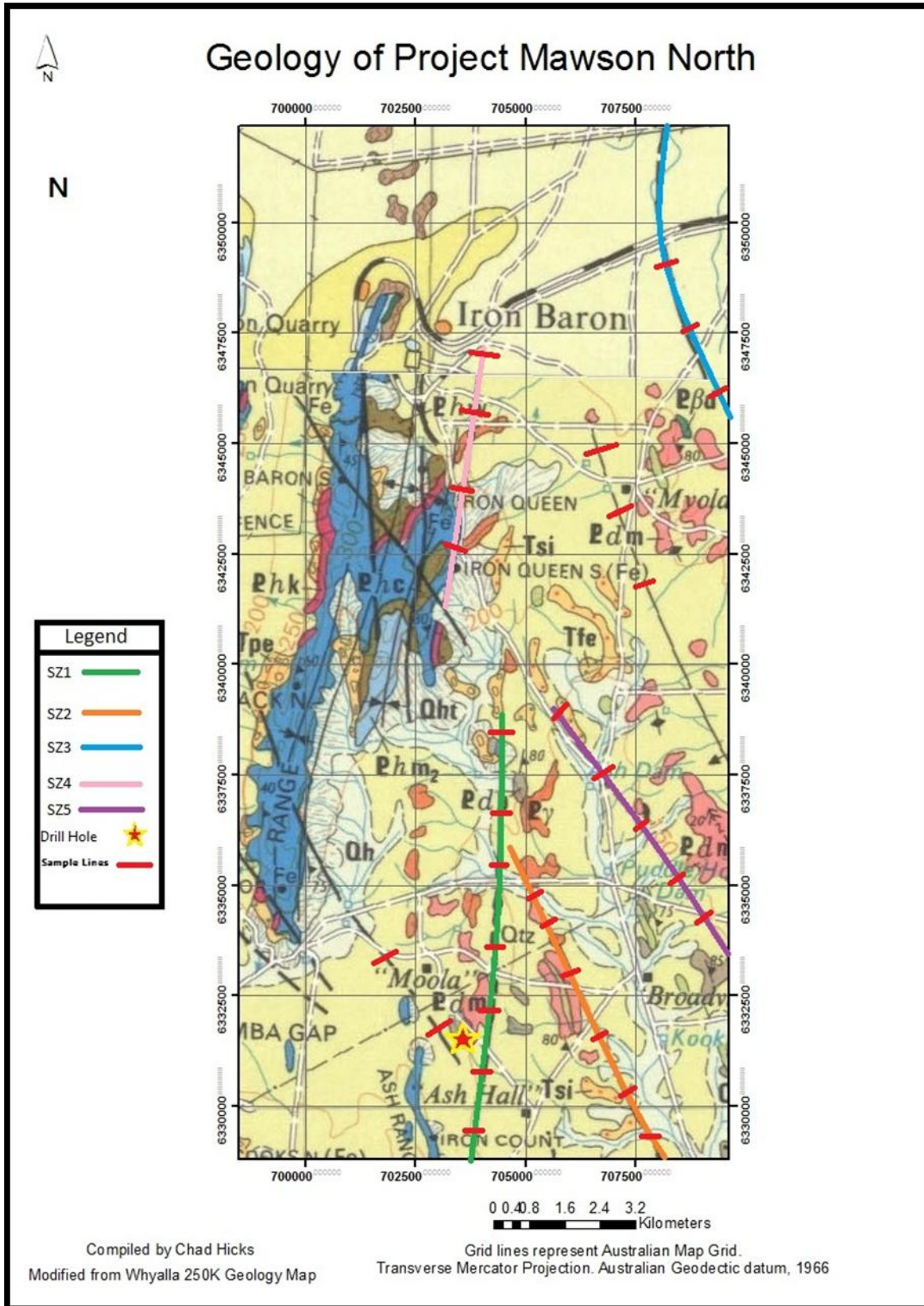


Figure 85.





Figure 86.



## Tables



**Table 1.** Previous Exploration undertaken within the area (source: Parker, 1998)

**Myola EL 2228**  
**Previous Mineral Exploration**

Company Name	EL #	Anomalous / intersecting results
Broken Hill Proprietary Company Ltd	SML539	Diamond/ percussion holes ST1, ST2 are in Equinox tenement. Though BIF-suite lithologies were encountered, no anomalous BM values recorded. Potential for high grade iron ore was deemed to be limited.
Dampier Mining Co Ltd	144	
Director of Mines	145	
Director of Mines	146	
Nissho Iwai Co (Aust) Pty Ltd	262	Limited amounts of radioactive clays were found to contain Th rather than U. Located the Th-bearing horizon with minor U in the Carpentarian Corunna sequence, & noted the U anomalous nature of the Burkitt Granite. Did not find palaeochannels with U.
Broken Hill Proprietary Company Ltd	266	Percussion drill holes MY9-23, MY28-61, EEP1,2,3,4 are all in Equinox tenement. 2 of 25 holes had Cu >600ppm. EEP3 had weakly anomalous Cu. No iron ore has been located. SEE SUMMARY
Broken Hill Proprietary Company Ltd	266	Geochem assays of boreholes anomalous but not high. EEP7,8 on Moonabie Anomaly; EEP9,10 on Nonowie Anomaly; EEP5,6 (failed) on Kooralla Anomaly; EEP11,12,13,14 on Arno Bay Anomaly.
Samedan Oil Corp	398	6 shallow core holes confirmed stratabound Pb/ Ag & Cu/Pb/Ag/Co minlzn in Mt Laura Fm. Breccias adjacent to Angle Dam Porphyry contain minor Cu/Ag minlzn in composites of altered sediments and vein components. SEE SUMMARY
Pancontinental Mining Ltd / Power reactor & Nuclear	432	Absence of Middle Proterozoic sandstone cover rock considerably downgrades potential of EL for "unconformity-vein type" U minlzn. All of U anomalies in EL432 are attributable to strong iron & manganese scavenging of U.
Stockdale Prospecting Ltd	451	Majority of results for kimberlite indicators negative. Rare samples contained kimberlitic ilmenite. U anomalism found in several locations. SEE SUMMARY
Stockdale Prospecting Ltd	454	U analysis very poor. Best = 2.4ppm in NW of tenement. Reanalysis of 20 stream sediment samples- one was found to contain kimberlitic ilmenite (N6890)
Stockdale Prospecting Ltd (JV)	537	Follow-up stream & loam sampling for kimberlitic indicators were subsequently used for U search. Anomalous Cu, Pb, Zn values were located in Hutchison Gp.
Esso Exploration & Production Australia Pty Ltd	588	Poor results gained from U expln. Results of alpha cup survey completed over area of gneisses, Myola metavolcanics & supergene enriched iron-Fm Hutchison metaseds failed to delineate areas of further expln. Geol mapping indicates low potential for BM.
Esso Exploration & Production Australia Pty Ltd	644	Several anomalous radiation areas were found, but mainly due to K40. Th conc > U conc. BM assays in UP5 are low - max U3O8=15ppm, ThO2=35ppm. Sampling across BIF= some encouraging values. SEE SUMMARY
Samedan Oil Corp / Esso Exploration & Production	692	
BHP Minerals Ltd / Dampier Mining Co Ltd	766	Search for carbonaceous seds. of Tertiary age possibly preserved on a series of fault blocks in area. Drill holes intersected beds of oil shale & lignite. Almost continued gradation from lignite to oil shale as ash content increases.

Table 1 continued.

<b>Myola EL 2228 Previous Mineral Exploration</b>		
<b>Company Name</b>	<b>EL #</b>	<b>Anomalous / intersecting results</b>
BHP Minerals Ltd / Dampier Mining Co Ltd	786	Depth to basement calculations and CRAE holeRHC7 suggest area sth of Charleston Fault & E of Moonabie Fault contains too thick a sequence above the Eocene to be of economic interest.
BHP Minerals Ltd	863	No kimberlite indicators found, no economic Fe grades intersected and BM values were at background to weakly anomalous levels. SEE SUMMARY
Stockdale Prospecting Ltd	874	Became EL1193 in joint venture. U and diamond prospectivity of region downgraded, however BM results were anomalous. SEE SUMMARY.
Stockdale Prospecting Ltd (JV)	965	Anomalous Cu,Pb,Zn values were located in Hutchison Gp. Existing drillhole material has demonstrated the existence of primary Cu,Pb,Zn,Mn,Ba,Ag in Lower Proterozoic dolomite, graphitic schist and iron formation. Becomes EL1193 in joint venture.SEE SUMMARY
Samedan Oil Corp.	1041	Best results: 2.2% Cu and 51g/t Ag intersected in breccias in FW.1. Mineralization is in a composite of altered sediments and vein components. SEE SUMMARY
Shell Co of Australia Ltd	1116	Geochemical results are low. Only 14 of drillholes penetrated to bedrock because of water & fine sands. Significantly elevated but not outstandingly anomalous values were recorded in 8 samples. 270ppm Cu, 630ppm Zn, 720ppm Pb, 12%Fe, 1.15%Mn.
Shell Co of Australia Ltd	1117	
Shell Co Of Australia Ltd / WMC Ltd / Poseidon Ltd	1117	A Pb-Zn anomalous sub-basin was outlined at Miltalie Nth. SEE SUMMARY
Aberfoyle Exploration Pty Ltd / Mobil Energy Minerals Ltd	1193	3 percussion holes drilled on Katunga Hill [KHPD1] & Iron Queen [IQPD1 &2] prospects found no significant BM values. EM seems to be ineffective in this deeply weathered environment and drill targets are likely to be deep. SEE SUMMARY
Aberfoyle Exploration Pty Ltd	1193	No gossans were found. Apart from one elevated Cu value in the spot samples which correlates with a large amount of Mn there is no suggestion of a base metal presence.
Shell Co of Australia Ltd (drilling by Billiton Aust Ltd)	1230	Stratiform BM potential in Early Proterozoic Hutchison Gp metasediments was downgraded. Anomalous bedrock Zn in 22 RAB holes at Moores Dam. Drillholes BILLITONRLG1,3,8,7,9 are in Equinox tenement. SEE SUMMARY
PNC Exploration (Aust) Pty Ltd	1241	Drill holes did not intersect any significant U mineralisation. Highest BM assay is 370ppm Zn in M1. SEE SUMMARY
PNC Exploration (Aust) Pty Ltd	1339	Secondary U-Cu minlzn intersected in 2 holes at contact with dolerite dyke. Drillhole cuttings & groundwater from RAB holes have generally low geochem values - elevated U, Cu related to Roopena Fault. Only drillhole PNCRP3 in Equinox tenement. SEE SUMMARY
Gypcel Pty Ltd	1410	
Pondray Pty Ltd (drilling by Perilya Mines NL)	1532	Drillholes PERILYAGD1-5, PERILYAP1,10,11,23,30,38,39,43,44,50,56,60,61,64,66,69,70,73,76,81,82,83,89 are in Equinox tenement. SEE SUMMARY

Table 1 continued.

**Myola EL 2228  
Previous Mineral Exploration**

Company Name	EL #	Anomalous / intersecting results
Pondray Pty Ltd	1551	Some weakly anomalous Pb & Zn values were delineated. Low quality kaolinite occurrence was outlined. SEE SUMMARY
Burmine Ltd	1581	
Broken Hill Proprietary Company Ltd	1663	
Aberfoyle Resources Ltd	1735	Max Pb = 2.88%, max Cu = 0.67%. Drilling downgraded anomalous zones. No targets were deemed worthy of detailed follow up. SEE SUMMARY
Western Mining Corp Ltd	1775	
Aberfoyle Resources Ltd / Kokong Holdings Pty Ltd	1814	RAB holes best results: 1.01% Zn, 0.3% Pb. Cu rarely exceeds 250ppm. A clear relationship between the magnetics and surface geochemistry is evident at "Line C". SEE SUMMARY
Acacia Resources Ltd, DB Clarke	1831	4 geophysical targets delineated. No signif. assay results so sthn portion of EL relinq. Target areas based on mag. anomalies relating to Fe-rich units/ jaspilite of Hutchison Gp; nth-sth mag. horizons/ BIF's, & an area of subcropping Charleston Granite.
Pondray Pty Ltd	1892	
North Mining Ltd	1927	
Australasian Granite Pty Ltd	2052	

**Table 2.** Previous exploration undertaken by Helix Resources and the time when they were undertaken

<b>Year</b>	<b>Type of Exploration</b>
1999	Stream sediment sampling
1999	Calcrete sampling
1999	Soil Traverses
1999	Rock chip sampling and Geological Mapping
1999	Ground Magnetism and Geophysics
1999	Drill core logging and re-assaying
2000	RAB Drilling: Moola Prospect
2000	RC Drilling: Moola Prospect
2000	Calcrete sampling: Moola Nth
2000	RC and Diamond Drilling: Princess Prospect
2000	RAB/Aircore Drilling: Highway, Melody, Monarch SE Prospects
2000	Ground Electromagnetics: Moola, Princess, Highway, Melody Prospects
2001	Princess Time Domain Induced Polarisation Survey
2001	Highway Frequency Domain Magnetometric Resistivity/Induced Polarisation Survey
2001	Moola Fixed Loop TEM Survey



Regolith Expression of Cu-Au mineralisation within the Northern region of the Project Mawson area,  
NE Eyre Peninsula, South Australia

---

**Table 3.** Significant results acquired from work undertaken by Helix Resources (source: Wilson, 1999, 2000, 2004; Cairns, 2003)

Exploration Method	Prospect	Hole	Easting	Northing	Result
RC drilling Results	Moola	MRC003	9535	49050	52m @0.57% Cu 12m @1.0% Cu 12m @ 9 g/t Ag
RC drilling Results	Moola	MRC006	9530	48900	32m @0.27% Cu 8m @ 7 g/t Ag
RC drilling Results	Moola	MRC008	9530	48975	46m @ 0.31% Cu 4m @ 0.11 g/t Au 4m @0.32 g/t Au
RC drilling Results	Moola	MRC009	9615	49600	16m @0.15% Pb 16m @0.21% Zn
RC drilling Results	Moola	MRC010	9575	49600	8m @ 0.17% Cu 20m @0.16% Cu 8m @ 0.16 g/t Au and 1.0g/t Ag
RC drilling Results	Moola	MRC012	9560	49390	40m @ 0.11 % Cu 8m @ 0.1 g/t Au 28m @ 0.25% Cu
RC drilling Results	Moola	MRC014	9290	48300	48m @ 0.21% Cu and 1.0 g/t Ag 16m @ 0.15 g/t Au
RC drilling Results	Moola	MRC015	9300	48100	20m @ 0.21% Cu and 1.0 g/t Ag 4m @ 0.18 g/t Au 8m @ 0.13 g/t Au
Drill Assay Results	Moola	MBR 110	9640	49250	0.25% Cu
Drill Assay Results	Moola	MBR 112	9560	49250	0.1% Cu 0.13% Cu
Drill Assay Results	Moola	MBR 115	9560	49100	0.35% Cu
Drill Assay Results	Moola	MBR 117	9560	48900	0.5%Cu 1.0% Cu 0.2% Zn 8g/t Au
Drill Assay Results	Moola	MBR 169	9560	49000	0.45% Cu 1.2% Cu 0.15 g/t Au
Drill Assay Results	Moola	MBR 171	9560	49050	0.80% Cu 1.1% Cu 8 g/t Ag
Drill Assay Results	Moola	MBR 172	9560	48950	0.38% Cu

**Table 4.** Table summarising exploration targets identified by helix and possible exploration tools that could be used to further exploration(source: Wilson, 2000)

Prospect	Identified Exploration Target	Suggested Future Exploration
Princess	Shallow chargeable anomaly within PRCD1A- Princess IP  &	A shallow RAB / RC hole should test this anomaly and may be completed as part of a larger program incorporating the Moola FLTEM anomalies.
Princess	Deep chargeable anomaly within PRCD1A- Princess IP	A deep drill hole would be needed to test this anomaly, although it is suggested that infill IP lines be completed to better define the centre of the anomaly.
Highway	Zones of higher conductivity that could possibly be fractures or shears within the basement lithology, which may have the potential to host mineralisation -MMR	A program of RAB drilling
Moola	An extensive but weak conductor dipping shallowly to the west – northwest, carbonaceous shale or perhaps a weakly disseminated sulphide unit - FLTEM	A small, shallow RAB / RC drilling would be required to test the potential of the two conductor
Moola	A conductor source directly below the loop, defining a  weak, broad, flat lying conductor located at depths of between 45 – 50m, possibly due to some sort of supergene enrichment-FLTEM	A small, shallow RAB / RC drilling would be required to test the potential of the two conductor
Moola	A deeper conductor which is more extensive than the one above and is likely to be the same conductor as the extensive but weak anomaly also identified above - FLTEM	A small, shallow RAB / RC drilling would be required to test the potential of the two conductor

**Table 5.** Calcrete samples taken along old Helix workings to check accuracy of existing data

Current Sample Locations		Helix Sample Locations	
easting	northing	easting	northing
703607	6334797	703608	6334796
704394	6325111	704394	6325111
703002	6334800	703022	6334538
704025	6325582	704025	6325581
704427	6325585	704428	6325588
704007	6334824	704006	6334825
703421	6335300	703421	6335303
702994	6335312	702999	6335307
704581	6334797	704582	6334799
705009	6335288	705007	6335288
703206	6334796	703205	6334802
703171	6325626	703189	6325633
703584	6325621	703580	6325617
703395	6334802	703395	6334804
704883	6325572	704863	6325572
703592	6325100	703592	6325102
703177	6334505	703177	6334505
704566	6335217	704564	6335219
703596	6334535	703597	6334535

**Table 6.** Western myall Cu concentrations normalized to equal original pearl bluebush data

Western Myall (Cu)	Western Myall Normalized (Cu)	Pearl Bluebush	Calculation for constant
8.77	5.76189	5.38	$(y_2 - y_1) / (x_2 - x_1)$
13.89	9.12573	7.84	
9.11	5.98527	9.09	
6.45	4.23765	5.85	From Figure 61.
5.86	3.85002	3.34	$(8.4 - 3.8) / (12.4 - 5.4)$
5.05	3.31785	3.31	0.657
5.41	3.55437	2.2	
10.72	7.04304	7.86	

**Table 7.** Pearl bluebush Cu concentrations normalized to equal original western myall data

Pearl Bluebush (Cu)	Pearl bluebush Normalized (Cu)	Western Myall (Cu)	Calculation for constant
5.38	7.21996	8.77	$(y_2 - y_1) / (x_2 - x_1)$
7.84	10.52128	13.89	
9.09	12.19878	9.11	
5.85	7.8507	6.45	From Figure 61.
3.34	4.48228	5.86	$(8.4 - 3.8) / (12.4 - 5.4)$
3.31	4.44202	5.05	0.657
2.2	2.9524	5.41	$(1 - 0.657) + 1$
7.86	10.54812	10.72	1.342



**Table 8.** Divisions used to describe the correlations between target elements within Spearman's matrix

<b>Spearman's Correlation</b>	
<b>Very Weak</b>	<b>&lt;20</b>
<b>Weak</b>	<b>20-40</b>
<b>Moderate</b>	<b>40-60</b>
<b>High</b>	<b>60-80</b>
<b>Very High</b>	<b>80-100</b>

**Table 9.** Locations and concentrations of high Cu concentrations and the species it was found within

<b>northing</b>	<b>easting</b>	<b>Western myall (Cu)</b>	<b>northing</b>	<b>easting</b>	<b>Pearl bluebush (Cu)</b>
6331269	703670	13.04	6334999	703060	7.06
6331181	703767	19.42	6335049	703297	7.86
6331222	703820	33.4	6335117	703551	7.01
6331271	703848	43.78	6335124	703810	9.81
6331373	703756	13.89	6335161	704053	9.75
6331276	703809	36.77	6339408	703252	7.32
6331731	703900	21.84	6331360	703737	8.71
6331853	703822	20.22	6331209	703869	8.14
6331855	703945	13.01	6331369	703760	7.84
6331770	703806	11.35	6331778	703753	9.25
6330946	706559	11.44	6331768	703813	10.01
6335100	704466	16.34	6331780	703845	9.09
6349205	706922	11.5	6330945	706811	7.65
6349346	707233	10.85	6331244	705348	7.25
6349498	707569	12.92	6331444	705090	7.16

**Table 10.** Spearman's Correlation Matrix for Western Myall target elements

Spearman	Cu_ppm	Pb_ppm	Zn_ppm	Ag_ppb	Fe_pct	U_ppm	Au_ppb	La_ppm	Al_pct	Zr_ppm	Y_ppm	Ce_ppm	Sn_ppm
<b>Cu_ppm</b>	1	0.05	0.41	-0.16	0.29	-0.14	-0.46	0.44	-0.35	0.17	0.57	0.43	0.12
<b>Pb_ppm</b>	0.05	1	0.078	0.5	0.4	0.28	0.68	-0.14	0.66	0.27	-0.034	-0.22	0.14
<b>Zn_ppm</b>	0.41	0.078	1	0.049	0.14	-0.12	-0.24	0.22	-0.049	0.2	0.23	0.22	0.083
<b>Ag_ppb</b>	-0.16	0.5	0.049	1	0.19	0.012	0.56	-0.42	0.51	0.088	-0.33	-0.43	0.14
<b>Fe_pct</b>	0.29	0.4	0.14	0.19	1	0.19	0.2	0.17	0.36	0.86	0.17	0.07	0.27
<b>U_ppm</b>	-0.14	0.28	-0.12	0.012	0.19	1	0.8	0.036	0.11	0.23	0.2	0.078	0.34
<b>Au_ppb</b>	-0.46	0.68	-0.24	0.56	0.2	0.8	1	-0.65	0.86	0.12	-0.49	-0.64	
<b>La_ppm</b>	0.44	-0.14	0.22	-0.42	0.17	0.036	-0.65	1	-0.33	0.33	0.82	0.97	0.055
<b>Al_pct</b>	-0.35	0.66	-0.049	0.51	0.36	0.11	0.86	-0.33	1	0.35	-0.39	-0.38	0.018
<b>Zr_ppm</b>	0.17	0.27	0.2	0.088	0.86	0.23	0.12	0.33	0.35	1	0.22	0.23	0.31
<b>Y_ppm</b>	0.57	-0.034	0.23	-0.33	0.17	0.2	-0.49	0.82	-0.39	0.22	1	0.87	-0.001
<b>Ce_ppm</b>	0.43	-0.22	0.22	-0.43	0.07	0.078	-0.64	0.97	-0.38	0.23	0.87	1	0.031
<b>Sn_ppm</b>	0.12	0.14	0.083	0.14	0.27	0.34	NaN	0.055	0.018	0.31	-0.001	0.031	1

**Table 11.** Spearman’s Correlation Matrix for Pearl Bluebush target elements

<b>Spearman</b>	<b>Cu_ppm</b>	<b>Au_ppb</b>	<b>U_ppm</b>	<b>Pb_ppm</b>	<b>Zn_ppm</b>	<b>Ag_ppb</b>	<b>Fe_pct</b>	<b>Al_pct</b>	<b>Zr_ppm</b>	<b>Y_ppm</b>	<b>Ce_ppm</b>	<b>La_ppm</b>	<b>Sn_ppm</b>
<b>Cu_ppm</b>	1	0.22	0.53	0.26	0.4	0.16	0.37	0.49	0.56	0.62	0.5	0.56	0.19
<b>Au_ppb</b>	0.22	1	0.33	0.34	0.33	0.2	0.39	0.32	0.42	0.35	0.42	0.35	0.31
<b>U_ppm</b>	0.53	0.33	1	0.54	0.41	0.25	0.8	0.71	0.76	0.75	0.74	0.79	0.37
<b>Pb_ppm</b>	0.26	0.34	0.54	1	0.57	0.35	0.78	0.68	0.74	0.63	0.75	0.72	0.7
<b>Zn_ppm</b>	0.4	0.33	0.41	0.57	1	0.48	0.57	0.51	0.55	0.49	0.58	0.49	0.52
<b>Ag_ppb</b>	0.16	0.2	0.25	0.35	0.48	1	0.4	0.28	0.33	0.26	0.37	0.26	0.29
<b>Fe_pct</b>	0.37	0.39	0.8	0.78	0.57	0.4	1	0.81	0.86	0.75	0.85	0.83	0.66
<b>Al_pct</b>	0.49	0.32	0.71	0.68	0.51	0.28	0.81	1	0.92	0.94	0.9	0.9	0.63
<b>Zr_ppm</b>	0.56	0.42	0.76	0.74	0.55	0.33	0.86	0.92	1	0.93	0.96	0.96	0.65
<b>Y_ppm</b>	0.62	0.35	0.75	0.63	0.49	0.26	0.75	0.94	0.93	1	0.9	0.93	0.57
<b>Ce_ppm</b>	0.5	0.42	0.74	0.75	0.58	0.37	0.85	0.9	0.96	0.9	1	0.95	0.67
<b>La_ppm</b>	0.56	0.35	0.79	0.72	0.49	0.26	0.83	0.9	0.96	0.93	0.95	1	0.63
<b>Sn_ppm</b>	0.19	0.31	0.37	0.7	0.52	0.29	0.66	0.63	0.65	0.57	0.67	0.63	1

**Table 12.** Spearman's Correlation Matrix for Calcrete target elements

<b>Spearman</b>	<b>Au ppb</b>	<b>Ag ppm</b>	<b>Al ppm</b>	<b>Ca pct</b>	<b>Ce ppm</b>	<b>Co ppm</b>	<b>Cu ppm</b>	<b>Fe pct</b>	<b>La ppm</b>	<b>Pb ppm</b>	<b>Sn ppm</b>	<b>U ppm</b>	<b>Y ppm</b>	<b>Zn ppm</b>	<b>Zr ppm</b>
<b>Au_ppb</b>	1	0.085	-0.034	0.14	-0.11	0.21	0.42	-0.26	-0.11	-0.38	-0.14	-0.31	-0.075	-0.086	-0.043
<b>Ag_ppm</b>	0.085	1	-0.12	-0.13	0.035	0.3	-0.075	0.25	0.032	0.29	-0.074	-0.05	4.00E-04	0.24	-0.21
<b>Al_ppm</b>	-0.034	-0.12	1	-0.77	0.75	0.42	0.17	0.53	0.65	0.38	0.9	-0.012	0.54	0.62	0.83
<b>Ca_pct</b>	0.14	-0.13	-0.77	1	-0.68	-0.26	0.086	-0.69	-0.63	-0.69	-0.88	0.18	-0.37	-0.64	-0.68
<b>Ce_ppm</b>	-0.11	0.035	0.75	-0.68	1	0.56	0.076	0.53	0.93	0.47	0.71	-0.12	0.67	0.62	0.52
<b>Co_ppm</b>	0.21	0.3	0.42	-0.26	0.56	1	0.29	0.32	0.46	0.27	0.28	-0.26	0.44	0.58	0.12
<b>Cu_ppm</b>	0.42	-0.075	0.17	0.086	0.076	0.29	1	-0.032	-0.016	-0.18	-0.11	-0.06	0.16	0.27	0.18
<b>Fe_pct</b>	-0.26	0.25	0.53	-0.69	0.53	0.32	-0.032	1	0.52	0.88	0.6	0.044	0.36	0.77	0.41
<b>La_ppm</b>	-0.11	0.032	0.65	-0.63	0.93	0.46	-0.016	0.52	1	0.49	0.65	-0.18	0.76	0.6	0.42
<b>Pb_ppm</b>	-0.38	0.29	0.38	-0.69	0.47	0.27	-0.18	0.88	0.49	1	0.51	-0.023	0.28	0.7	0.26
<b>Sn_ppm</b>	-0.14	-0.074	0.9	-0.88	0.71	0.28	-0.11	0.6	0.65	0.51	1	-0.095	0.44	0.55	0.82
<b>U_ppm</b>	-0.31	-0.05	-0.012	0.18	-0.12	-0.26	-0.06	0.044	-0.18	0.023	-0.095	1	-0.18	-0.055	0.12
<b>Y_ppm</b>	-0.075	4.00E-04	0.54	-0.37	0.67	0.44	0.16	0.36	0.76	0.28	0.44	-0.18	1	0.58	0.34
<b>Zn_ppm</b>	-0.086	0.24	0.62	-0.64	0.62	0.58	0.27	0.77	0.6	0.7	0.55	-0.055	0.58	1	0.43
<b>Zr_ppm</b>	-0.043	-0.21	0.83	-0.68	0.52	0.12	0.18	0.41	0.42	0.26	0.82	0.12	0.34	0.43	1



**Table 13.** Western Myall Sn results and sample locations for the Project Mawson area

<b>northing</b>	<b>easting</b>	<b>Sn (ppm)</b>	<b>northing</b>	<b>easting</b>	<b>Sn (ppm)</b>	<b>northing</b>	<b>easting</b>	<b>Sn (ppm)</b>	<b>northing</b>	<b>easting</b>	<b>Sn (ppm)</b>
6331269	703670	0.01	6331033	705484	0.01	6339388	704413	0.01	6348276	704935	0.02
6331255	703683	0.01	6331465	705169	0.01	6339380	704728	0.01	6348452	705260	0.01
6331217	703717	0.01	6331957	704178	0.01	6338982	706941	0.04	6348578	705536	0.01
6331181	703767	0.01	6332032	704344	0.03	6339128	706583	0.01	6348692	705783	0.01
6331222	703820	0.01	6332221	704091	0.01	6339461	706497	0.01	6348820	706063	0.02
6331271	703848	0.01	6332436	703839	0.01	6339128	706042	0.01	6348958	706374	0.01
6331373	703756	0.01	6332560	703620	0.54	6339539	705478	0.01	6349085	706656	0.01
6331276	703809	0.01	6332401	703266	0.01	6339317	705295	0.01	6349205	706922	0.01
6331875	703804	0.01	6332196	702654	0.01	6342704	704028	0.01	6349346	707233	0.01
6331862	703885	0.01	6334677	701866	0.02	6342790	704299	0.01	6349498	707569	0.01
6331731	703900	0.01	6334782	702351	0.01	6343017	704590	0.01	6349594	707781	0.01
6331778	703730	0.01	6334888	702704	0.01	6343158	705089	0.01	6349846	708345	0.03
6331806	703696	0.01	6335029	703239	0.01	6343014	705565	0.01			
6331820	703727	0.01	6335209	703617	0.01	6343597	706361	0.01			
6331853	703822	0.01	6335231	704144	0.01	6343705	706569	0.02			
6331855	703945	0.01	6335100	704466	0.01	6343866	707108	0.01			
6331774	703850	0.01	6335241	705138	0.01	6344072	707694	0.01			
6331770	703806	0.01	6335048	705703	0.11	6344204	707975	0.01			
6331012	706337	0.01	6335179	706040	0.01	6344324	708300	0.01			
6330946	706559	0.01	6334992	706736	0.01	6344385	708576	0.01			
6330939	706906	0.01	6339418	702987	0.01	6347528	704192	0.01			
6330920	706994	0.01	6339394	703913	0.01	6347768	704418	0.01			
6330994	705834	0.01	6339390	704144	0.01	6348031	704665	0.01			

**Table 14.** Pearl Bluebush Sn results and sample locations for the Project Mawson area

northing	easting	Sn (ppm)	northing	easting	Sn (ppm)	northing	easting	Sn (ppm)	northing	easting	Sn (ppm)
6334681	701882	0.06	6339375	704237	0.04	6349056	706589	0.04	6339401	703962	0.05
6334729	702117	0.05	6339384	704564	0.06	6349189	706886	0.04	6331875	704016	0.05
6334790	702345	0.08	6339390	704807	0.06	6349330	707199	0.05	6331869	704100	0.01
6334866	702572	0.08	6339370	705015	0.05	6349493	707550	0.03	6330945	706811	0.07
6334909	702831	0.06	6339325	705305	0.05	6349687	707974	0.03	6330941	706548	0.03
6334999	703060	0.09	6339322	705532	0.04	6349831	708298	0.04	6330952	706268	0.01
6335049	703297	0.04	6339284	706053	0.06	6331381	703661	0.06	6330964	705997	0.02
6335117	703551	0.12	6339097	706930	0.05	6331416	703687	0.05	6331001	705892	0.01
6335124	703810	0.12	6342686	704036	0.05	6331391	703741	0.03	6331041	705599	0.05
6335161	704053	0.07	6342778	704313	0.03	6331360	703737	0.05	6331244	705348	0.04
6335189	704304	0.05	6342951	704529	0.04	6331244	703645	0.03	6331444	705090	0.03
6335189	704559	0.09	6343057	704764	0.03	6331221	703720	0.04	6332002	704383	0.03
6335156	704831	0.03	6343135	705013	0.03	6331183	703767	0.12	6331830	704596	0.04
6335126	705114	0.05	6343231	705380	0.05	6331209	703869	0.04	6331689	704790	0.04
6335123	705389	0.07	6343292	705688	0.06	6331299	703885	0.03	6331669	703213	0.03
6335148	705675	0.05	6343398	705915	0.04	6331369	703760	0.04	6331503	703450	0.04
6335159	705887	0.03	6343512	706245	0.09	6331324	703622	0.01	6331795	703303	0.04
6335132	706176	0.08	6343891	706580	0.12	6331186	703654	0.04	6332069	702495	0.05
6335096	706468	0.04	6343706	707115	0.05	6331172	703655	0.04	6332250	702864	0.04
6347323	704059	0.06	6344057	707642	0.03	6331116	703698	0.04	6332372	703080	0.04
6347642	704344	0.03	6344222	708041	0.02	6331376	705890	0.03	6332516	703348	0.06
6347861	704533	0.03	6348074	704703	0.05	6331778	703753	0.04	6335121	705779	0.04
6339420	702990	0.05	6348308	704971	0.04	6331768	703813	0.03	6335055	706559	0.05
6339408	703252	0.06	6348466	705287	0.03	6331780	703845	0.05	6344013	707429	0.07
6339403	703482	0.04	6348614	705611	0.06	6331770	703920	0.03	6344272	708556	0.03

**Table 15.** Concentration of Cu and Au from calcrete and western myall which are proximal to one another

<b>Western myall (<i>Acacia papyrocarpa</i>)</b>				<b>Pearl bluebush (<i>Maireana sedifolia</i>)</b>			
<b>northing</b>	<b>easting</b>	<b>Au</b>	<b>Cu</b>	<b>northing</b>	<b>easting</b>	<b>Au</b>	<b>Cu</b>
6349205	706922	0.1	11.5	6349189	706886	0.5	16.1
6349498	707569	0.1	12.92	6349493	707550	0.5	18.2
6343866	707108	0.1	8.23	6343706	707115	0.5	20
6342790	704299	0.1	5.05	6342778	704313	5	85.8
6342704	704028	0.1	5.86	6342686	704036	0.5	28.8
6339317	705295	0.1	5.41	6339325	705305	1	19.4
6339128	706042	0.1	9.51	6339284	706053	3	75.5
6334677	701866	0.1	6.44	6334681	701882	1	20.3
6334782	702351	0.4	6.45	6334790	702345	0.5	28.7

**Table 16.** Errors Analysis for pearl bluebush

Element	Detection Limit	Minimum	Maximum	Standard deviation	Duplicate Error	Duplicate error (ACME)	Standard (V14) Error	V14 (mean)
Cu	0.01ppm	0.050	1.460	0.495	0.097	0.031	0.036	4.655
Pb	0.01ppm	0.030	0.200	0.061	0.012	0.024	0.019	0.852
Zn	0.1ppm	0.000	0.900	0.295	0.058	0.040	0.038	14.400
Ag	2ppb	0.000	3.000	0.919	0.180	0.245	0.351	25.545
Ni	0.1ppm	0.000	0.200	0.092	0.018	0.047	0.023	1.427
Fe	0.001%	0.001	0.052	0.016	0.003	0.006	0.000	0.015
U	0.01ppm	0.000	0.010	0.004	0.001	0.000	0.000	0.005
Au	0.2ppb	0.000	0.400	0.125	0.024	0.028	0.442	6.682
La	0.01ppm	0.020	0.120	0.032	0.006	0.012	0.002	0.030
Al	0.01%	0.000	0.010	0.005	0.001	0.018	0.001	0.143
Sn	0.02ppm	0.000	0.030	0.009	0.002	0.002	0.001	0.041
Zr	0.01ppm	0.000	0.110	0.046	0.009	0.039	0.008	0.052
Y	0.001ppm	0.004	0.116	0.036	0.007	0.020	0.001	0.021
Ce	0.01ppm	0.010	0.470	0.156	0.031	0.048	0.001	0.060



**Table 17.** Errors Analysis for western myall

<b>Element</b>	<b>Detection Limit</b>	<b>Minimum</b>	<b>Maximum</b>	<b>Duplicate Error</b>	<b>Duplicate Error (ACME)</b>	<b>Sample (V14) Error</b>	<b>(V14 Mean)</b>
<b>Cu</b>	0.01ppm	0.3	2.75	0.185207222	1.456527995	0.060862902	4.71
<b>Pb</b>	0.01ppm	0	0.17	0.014131182	0.006533333	0.035382905	0.93
<b>Zn</b>	0.1ppm	0.7	9	0.627634273	0.862630946	0.533473084	14.79
<b>Ag</b>	2ppb	0	2	0.157013136	0.653333333	0.368955451	24.38
<b>Fe</b>	0.001%	0.001	0.01	0.000745857	0.000653333	0.000259862	0.014
<b>U</b>	0.01ppm	0	0.01	0.00113413	0	0	0.01
<b>Au</b>	0.2ppb	0	0.2	0.017324116	0.113160653	0.574426671	6.85
<b>La</b>	0.01ppm	0	0.22	0.022445072	0.164288761	0.001822858	0.034
<b>Al</b>	0.01%	0	0.01	0.000911429	0	0.002044581	0.141
<b>Sn</b>	0.02ppm	0	0.53	0.045572634	0.003772022	0.001732412	0.038
<b>Zr</b>	0.01ppm	0	0.05	0.004618475	0	0.010476641	0.055
<b>Y</b>	0.001ppm	0.002	0.907	0.076183344	0.103683266	0.001101527	0.02
<b>Ce</b>	0.01ppm	0	1.23	0.109151752	0.032228168	0.003571458	0.059

**Table 18.** Errors Analysis for Calcrete

Element	Detection Limit	Minimum	Maximum (Samples)	Duplicate Error	Duplicate error (Genalysis)	Standard (AE19) Error	AE19 (mean)
<b>Au</b>	1 ppb	0.000	3.500	0.561	0.377	0.200	71.750
<b>Ag</b>	0.02 ppm	0.000	0.020	0.004	0.008	0.016	1.173
<b>Al</b>	20 ppm	602.000	10980.000	1769.764	662.997	283.617	18996.000
<b>As</b>	0.5 ppm	0.500	2.000	0.259	0.136	0.016	0.800
<b>Ca</b>	0.01%	0.370	5.040	0.692	0.631	0.286	13.743
<b>Co</b>	0.1 ppm	0.000	3.200	0.484	0.173	0.263	43.430
<b>Cu</b>	0.2 ppm	2.300	10.700	1.399	0.635	1.013	105.950
<b>Fe</b>	0.01%	0.060	0.840	0.132	0.079	0.088	4.800
<b>La</b>	0.01 ppm	0.090	9.730	1.477	0.674	0.273	12.890
<b>Pb</b>	0.5 ppm	0.000	3.800	0.620	0.360	0.942	53.480
<b>Sn</b>	0.05 ppm	0.020	0.330	0.051	0.026	0.039	2.520
<b>U</b>	0.01 ppm	0.020	0.200	0.028	0.038	0.224	13.610
<b>Y</b>	0.02 ppm	0.210	7.100	1.205	0.505	0.011	1.080
<b>Zn</b>	1 ppm	0.000	15.000	2.448	0.998	1.617	118.250

**Table 19.** Level of certainty for each Calcrete Sample based on Ca % taken from Appendix 2

sample	northing	easting	Ca	Level of certainty	sample	northing	easting	Ca	Level of certainty	sample	northing	easting	Ca	Level of certainty
1	6334681	701882	23.23	Very High	20	6335096	706468	1.75	Low	39	6343891	706580	10.59	High
2	6334681	701882	23.12	Very High	21	6347323	704059	25.88	Very High	40	6343706	707115	12.84	High
3	6334729	702117	15.66	High	22	6347642	704344	20.88	Very High	41	6344057	707642	25.16	Very High
4	6334790	702345	16.99	High	23	6347861	704533	24.07	Very High	42	6344222	708041	26.3	Very High
5	6334866	702572	11.46	High	24	6339430	703754	10.48	High	43	6348074	704703	22.67	Very High
6	6334909	702831	1.11	Low	25	6339401	703962	8.32	Mid	44	6349831	708298	15.71	High
7	6334999	703060	10.3	Mid	26	6339384	704564	23.43	Very High	45	6348776	705969	19.95	Very High
8	6334999	703060	6.11	Mid	27	6339390	704807	11.54	High	46	6348916	706276	16.82	High
9	6335049	703297	4.76	Low	28	6339370	705015	18.58	High	47	6349056	706589	14	High
10	6335117	703551	13.8	High	29	6339325	705305	22.84	Very High	48	6349189	706886	24.84	Very High
11	6335124	703810	11.75	High	30	6339322	705532	21.31	Very High	49	6349330	707199	27.03	Very High
12	6335161	704053	9.4	Mid	31	6339284	706053	12.51	High	50	6349493	707550	26.61	Very High
13	6335189	704304	8.17	Mid	32	6342686	704036	23.8	Very High	51	6349687	707974	15.21	High
14	6335189	704559	20.94	Very High	33	6342778	704313	19.49	Very High	52	6349831	708298	25.72	Very High
15	6335156	704831	12.03	High	34	6342951	704529	23.41	Very High	53	6344272	708556	26.82	Very High
16	6335126	705114	0.89	Low	35	6343057	704764	6.24	Mid	54	6331444	705090	28.15	Very High
17	6335123	705389	11.19	High	36	6343135	705013	7.94	Mid	55	6331830	704596	28.6	Very High
18	6335148	705675	23.61	Very High	37	6343398	705915	22.42	Very High	56	6332069	702495	28.02	Very High
19	6335132	706176	5.47	Low	38	6343512	706245	16.59	High	57	6344272	708556	24.57	Very High

**Table 20.** Concentrations of target elements for Helix calcrete and current calcrete overlap

Sample no	Source	easting	northing	Au	Ag	As	Ca	Co	Cu	Mo	Ni	Pb	Sb	Zn
1	Current Data	703607	6334797	8	0.05	4	17.14	5.9	45.3	0.3	11.3	6.7	0.15	24
1	Helix Data	703608	6334796	3.9	0	5	0	0	49	X	19	10	0	46
2	Current Data	704394	6325111	3	0.02	1.3	21.43	6.7	28	0.1	7.7	2.4	0.09	10
2	Helix Data	704394	6325111	1.2	0	0	0	0	33	X	10	6	0	29
3	Current Data	703002	6334800	5	0.04	5.2	2.84	10.8	101.4	2.5	21.8	9.5	0.21	64
3	Helix Data	703022	6334538	3.6	0	0	0	0	39	X	0	4	1	11
4	Current Data	704025	6325582	2	0.02	0.9	23.68	8.8	12.5	0.1	9.2	2	0.08	10
4	Helix Data	704025	6325581	0.8	0	0	0	0	14	X	18	6	0	27
5	Current Data	704427	6325585	1	0.02	3.3	17.37	8.4	24.5	0.3	12.4	4.4	0.13	18
5	Helix Data	704428	6325588	3.1	0	5	0	0	24	X	33	7	0	32
6	Current Data	704007	6334824	2	0.04	3.1	13.18	7.4	37.2	0.3	15	8.6	0.14	42
6	Helix Data	704006	6334825	2.9	0	0	0	0	43	X	24	12	0	62
7	Current Data	703421	6335300	3	0.21	3	17.95	9.5	34.7	0.3	15.7	8	0.16	37
7	Helix Data	703421	6335303	3.2	0	0	0	0	41	X	18	9	0	52
8	Current Data	702994	6335312	2	0.04	3.9	7.56	9.8	26.3	0.3	17.8	8.4	0.28	40
8	Helix Data	702999	6335307	3.1	0	0	0	0	32	X	22	11	0	50
9	Current Data	704581	6334797	X	0.04	4.8	3.04	7.8	29.7	0.4	13.2	4.8	0.14	28
9	Helix Data	704582	6334799	1.6	0	0	0	0	36	X	16	7	0	32
10	Current Data	705009	6335288	2	0.06	8.5	7.95	5.3	20.2	0.5	10.4	10.1	0.24	20
10	Helix Data	705007	6335288	1.8	0	5	0	0	23	X	18	17	0	29
11	Current Data	703206	6334796	1	0.06	4.4	2.98	6.9	39.5	0.4	13.4	7.7	0.11	34
11	Helix Data	703205	6334802	0.8	0	5	0	0	25	X	14	11	0	40
12	Current Data	703171	6325626	3	0.03	1.9	20.28	4	30.5	0.2	6.6	3.3	0.07	8
12	Helix Data	703189	6325633	3.1	0	5	0	0	34	X	16	9	0	42
13	Current Data	703584	6325621	X	0.02	2.1	21.68	6.8	33.3	0.2	13.1	3.3	0.12	15
13	Helix Data	703580	6325617	1.5	0	0	0	0	20	X	21	7	0	33
14	Current Data	703395	6334802	4	0.03	4.6	16.65	8.5	43.7	0.2	14.8	6.9	0.17	34
14	Helix Data	703395	6334804	2.7	0	0	0	0	52	X	23	11	0	60



Table 20 continued.

Sample no	Source	easting	northing	Au	Ag	As	Ca	Co	Cu	Mo	Ni	Pb	Sb	Zn
15	Current Data	704883	6325572	3	0.07	2.1	20.74	9	27.8	0.2	14	4	0.21	20
15	Helix Data	704863	6325572	3.6	0	0	0	0	26	X	16	8	0	31
16	Current Data	703592	6325100	4	0.04	7.7	11.66	11.6	26.8	0.4	24.3	5.7	0.15	32
16	Helix Data	703592	6325102	2.1	0	0	0	0	28	X	18	5	0	19
17	Current Data	703177	6334505	X	0.04	7.8	3.93	3.8	17.7	0.5	7.2	6.8	0.26	15
17	Helix Data	703177	6334505	1.9	0	0	0	0	42	X	10	8	0	26
18	Current Data	704566	6335217	X	0.12	7.9	8	33.4	35.2	0.6	15.1	11.9	0.2	60
18	Helix Data	704564	6335219	1.0	0	5	0	0	19	X	11	16	0	39
19	Current Data	703596	6334535	3	0.03	4.8	12.33	7.3	32.2	0.3	13.3	6.4	0.16	28
19	Helix Data	703597	6334535	1.5	0	0	0	0	31	X	15	8	0	39
15	Current Data	704883	6325572	3	0.07	2.1	20.74	9	27.8	0.2	14	4	0.21	20
15	Helix Data	704863	6325572	3.6	0	0	0	0	26	X	16	8	0	31
16	Current Data	703592	6325100	4	0.04	7.7	11.66	11.6	26.8	0.4	24.3	5.7	0.15	32
16	Helix Data	703592	6325102	2.1	0	0	0	0	28	X	18	5	0	19
17	Current Data	703177	6334505	X	0.04	7.8	3.93	3.8	17.7	0.5	7.2	6.8	0.26	15
17	Helix Data	703177	6334505	1.9	0	0	0	0	42	X	10	8	0	26
18	Current Data	704566	6335217	X	0.12	7.9	8	33.4	35.2	0.6	15.1	11.9	0.2	60
18	Helix Data	704564	6335219	1.0	0	5	0	0	19	X	11	16	0	39

**Table 21.** Mechanisms of Dispersion (source: Aspandiar, 2006)

Table 9. Summary of different mechanisms having the potential to transfer metals upwards through transported cover.

	Mechanism	Process summary	Limiting Factors
<b>Phreatic</b>	Convection (Heat)	Faster upward migration of ions due to density or subtle heat generated currents	<ul style="list-style-type: none"> <li>• Sulphide rich oxidizing deposit needed</li> <li>• Effectiveness over deposit not fully proved or explored</li> <li>• Limited to water table</li> </ul>
	Dilatancy pumping	Groundwater pumped upwards due to compressional stress along faults/fractures. Arid climates favour rapid evaporation and restriction of metals	<ul style="list-style-type: none"> <li>• Requires neotectonic active areas - faults through transported cover and</li> <li>• Confirmation of visible groundwater effusion after earthquakes</li> </ul>
	Bubble	Metal ions attach to upward streaming carrier gas bubbles (CO <sub>2</sub> )	<ul style="list-style-type: none"> <li>• Fate of bubbles and attached particles on unclear above water table</li> </ul>
	SP (electrochemical)	Electrical currents set around from sulphide ore with concentration of cations at edges	<ul style="list-style-type: none"> <li>• Process is limited to shallow cover</li> <li>• Relies on diffusion process to pass through thick cover</li> </ul>
	Redox Gradient (electrochemical)	Redox differences between oxidizing near surface and reducing base of cover. Faster migration in voltaic gradient	<ul style="list-style-type: none"> <li>• Needs saturation conditions and associated redox gradient for effective transfer</li> </ul>
	Diffusion (indirect effects)	Diffusion along concentration gradient from base of cover to surface	<ul style="list-style-type: none"> <li>• Very slow process with only H<sup>+</sup> migrating fast enough through saturated cover</li> </ul>
<b>Vadose</b>	Capillary	Surface tension related rise of groundwater above WT. Evaporation at surface drives suction upwards	<ul style="list-style-type: none"> <li>• Upward extent unclear and operation in heterogenous textural materials unproven</li> </ul>
	Gaseous diffusion	Oxidizing ore body produced gases (CO <sub>2</sub> , COS, SO <sub>2</sub> , CH <sub>4</sub> ) and volatiles (Hg, AsH <sub>3</sub> ) diffusion through porous media	<ul style="list-style-type: none"> <li>• Migration along preferential pathways (structural conduits).</li> <li>• Gas signal complicated by biological released gases</li> <li>• Temporal stability of many gases limited</li> </ul>
	Barometric pumping	Rapid advective transport of gases in fractured media via barometric pumping	<ul style="list-style-type: none"> <li>• Limited to fractured media</li> </ul>
	Gas Convection	Air temperature differences drive hotter gases from ore body upwards	<ul style="list-style-type: none"> <li>• Limited to hilly regions or for low relief regions, permeable covers, high sulphide contents and oxidizing conditions</li> </ul>
	Plant uptake and release to surface via litter	Absorption of metals from water table or anomalous zone, accumulation in organs and release to ground via litter	<ul style="list-style-type: none"> <li>• Species, landform and climate related</li> <li>• Root penetration depths maybe localized</li> <li>• Species related uptake unclear</li> <li>• Rate of transfer to surface and homogenization requires study</li> </ul>
	Plant uptake and release to soil - Hydraulic lift	Water absorption from depth (water table) and release near surface (upper soil horizon)	<ul style="list-style-type: none"> <li>• Metal transfer with water not confirmed.</li> <li>• Depth from which water lifted poorly constrained.</li> <li>• Limited understanding of the process</li> </ul>
	Bioturbation and gravity (mechanical)	Vertical and lateral movement of material from depth to surface by burrowing activities of conveyor belt organisms (termites and ants) - bioturbation	<ul style="list-style-type: none"> <li>• In many areas limited by depth of bioturbation (&lt;3 m)</li> <li>• Further information on burrowing depths of ants &amp; termites in dry settings</li> </ul>